Numerical Modelling of Process Kinetics during TLP-bonding and Other Diffusion-Controlled Processes

by

Yunhong Zhou

A thesis submitted in conformity with the requirements
for the Degree of Doctor of Philosophy
Department of Metallurgy and Materials Science
University of Toronto

ISBN 0-315-92809-3

Name YUN MING ZHOU

Dissertation Abstracts International is arranged by broad, general subject categories. Please select the one subject which most nearly describes the content of your dissertation. Enter the corresponding four-digit code in the spaces provided.

Material Science Metallurgy

SUBJECT TERM

0794

SUBJECT CODE

U·M·I

Subject Categories

THE HUMANITIES AND SOCIAL SCIENCES

COMMUNICATIONS AND THE ARTS

Architecture 0729
Art History 0377
Cinema 0900
Dance 0378
Fine Arts 0357
Information Science 0723
Journalism 0391
Library Science 0399
Mass Communications 0708
Music 0413
Speech Communication 0459
Theater 0465

EDUCATION

General 0515
Administration 0514
Adult and Continuing 0516
Agricultural 0517
Art 0273
Bilingual and Multicultural 0282
Business 0688
Community College 0275
Curriculum and Instruction 0727
Early Childhood 0518
Elementary 0524
Finance 0277
Guidance and Counseling 0519
Health 0680
Higher 0745
History of 0520
Home Economics 0278
Industrial 0521
Language and Literature 0279
Mathematics 0280
Music 0522
Philosophy of 0998
Physical 0523
Psychology 0525
Reading 0535
Religious 0527
Sciences 0714
Secondary 0533
Social Sciences 0534
Sociology of 0340
Special 0529
Teacher Training 0530
Technology 0710
Tests and Measurements 0288
Vocational 0747

LANGUAGE, LITERATURE AND LINGUISTICS

Language
- General 0679
- Ancient 0289
- Linguistics 0290
- Modern 0291

Literature
- General 0401
- Classical 0294
- Comparative 0295
- Medieval 0297
- Modern 0298
- African 0316
- American 0591
- Asian 0305
- Canadian (English) 0352
- Canadian (French) 0355
- English 0593
- Germanic 0311
- Latin American 0312
- Middle Eastern 0315
- Romance 0313
- Slavic and East European 0314

PHILOSOPHY, RELIGION AND THEOLOGY

Philosophy 0422
Religion
- General 0318
- Biblical Studies 0321
- Clergy 0319
- History of 0320
- Philosophy of 0322

Theology 0469

SOCIAL SCIENCES

American Studies 0323
Anthropology
- Archaeology 0324
- Cultural 0326
- Physical 0327

Business Administration
- General 0310
- Accounting 0272
- Banking 0770
- Management 0454
- Marketing 0338

Canadian Studies 0385
Economics
- General 0501
- Agricultural 0503
- Commerce-Business 0505
- Finance 0508
- History 0509
- Labor 0510
- Theory 0511

Folklore 0358
Geography 0366
Gerontology 0351
History
- General 0578
- Ancient 0579
- Medieval 0581
- Modern 0582
- Black 0328
- African 0331
- Asia, Australia and Oceania 0332
- Canadian 0334
- European 0335
- Latin American 0336
- Middle Eastern 0333
- United States 0337

History of Science 0585
Law 0398
Political Science
- General 0615
- International Law and Relations 0616
- Public Administration 0617

Recreation 0814
Social Work 0452
Sociology
- General 0626
- Criminology and Penology 0627
- Demography 0938
- Ethnic and Racial Studies 0631
- Individual and Family Studies 0628
- Industrial and Labor Relations 0629
- Public and Social Welfare 0630
- Social Structure and Development 0700
- Theory and Methods 0344

Transportation 0709
Urban and Regional Planning 0999
Women's Studies 0453

THE SCIENCES AND ENGINEERING

BIOLOGICAL SCIENCES

Agriculture
- General 0473
- Agronomy 0285
- Animal Culture and Nutrition 0475
- Animal Pathology 0476
- Food Science and Technology 0359
- Forestry and Wildlife 0478
- Plant Culture 0479
- Plant Pathology 0480
- Plant Physiology 0817
- Range Management 0777
- Wood Technology 0746

Biology
- General 0306
- Anatomy 0287
- Biostatistics 0308
- Botany 0309
- Cell 0379
- Ecology 0329
- Entomology 0353
- Genetics 0369
- Limnology 0793
- Microbiology 0410
- Molecular 0307
- Neuroscience 0317
- Oceanography 0416
- Physiology 0433
- Radiation 0821
- Veterinary Science 0778
- Zoology 0472

Biophysics
- General 0786
- Medical 0760

EARTH SCIENCES

Biogeochemistry 0425
Geochemistry 0996
Geodesy 0370
Geology 0372
Geophysics 0373
Hydrology 0388
Mineralogy 0411
Paleobotany 0345
Paleoecology 0426
Paleontology 0418
Paleozoology 0985
Palynology 0427
Physical Geography 0368
Physical Oceanography 0415

HEALTH AND ENVIRONMENTAL SCIENCES

Environmental Sciences 0768
Health Sciences
- General 0566
- Audiology 0300
- Chemotherapy 0992
- Dentistry 0567
- Education 0350
- Hospital Management 0769
- Human Development 0758
- Immunology 0982
- Medicine and Surgery 0564
- Mental Health 0347
- Nursing 0569
- Nutrition 0570
- Obstetrics and Gynecology 0380
- Occupational Health and Therapy 0354
- Ophthalmology 0381
- Pathology 0571
- Pharmacology 0419
- Pharmacy 0572
- Physical Therapy 0382
- Public Health 0573
- Radiology 0574
- Recreation 0575
- Speech Pathology 0460
- Toxicology 0383

Home Economics 0386

PHYSICAL SCIENCES

Pure Sciences

Chemistry
- General 0485
- Agricultural 0749
- Analytical 0486
- Biochemistry 0487
- Inorganic 0488
- Nuclear 0738
- Organic 0490
- Pharmaceutical 0491
- Physical 0494
- Polymer 0495
- Radiation 0754

Mathematics 0405
Physics
- General 0605
- Acoustics 0986
- Astronomy and Astrophysics 0606
- Atmospheric Science 0608
- Atomic 0748
- Electronics and Electricity 0607
- Elementary Particles and High Energy 0798
- Fluid and Plasma 0759
- Molecular 0609
- Nuclear 0610
- Optics 0752
- Radiation 0756
- Solid State 0611

Statistics 0463

Applied Sciences

Applied Mechanics 0346
Computer Science 0984
Engineering
- General 0537
- Aerospace 0538
- Agricultural 0539
- Automotive 0540
- Biomedical 0541
- Chemical 0542
- Civil 0543
- Electronics and Electrical 0544
- Heat and Thermodynamics 0348
- Hydraulic 0545
- Industrial 0546
- Marine 0547
- Materials Science 0794
- Mechanical 0548
- Metallurgy 0743
- Mining 0551
- Nuclear 0552
- Packaging 0549
- Petroleum 0765
- Sanitary and Municipal 0554
- System Science 0790

Geotechnology 0428
Operations Research 0796
Plastics Technology 0795
Textile Technology 0994

PSYCHOLOGY

General 0621
Behavioral 0384
Clinical 0622
Developmental 0620
Experimental 0623
Industrial 0624
Personality 0625
Physiological 0989
Psychobiology 0349
Psychometrics 0632
Social 0451

THE UNIVERSITY OF TORONTO LIBRARY
MANUSCRIPT THESIS - DOCTORAL
AUTHORITY TO DISTRIBUTE

NOTE: The AUTHOR will sign in one of the two places indicated. It is the intention of the University that there be NO RESTRICTION on the distribution of the publication of theses save in exceptional cases.

(a) Immediate publication in microform by the National Library is authorized.

Author's signature _____ Date Jan. 6, 1994

- OR -

(b) Publication by the National Library is to be postponed until _____ 19____ (normal maximum delay is two years). Meanwhile this thesis may not be consulted in the University Library except with written permission on each occasion from me.

Author's signature _____ Date _____

This restriction is authorized for reasons which seem to me, as Chair of the Graduate Department of _____, to be sufficient.

Signature of Graduate Department Chair _____

Date _____

BORROWERS undertake to give proper credit for any use made of the thesis, and to obtain the consent of the author if it is proposed to make extensive quotations, or to reproduce the thesis in whole or in part.

Signature of borrower	Address	Date

1989

Numerical Modelling of Process Kinetics during TLP-bonding and Other Diffusion-Controlled Processes

by **Yunhong Zhou**

A thesis submitted in conformity with the requirements
for the Degree of Doctor of Philosophy
Department of Metallurgy and Materials Science
University of Toronto

Abstract

The process kinetics during Transient Liquid Phase (TLP) bonding and other diffusion-controlled, two-phase moving interface problems have been examined using numerical modelling and experimental testing. The review section produces a general background of kinetic modelling of two-phase diffusion-controlled processes. Considerable emphasis is placed on the effect of grain boundary regions on process kinetics, and on previous modelling studies.

Nickel base metals with different grain sizes were TLP-bonded using Ni-19at.%P filler metal. The experiment results produced when bonding single-crystal nickel closely correspond with the calculated output of a one-dimensional model developed in the present thesis. The results of influence of base metal grain boundary regions on the process kinetics form the basis for the subsequent development of two-dimensional finite difference models that accounted for grain boundary-related phenomena.

The one-dimensional, fully implicit finite difference model developed in this thesis permits the calculation of solute distribution and the location of the migrating interface in any diffusion-controlled, two-phase moving interface process. The computed results are in good agreement with experimental results produced in the present thesis, and with results found in the literature (on the solution treatment of α/β brass diffusion couples). The numerical calculation is very fast and accurate. Also, the one-dimensional model permits selection of optimum parameters during TLP-bonding.

The two-dimensional finite difference models developed to examine the effect of grain boundary regions on process kinetics take into account grain boundary diffusion, grain boundary migration and grain boundary grooving (or liquid penetration during TLP-bonding). Modelling has confirmed that the influence of grain boundary regions depends on the grain size, the ratio of grain boundary diffusion and lattice diffusion coefficients. Grain boundary migration only affects the total amount diffused during part of the holding period. The grain boundary grooving model takes into account: (1) volume diffusion in each phase, (2) the excess chemical potential resulting from the gradient interfacial curvature, and (3) the excess chemical potential resulting from the balance between the grain boundary energy and interfacial energy at the grain boundary triple junction. This model correctly simulates liquid-solid interface movement at base metal grain boundary regions during TLP-bonding.

To My Parents and My Wife

Acknowledgements

I would like to express my sincere gratitude to my supervisor, Professor T.H. North for providing guidance and support throughout this study. In addition, I would like to acknowledge the excellent advice provided by Professor K. Ikeuchi (Welding Research Institute, Osaka University, Japan).

Also, the author would also like to acknowledge useful discussions with Professor W.A. Miller, Professor J.W. Rutter, Professor K.T. Aust, Professor Z. Wang (all at University of Toronto), Professor Y. Nakao (Department of Welding and Production Engineering, Osaka University, Japan), Dr. E.R. Wallach (Department of Materials Science and Metallurgy, University of Cambridge, U.K.), Dr. K. Saida (Department of Welding and Production Engineering, Osaka University, Japan) and Professor G.E. Peng (Department of Second Mechanical Engineering, Chongqing University, P.R. China). Special thanks must go to Mr. W. Fearis for his considerable assistance in terms of experimental advice and support.

Finally, I wish to acknowledge financial support through the Ontario Government and the University of Toronto.

Page#

Table of Contents

List of Figures

List of Tables

Chapter 1

Introduction

1.1. Two-Phase Diffusion-Controlled Processes

Diffusion-controlled growth or dissolution of an unstable phase is important in a range of metallurgical situations [Sekerka, 1975]. For example:

(a) in a solid-solid system when a second-phase grows and subsequently dissolves during solution heat-treatment [Heckel, 1975], or when an intermediate layer grows in a thermal barrier coating [Kidson and Miller, 1964];

(b) in a solid-liquid system when the liquid phase grows and/or shrinks during liquid phase sintering, or during Transient Liquid Phase (TLP) bonding [Kaysser, 1980; Tuah-Poku, 1988];

(c) in a solid-gas (vapor) system when an intermediate aluminide phase grows during aluminization of nickel-based alloy materials [Hickl and Heckel, 1975].

In the present thesis, two-phase diffusion processes are defined as those metallurgical situations in which the growth or/and dissolution of an unstable phase occurs through solute diffusion and interface movement (see Fig. 1-1 and a more detailed explanation is provided in Chapter 2).

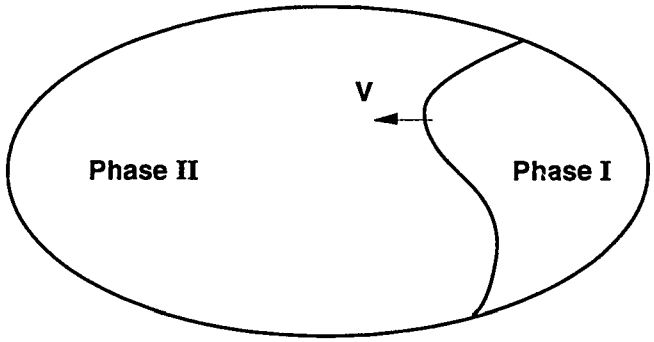

Fig. 1-1 Two-phase diffusion-controlled processes (the growth or/and dissolution of unstable phase I depends on solute diffusion and on interface movement).

1.2. Modelling of Process Kinetics

A number of investigators have modelled the growth or/and dissolution of unstable phases [e.g., Tanzilli and Heckel, 1971; Lanam and Heckel, 1971; Karlsson and Larsson, 1975; and Nakagawa et al, 1991]. However, major problems still remain. For example:

(1) Modelling of the TLP-bonding process still requires much work, since almost all the research to-date has depended on the application of analytical methods [e.g., Niemann and Garret, 1974; Sekerka, 1975; Ikawa and Nakao, 1977; Onzawa et al, 1978; and Tuah-Poku et al, 1988; Nakao et al, 1990; and Liu et al, 1991]. These analytical approaches treat the joining process as a number of discrete stages -- dissolution, isothermal solidification and homogenization. However, this is not what actually occurs during TLP-bonding. For example, the completion time required during the homogenization stage

depends on the solute distribution immediately following completion of isothermal solidification. Nakagawa et al [1991] have pointed out that at very low heating rates, solidification can occur when heating from the filler metal melting point to the bonding temperature. This situation cannot be modelled using analytical methods. In addition, the analytical calculations for each stage in TLP-bonding depend on error function and parabolic law assumptions that are only approximate solutions.

(2) A review of the numerical-modelling literature concerning the growth or/and dissolution of unstable phases confirms that extremely long calculation times are involved. This occurs because explicit formulae are employed during such calculations. This is an especially severe problem, when an attempt is made to model a complex process such as Transient Liquid Phase bonding (since the processing time is extremely long compared with the calculation time step needed for stability of the numerical solution). In this connection, computations of other complex situations, e.g., microsegregation during binary alloy casting, have taken several days to perform using computer workstations [Battle and Pehlke, 1990].

(3) Almost all practical situations involve polycrystalline materials and grain boundary regions enhance mass transport. Consequently, the presence of grain boundary regions will markedly affect process kinetics. For example, the total amount of solute diffused during an "exchange experiment" is greatly influenced by the presence of grain boundaries [Lidiard and Tharmalingam, 1959]. Also, Kokawa et al. [1991] have also shown that the rate of isothermal

solidification is faster when finer-grained nickel base metal is employed during TLP-bonding. In this connection, only limited research has dealt with the numerical modelling of the influence of base metal grain boundary regions on the process kinetics during TLP-bonding and similar metallurgical processes.

1.3. Thesis Objectives

The objectives of the present study comprise:

(1) Develop a new numerical program for modelling diffusion-controlled growth or/and dissolution of unstable phases, with the specific aim of decreasing the calculation time and increasing the accuracy of the final calculation output;

(2) Use the numerical model (developed in (1) above) to analyze the Transient Liquid Phase Bonding process, and confirm the validity of calculated results by direct experiment;

(3) Develop numerical models that explain the influence of base metal grain boundary regions on the process kinetics during two-phase diffusion-controlled processes.

1.4. Thesis Layout

Fig. 1-2 shows a flow chart indicating chapters in this thesis. Chapter 1 provides a general background for the research carried out in this thesis. Chapter 2 examines the physical phenomena during two-phase diffusion-controlled processes and published modelling results. Detailed emphasis is placed on TLP-bonding and on solution treatment of α/β brass diffusion couples. The underlying features of analytical

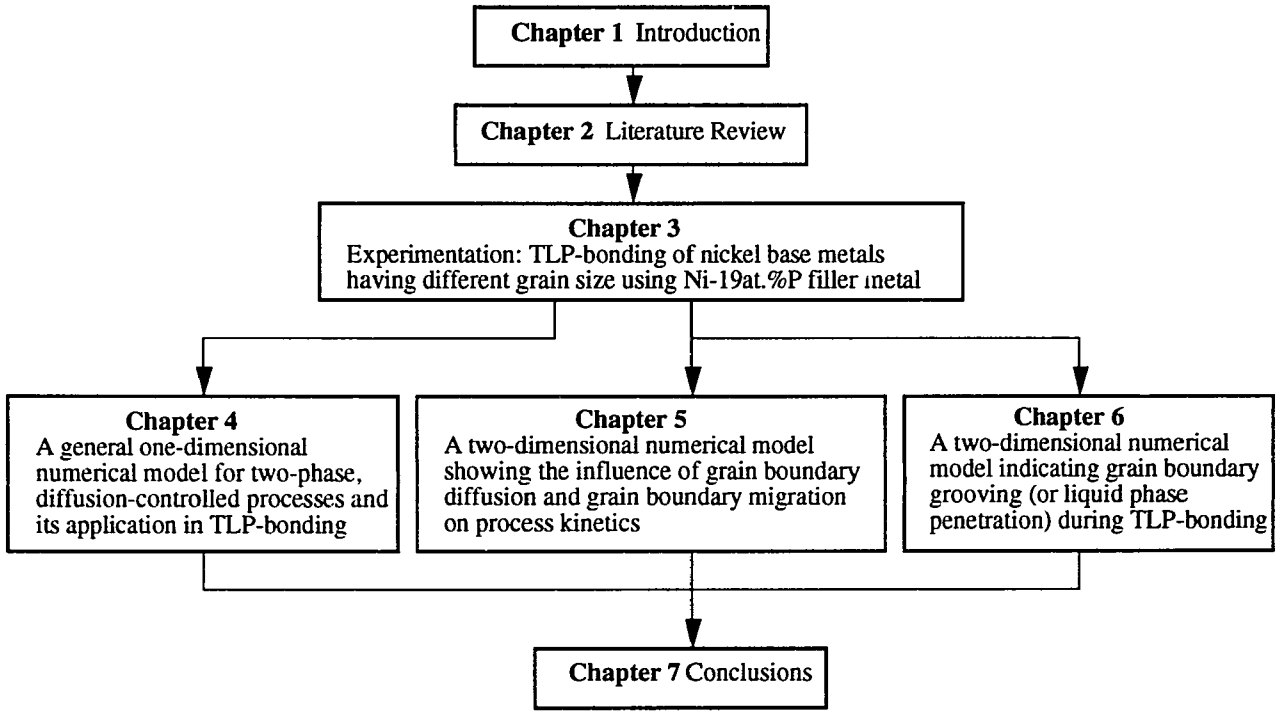

Fig. 1-2 Layout of thesis.

solutions (for diffusion equations) and the finite difference method are described. The influence of grain boundary regions (grain boundary diffusion, grain boundary migration and grain boundary grooving) on process kinetics are reviewed in depth. Chapter 3 describes the experimental results produced during TLP-bonding of nickel base metal. The experimental results produced during TLP-bonding of single-crystal nickel base metal are compared with the output of the one-dimensional numerical model developed in Chapter 4. The effect of base metal grain boundaries on the process kinetics during TLP-bonding of nickel base metal forms the basis for the two-dimensional finite difference models described in Chapters 5 and 6. The conclusions of this thesis are presented in Chapter 7.

Chapter 2

Literature Review

2.1. Two-Phase Diffusion-Controlled Processes

Solute transfer across the interface between two phases could lead to one phase growing and the other dissolving. As mentioned in Chapter 1, two-phase diffusion-controlled problems occur in a range of metallurgical situations and involve solid/solid, solid/liquid, or solid/gas systems. Two detailed examples are described below.

2.1.1. Transient Liquid Phase Bonding

Transient Liquid Phase (TLP) bonding is generally used during the repair of aero-engine turbine blades [Jahnke and Demny, 1983] and when joining components for electronic-circuits [Bernstein and Bartholomew, 1966]. TLP-bonding has a number of advantages -- the joint region has similar mechanical properties to the base metal and complex shapes can be readily fabricated [Duvall et al, 1974]. During TLP-bonding, an interlayer (filler metal) is clamped between the contacting metal surfaces and the entire assembly is heated to the bonding temperature. The filler metal will, at the bonding temperature, melt or react with the base metal to form a liquid zone and then this liquid will solidify isothermally. Following solidification, the joint region is homogenized at the same, or at some

lower, temperature. All stages of TLP-bonding proceed when the solute (the melting point depressant or MPD), which is initially concentrated in the filler metal, continuously diffuses away from the joint center region into the base metal.

Duvall et al [1974], when joining of Ni-Cr-(Co) alloys using Ni-B filler metal, considered that TLP-bonding comprised three different steps, namely, base metal dissolution, liquid phase isothermal solidification and joint homogenization. However, Tuah-Poku et al [1988] defined four stages during TLP-bonding of silver using pure copper filler metal, namely, dissolution of the interlayer (filler metal), homogenization of the liquid, isothermal solidification, and homogenization of the joint region. MacDonald and Eagar [1992] suggested that a further stage should be included to account for the effect of solute diffusion during the heating cycle to the bonding temperature.

There is some dispute concerning the definition of each stage during TLP-bonding. This applies particularly to the dissolution stage. Tuah-Poku et al [1988], analyzed the situation that occurred when a single element filler metal was employed during TLP-bonding, and suggested that filler metal melting and liquid zone widening at the bonding temperature were quite separate stages. However, when a single element filler metal is employed, the initial liquid phase forms as a result of both interlayer melting and base metal dissolution. It is easier to consider filler metal melting and liquid zone widening as a

single stage; this is also consistent with Duvall et al's definition.

In addition, the assumption that the heating cycle between the filler metal melting point and the bonding temperature has no influence on the progress of TLP-bonding is incorrect. For example, when a eutectic composition filler metal is employed during TLP-bonding, solute diffusion when heating from the filler metal melting point (T_M) to the bonding temperature (T_B) can allow solidification to begin before the bonding temperature is reached. Thus, Nakagawa et al [1991] indicated that isothermal solidification could occur between T_M and T_B when the heating rate is slow (around 1K/s) and when a thin (5μm) filler metal is employed. These results were produced when modelling TLP-bonding of nickel base metal using Ni-19at.%P filler metal. The likelihood of solidification prior to reaching the bonding temperature will increase markedly when a high diffusivity melting point depressant is contained in the filler metal. Based on the above comments, it is apparent that a new classification for the different stages during TLP-bonding is required.

It is convenient to describe the new classification of TLP-bonding using the binary eutectic alloy diagram shown in Fig. 2-1 and the time/temperature relation shown in Fig. 2-2. It is worth pointing out that this explanation equally applies when a single-element (pure) filler metal is used during TLP-bonding (see Figs. 2-1 and 2-3 (b)) and when an eutectic alloy filler metal is employed (see Figs. 2-1 and 2-3 (a)). This discussion can be easily extended to binary solid-solution

alloy systems.

Stage I. This is the heating stage, where the sample is heated from room temperature to the filler metal melting temperature (from point o to a in Fig. 2-2). During heating, interdiffusion occurs and the solute concentration $C_{\alpha s}$ at the interface between base metal and filler metal in base metal changes with temperature, following the solvus line in the phase diagram (see Fig. 2-1). Niemann and Garret [1974]

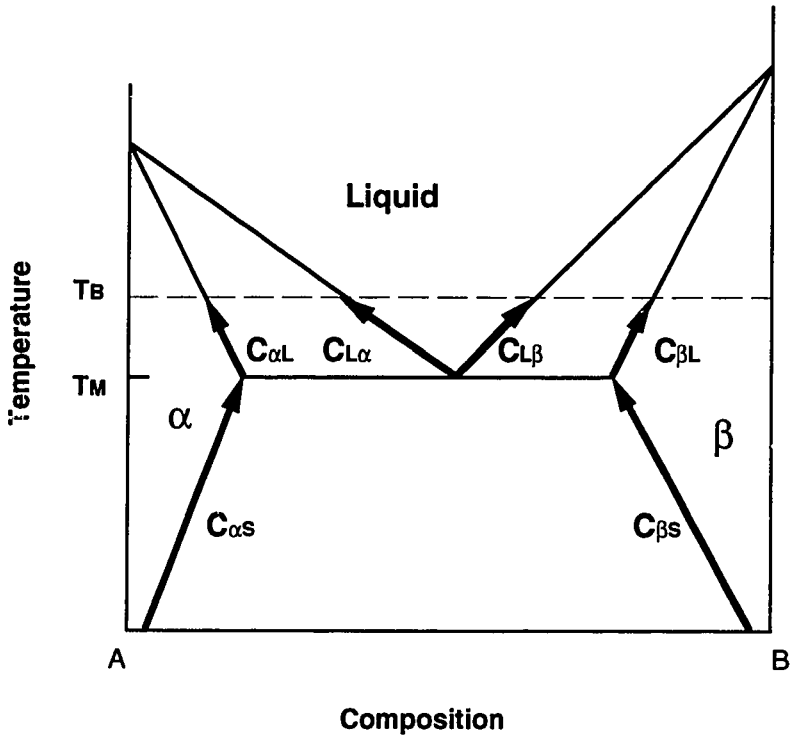

Fig. 2-1 Hypothetical binary phase diagram with a eutectic point.

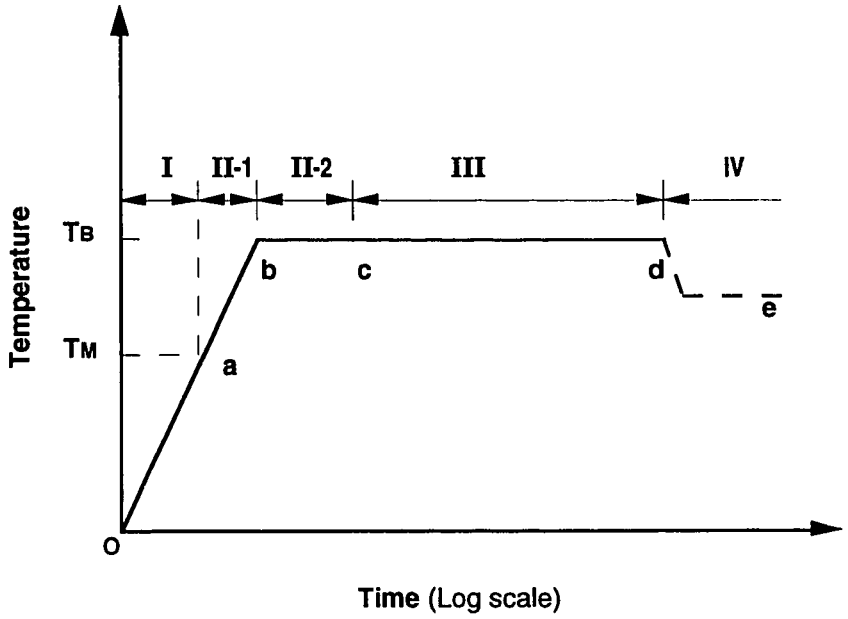

Fig. 2-2 Schematic showing the different stages during heating cycle of TLP-bonding, where T_B is the bonding temperature and T_M is the melting point of the filler metal.

pointed out that this heating stage is particularly important when the filler metal is very thin (since all the filler metal can be consumed during the heating cycle).

Stage II. This is the dissolution stage, when the base metal dissolves and the liquid zone widens (from point a to b and then to c in Fig. 2-2) and solute diffuses into the base metal. This stage can be

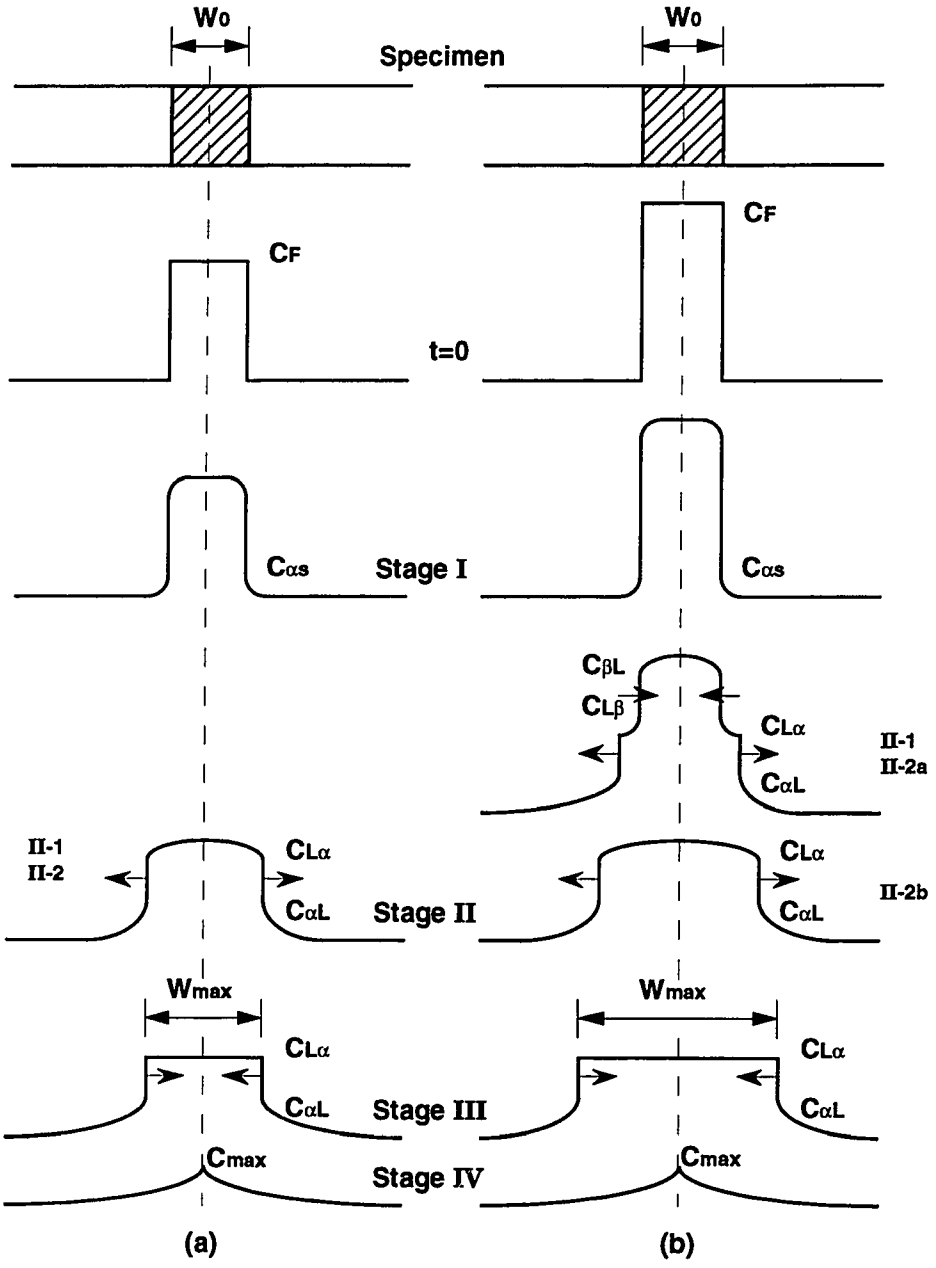

Fig. 2-3 Schematic showing concentration profiles during TLP-bonding using a eutectic filler metal (a) and a single-element filler metal (b).

sub-divided as follows:

(1) Stage II-1, when the temperature is raised from the melting point to the bonding temperature (from point a to b in Fig. 2-2) and the solute concentrations, $C_{L\alpha}$ and $C_{\alpha L}$,and $C_{L\beta}$ and $C_{\beta L}$ at the solid-liquid interfaces are changing with temperature following the solidus and liquidus lines in the binary diagram (see Fig. 2-1);

(2) Stage II-2, involves isothermal dissolution at the bonding temperature (from point b to c in Fig. 2-2). When a single-element filler metal B is employed in an eutectic system, three metallurgical phases (α, β and liquid) will be involved at beginning of dissolution stage (see stage II-1 and stage II-2a in Fig. 2-3 (b)) and then β phase disappears (see stage II-2b in Fig. 2-3 (b)). At the end of stage II, the liquid zone reaches its maximum width (see Fig. 2-3).

It is worth emphasizing that solidification can initiate during the heating cycle from the filler metal melting point when the heating rate is slow and the thin filler metal contains a high diffusivity melting point depressant. When this occurs, base metal dissolution may not occur and filler metal melting will be immediately followed by solidification (also see the paper by Nakagawa et al [1991])

Stage III. This is the isothermal solidification stage, where the liquid zone solidifies when the solute continuously diffuses into base metal at the bonding temperature (from point c to d in Fig. 2-2). The solute concentrations at the solid-liquid interface, $C_{L\alpha}$ and $C_{\alpha L}$, are unchanged during this stage and only the width of liquid zone decreases

until the joint is completely solidified. The solute distribution in liquid is uniform during almost all of the isothermal solidification stage [Nakagawa et al, 1991]. This stage is generally considered to be the most important since the completion time required for the entire TLP-bonding process is largely determined by the time required to complete the isothermal solidification stage. As a result, much research has been carried out on this aspect of the bonding process.

Stage IV. This is the homogenization stage, where solid-state solute redistribution occurs (from point d to e in Fig. 2-2). The homogenization temperature is not necessarily the same as that employed during stage I and II. This stage is terminated when the maximum solute concentration at the joint centerline reaches some preselected value.

This new classification redefines the critical dissolution stage, from the point when the temperature is raised above the melting point of the filler metal. It is worth stressing that TLP-bonding is a continuous process and Fig. 2-3 only provides a schematic understanding of the physical phenomena that occur during the process.

The crucial point in TLP-bonding is that the completed joint has a chemical composition located in the single phase region of the binary equilibrium phase diagram (if no intermediate phases are allowed at the final joint). The joining process approaches this end-point through solute diffusion. The formation of the liquid phase assures complete

wetting of the base metal and formation of a sound joint. It is also clear from Fig. 2-3 that use of a single-element filler metal will markedly increase the maximum liquid width and the time for joint completion (compared with the situation when an equivalent thickness, eutectic composition filler metal is used) [Tuah-Poku, 1988].

2.1.2. Solution Treatment of α/β Brass Diffusion Couples

When an α and β phase aggregate is solution-treated at a temperature where only α is stable, there will be a time-dependent transformation to the single phase α structure. However, if there is a large flux in the β layer (resulting from large variations in solubility with temperature and/or from a large interdiffusion coefficient at the solution temperature) it is possible for the α/β interface to move initially so that the amount of β phase increases. Finally, the β phase dissolves, when a rapid loss of the supersaturation in β phase occurs, and the final structure approaches the end-point defined by the equilibrium phase diagram [Heckel et al, 1975] (see Fig. 2-4). In a similar manner to TLP-bonding, solution treatment of an α and β brass diffusion couple can be considered as a number of different stages, e.g., interdiffusion, α phase dissolution, β phase dissolution and homogenization (when the average composition of test sample is in the single α phase region of the phase diagram).

It is generally assumed that local equilibrium exists at the moving interface during modelling of two-phase diffusion-controlled

problems. In practice, local equilibrium is not attained, e.g., Langer andSekerka [1975] presented a model that accounted for departures

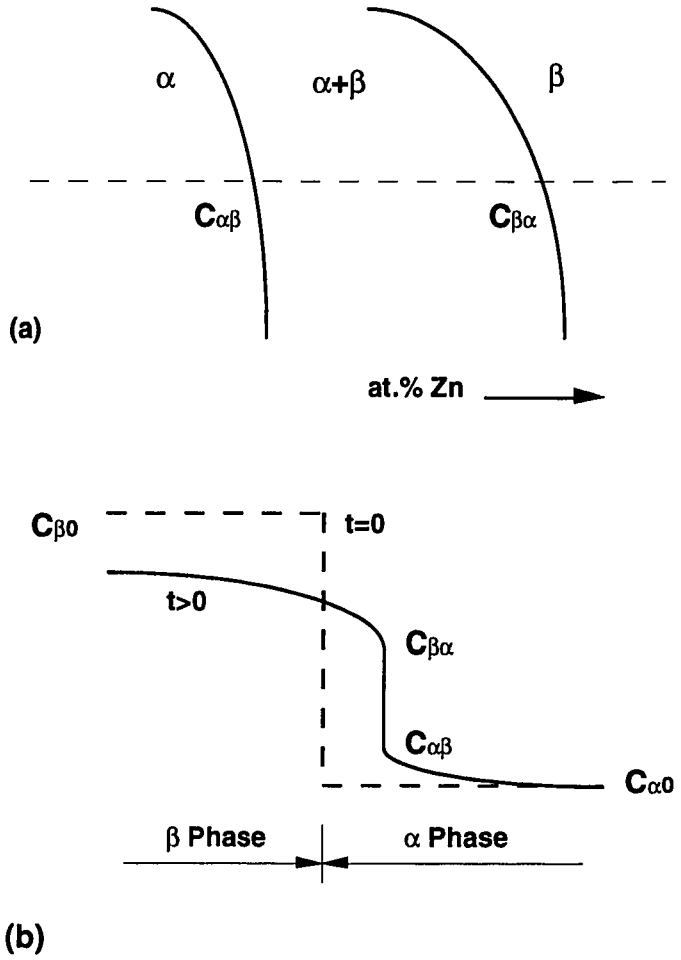

Fig. 2-4 Schematic showing (a) partial Cu-Zn phase diagram; (b) change in solute concentration profile across α/β brass diffusion couple (after Heckel et al, 1972).

from local equilibrium. However, the assumption of local equilibrium at the migrating interface is particularly convenient and it is for this reason that the assumption is employed during the present thesis.

2.1.3. Summary

This thesis considers diffusion-controlled, two-phase isothermal phase transformations where the whole system approaches the end-point defined by the equilibrium phase diagram through diffusional transport. The two principal features of such transformations are solute diffusion and interface migration. The process kinetics of two-phase diffusion-controlled transformations are influenced by all factors that affect diffusion.

2.2. Diffusion Equations in Structurally Homogeneous Materials

2.2.1. Fick's Diffusion Laws

The mathematical basis of diffusion was first established by Adolf Fick in 1855, and many text books have been published indicating mathematical solutions for particular diffusion processes, e.g. Crank's *Mathematics of Diffusion* [1975] and Shewmon's *Diffusion in Solids* [1989].

Fick's First Law is based on the hypothesis that the rate of transfer of the diffusing substance through unit area of a section is proportional to the concentration gradient measured normal to the section, i.e.,

$$J = - D \frac{\partial C}{\partial y}, \tag{2-1}$$

where J is the rate of transfer per unit area of section, C the concentration of diffusing substance, y is the space co-ordinate measured normal to the section, and D is the diffusion coefficient. Conservation of the diffusing substance at each point leads to **Fick's Second Law**:

$$\frac{\partial C}{\partial t} = \nabla(J). \tag{2-2}$$

Furthermore, if D is independent of composition, and also of location in the sample, the above equation becomes:

$$\frac{\partial C}{\partial t} = D \frac{\partial^2 C}{\partial y^2}. \tag{2-3}$$

In two dimensional space, this is:

$$\frac{\partial C}{\partial t} = D \left(\frac{\partial^2 C}{\partial x^2} + \frac{\partial^2 C}{\partial y^2} \right). \tag{2-4}$$

2.2.2. Solutions for One-Dimensional Diffusion Equations

Many useful analytical solutions for diffusion equations can be found in the literature [e.g., the texts by Crank, 1985 and by Shewmon,

1989]. A number of these solutions will be directly applied in the present study.

(1) Thin-Film Solution

Imagine that an infinitesimally thin layer of diffusant of concentration M is plated on to one end of a solute-free rod of infinite length and unit cross-section. If a similar solute-free rod is bonded to the plated-end of this rod (without any diffusion occurring) and the rod is annealed for time t so that diffusion occurs, the concentration of solute along the bar will be given by the relation:

$$C(y,t) = \frac{M}{2\sqrt{\pi Dt}} \exp\left(-\frac{y^2}{4Dt}\right), \tag{2-5}$$

and the total quantity of the solute diffused will be:

$$\int_{-\infty}^{\infty} C(y,t)dx = M. \tag{2-6}$$

(2) Thick Layer Solution

When the initial thickness (2h) of the diffusant source (C_0) is of the order of the diffusion distance ($\sqrt{Dt}$), and,

$$C(y,0) = C_0, \qquad h \geq y \geq 0 \tag{2-7}$$

$$C(y,0) = C_M, \qquad y > h \tag{2-8}$$

where C_M is initial concentration of diffusant in specimen, the solute concentration is:

$$C(y,t)= C_M+\frac{1}{2}(C_0-C_M)\left\{erf\left(\frac{y+h}{\sqrt{4Dt}}\right)-erf\left(\frac{y-h}{\sqrt{4Dt}}\right)\right\}. \quad (2\text{-}9)$$

(3) Solution For a Semi-Infinite Sample with a Constant Surface Composition

If the surface concentration of an initially solute-free specimen is maintained at some composition C_1 for all t>0 values, solute diffuses into the specimen and,

$$C(y,0) = C_M, \quad (2\text{-}10)$$

$$C(0,t) = C_1, \quad (2\text{-}11)$$

and the solute concentration in the specimen is:

$$C(y,t) = C_1+(C_M-C_1)erf\left(\frac{y}{\sqrt{4Dt}}\right). \quad (2\text{-}12)$$

The rate at which diffusant enters the specimen is given by the relation:

$$\left(D\frac{\partial C}{\partial y}\right)_{y=0}=\frac{D(C_M-C_1)}{\sqrt{\pi Dt}}. \quad (2\text{-}13)$$

The total amount M_t of diffusing substance, which has entered the medium at time t, is found by integrating the above equation with respect to t,

$$M_t = 2(C_1 - C_M)\sqrt{\frac{Dt}{\pi}}. \qquad (2\text{-}14)$$

2.3. Finite Difference Method

The analytical methods and solutions of diffusion equations are, for the most part, restricted to simple geometries, to simple initial and boundary conditions and to constant diffusion coefficients. In other words, it is either very difficult or impossible to obtain closed-form analytical solutions in most situations. However, numerical methods generally provide adequate numerical solutions more simply and efficiently. For this reason, numerical modelling is recognized as an essential tool that complements both analytical theory and experimental results in many branches of science and engineering (see Fig. 2-5).

Of the various numerical approaches, the finite difference method is by far the simplest to implement [Allen et al, 1988] and is employed in the present thesis. In the finite-difference method, the continuous derivatives in the partial differential equations are replaced by finite difference approximations at the grid-points and boundary points in the solute domain. This produces a set of algebraic equations which are solved using a computer.

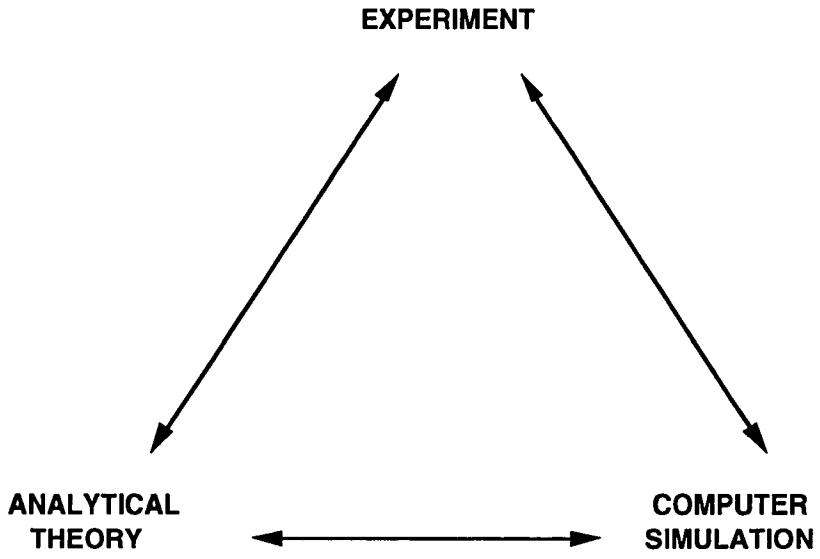

Fig. 2-5 Schematic illustrating of the roles of analytical theory, numerical simulation and experimental testing: the computer simulation can either be compared directly with a theory (to test the accuracy of the mathematical approximation) or with the experiment results (to test whether a model faithfully describes a real system), (after Binder, 1992).

2.3.1 Consistency, Stability and Convergence [Noye, 1982]

A finite difference equation is said to be *consistent* with a partial differential equation if, in the limit when the grid spacing tends to zero, the finite difference equation becomes the same as the partial differential equation at each point in the solution domain. The consistency is related to truncation errors, which are the differences

between the partial differential equation and its approximating finite difference equation. This can be easily evaluated using Taylor series expansion.

A set of finite difference equations is said to be *stable* if the cumulative effect of all the rounding-off errors is negligible. Therefore, the stability of a finite difference equation is concerned with the growth or decay of errors produced in the finite difference solution by the arithmetic operations. This stability depends on all the rounding-off errors introduced during the computation. Von Neumann's method [Noye, 1982] is often used in stability analyses, but is only really applicable to linear systems that have constant coefficients.

The solution of a finite difference equation, that approximates any given partial differential equation, is said to be *convergent* if, at each grid point in the solution domain, the finite difference solution approaches the solution of the partial differential equation (when the grid spacing tends to zero). The difference between the true solution of the partial differential equation and the exact solution of the approximating finite difference equation is called the discretization error. In general, the problem of convergence is a difficult one to investigate effectively. Fortunately, the convergence of the difference equations that approximate linear parabolic differential equations can be investigated using Lax's "equivalence theorem" [described in the paper by Lax and Richtmyer, 1956]. Lax's theorem states: "Given a properly posed linear initial value problem and a finite difference

approximation to it, that satisfies the consistency condition, stability is the necessary and sufficient condition for convergence."

2.3.2 Various Finite Difference Schemes [Allen et al, 1988]

Taking a one-dimensional diffusion problem as an example:

$$\frac{\partial C}{\partial t} = D\frac{\partial^2 C}{\partial y^2}. \tag{2-15}$$

A weighted average approximation for the above equation at (j,t+Δt) grid-point, is given by:

$$\frac{C_j^{t+\Delta t} - C_j^t}{\Delta t} = D\left(\theta\frac{C_{j+1}^{t+\Delta t} - 2C_j^{t+\Delta t} + C_{j-1}^{t+\Delta t}}{(\Delta y)^2} + (1-\theta)\frac{C_{j+1}^{t} - 2C_j^{t} + C_{j-1}^{t}}{(\Delta y)^2}\right), \tag{2-16}$$

where θ is a weighted constant, and the solution is unconditionally stable and convergent when $\frac{1}{2} \le \theta \le 1$. For $1 \le \theta < \frac{1}{2}$, we must employ the stability criterion:

$$\frac{D\Delta t}{(\Delta y)^2} \le \frac{1}{2(1-2\theta)}. \tag{2-17}$$

When θ = 0, Eq. (2-16) is an explicit scheme and its truncation error is $O(\Delta t + \Delta y^2)$. When θ = 1, Eq. (2-16) is an implicit scheme and its truncation error is $O(\Delta t + \Delta y^2)$. When θ = 0.5, this is the Crank-Nicolson scheme [Crank, 1975] and its truncation error is $O(\Delta t^2 + \Delta y^2)$. When the θ value is $\frac{1}{2} - \frac{(\Delta y)^2}{12D\Delta t}$, truncation error is $O(\Delta t^2 + \Delta y^4)$ and the solution is

also stable [Richtmyer, 1957].

It is necessary to point out that the economy of any particular numerical scheme must always be considered. Therefore, there is always a compromise between computational accuracy and economy.

2.4. Moving Interface Problems

2.4.1. Definition

Mathematically, the problem of diffusion-controlled growth or dissolution of an unstable phase is called a *Moving Boundary Problem* or *Stefan problem*, a reference to the early work of J. Stefan who, around 1890, was interested in the melting of the polar ice cap. In the present thesis the interface between phases is distinguished from a grain boundary region, by referring to it as a *moving interface*, not a moving boundary.

Consider one-dimensional melting of ice, where the ice sheet has length L and an initial temperature below the melting temperature. When the surface of the ice sheet is raised at time t=0 to a temperature above zero Celsius, melting occurs and the interface moves from the the surface into the sheet. This interface separates a region of water from one of ice at zero Celsius (see Fig. 2-6). Heat flow occurs in both the water and ice phases. The problem involves finding the temperature distribution in the water, $T_I(y,t)$, and in the ice, $T_{II}(y,t)$, and the position of the water phase, Y(t), at time t, where y is the space coordinate measured from the outer surface of the sheet

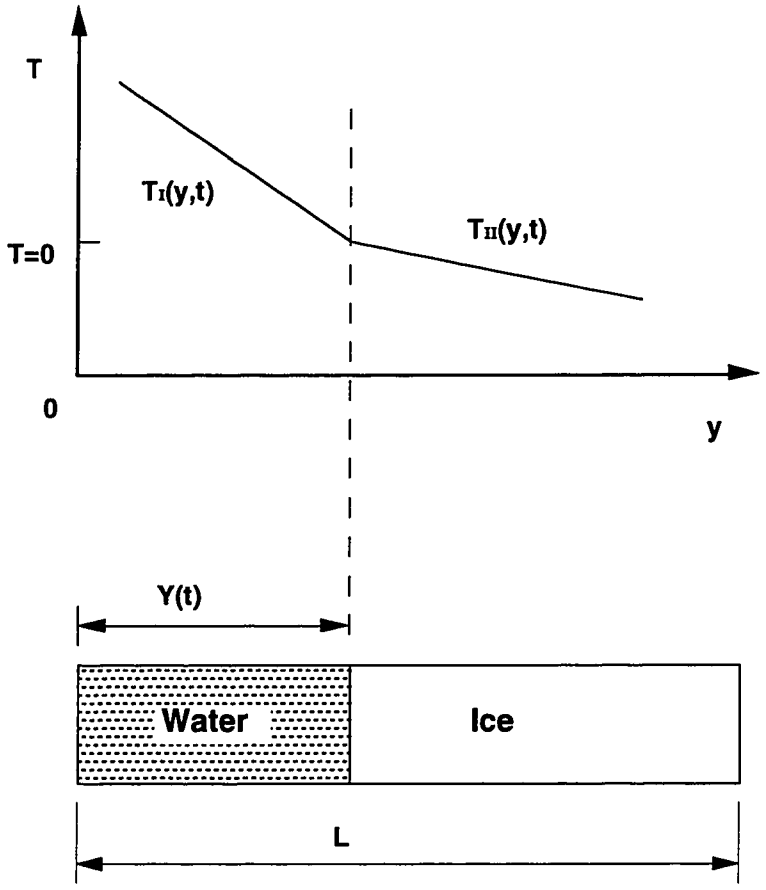

Fig. 2-6 Schematic of one-dimensional melting ice problem.

(y=0). In this situation,

$$c_i\rho_i\frac{\partial T_i}{\partial t} = K_i\frac{\partial^2 T_i}{\partial y^2}, \qquad i=I, II \qquad (2\text{-}18)$$

where c is the specific heat, ρ is the density, K is the heat conductivity, i=I refers to the water phase $0 < y < Y(t)$, and i=II refers to the ice phase $Y(t) < y < L$ (see Fig. 2-6). If ice and water have the same density ρ, the Stefan conditions at the interface are:

$$T_I(Y(t),t)=T_{II}(Y(t),t)=T_m=0, \tag{2-19}$$

and,

$$K_I\left(\frac{\partial T_{II}}{\partial y}\right)_{y=Y(t)} - K_{II}\left(\frac{\partial T_I}{\partial y}\right)_{y=Y(t)} = L_h\rho\frac{dY}{dt}. \tag{2-20}$$

where T_m is the melting point of ice and L_h is the latent heat of fusion.

Therefore, *moving interface problems* may be defined as time-dependent initial value problems, where parabolic partial differential equations with initial and boundary conditions, must be solved in a time-dependent space domain that has moving interfaces [Crank, 1985]. The rate of interface movement can be calculated from a flux balance equation at the moving interface, and this is sometimes called the Stefan condition. Moving interface problems are difficult to solve since the location of the moving interface is not known *a priori* and must be found as part of the problem solution.

2.4.2. Solutions for Moving Interface Problems

Moving interface problems occur in many branches of science and

engineering and have been a popular research area in recent years. Research to-date on moving interface problems in metallurgical processing has mainly been concerned with the diffusion and heat flow aspects of phase transformations or chemical reactions (also see §2.1). Moving interface problems have been tackled by a broad spectrum of researchers: engineers tackling practical problems, numerical analysts producing suitable numerical algorithms, and pure mathematicians deciding that the solutions to specific problems exist. Although many analytical and numerical solutions are available [Rubinstein, 1971 and Crank, 1984], very few analytical solutions are available in the closed form. Because of this, recent research has emphasized the development of numerical solutions, especially use of the finite difference method. In this connection, Fig. 2-7 shows some of the finite difference methods employed when solving moving interface problems. It is beyond the scope of this thesis to discuss this bulk of research in detail and the reader should consult the excellent review by Crank [1984]. The present thesis will emphasize the results of research on moving interface problems in the metallurgical field and apply existing mathematical principles and numerical algorithms during the solution of diffusion-controlled, two-phase moving interface problems.

2.4.2.1. Analytical Solutions

Typical analytical solutions can be found in texts such as *Diffusion in Solids, Liquids, Gases* by W. Jost [1960]. In addition, an

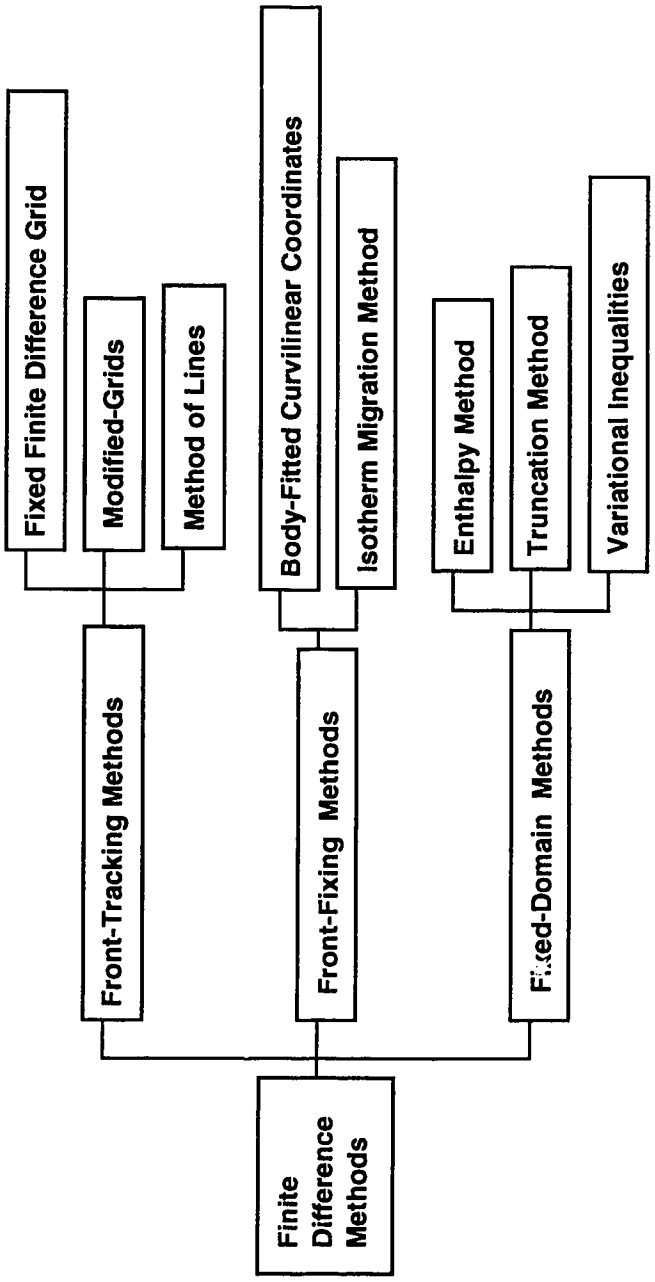

Fig. 2-7 Various finite difference methods for moving interface problems.

extensive review concerning diffusion-controlled moving interface problems and their analytical solutions has been presented by Sekerka et al [1975]. However, the available analytical solutions involve one-dimensional cases of an infinite or semi-infinite region, that have simple initial and boundary conditions, and constant thermal and diffusion properties. Analytical solutions for the moving interface generally take the form of functions of the single variable $x/\sqrt{t}$. These solutions are known as similarity solutions (they have been sometimes been termed square-root relations or parabolic law relations in the metallurgical field). Danckwerts [1950] presented a general solution for unsteady-state linear heat conduction or diffusion problems. In Danckwerts' paper, it was assumed that two phases meet at the moving interface Y(t) for semi-infinite media (see Fig. 2-8),

$$\frac{\partial C_I(y,t)}{\partial t} = D_I \frac{\partial^2 C_I(y,t)}{\partial y^2}, \qquad -\infty \le y \le Y(t) \qquad (2\text{-}21)$$

and,

$$\frac{\partial C_{II}(y,t)}{\partial t} = D_{II} \frac{\partial^2 C_{II}(y,t)}{\partial y^2}. \qquad Y(t) \le y \le \infty \qquad (2\text{-}22)$$

When the error function solution is applied to each phase,

$$C_I(y,t) = A_1 + A_2 \operatorname{erf}\left(\frac{y}{2\sqrt{D_I t}}\right), \qquad (2\text{-}23)$$

and,

$$C_{II}(y,t) = A_3 + A_4 \operatorname{erf}\left(\frac{y}{2\sqrt{D_{II} t}}\right), \qquad (2\text{-}24)$$

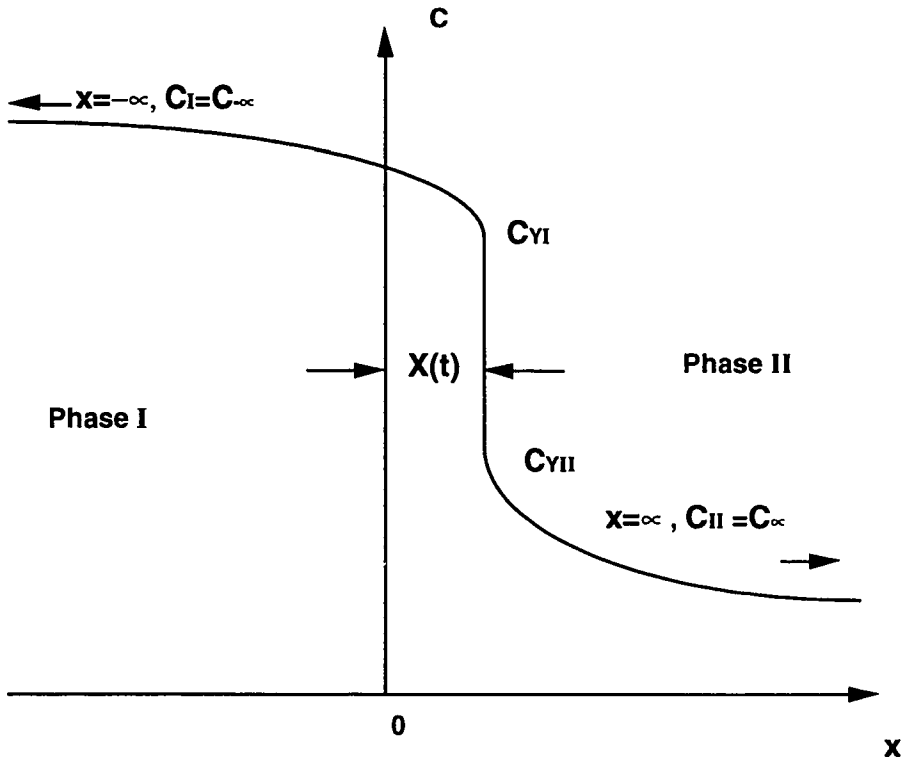

Fig. 2-8 A general model for a semi-infinite, diffusion-controlled, two-phase moving interface problem (after Danckwerts, 1950).

where A_1, A_2, A_3, and A_4 are constants. Using the appropriate boundary conditions, we obtain,

$$C_I(-\infty,t) = A_1 - A_2 = C_{-\infty}, \qquad (2\text{-}25)$$

and,

$$C_{II}(\infty,t) = A_3 + A_4 = C_\infty. \tag{2-26}$$

At the moving interface, we have:

$$C_I(Y,t) = A_1 + A_2\,\mathrm{erf}\left(\frac{Y}{2\sqrt{D_I t}}\right) = C_{YI}, \tag{2-27}$$

and,

$$C_{II}(Y,t) = A_3 + A_4\,\mathrm{erf}\left(\frac{Y}{2\sqrt{D_{II} t}}\right) = C_{YII}. \tag{2-28}$$

Since Eqs. (2-27) and (2-28) must be satisfied for all values of t, Y must be proportional to $\sqrt{t}$, i.e.,

$$Y = 2\beta\sqrt{t}, \tag{2-29}$$

where β is a constant. Substituting Eqs. (2-23)-(2-29) in the equation governing interface movement,

$$(C_{YI}-C_{YII})\frac{dY(t)}{dt} = -D_I\left(\frac{\partial C_I(y,t)}{\partial y}\right)_{y=Y(t)} - D_{II}\left(\frac{\partial C_{II}(y,t)}{\partial y}\right)_{y=Y(t)}, \tag{2-30}$$

we can can derive,

$$(C_{YI}-C_{YII})\beta\sqrt{\pi} - \frac{\sqrt{D_I}(C_{-\infty}-C_{YI})}{1+\mathrm{erf}\left(\frac{\beta}{\sqrt{D_I}}\right)}\exp\left(-\frac{\beta^2}{D_I}\right) + \frac{\sqrt{D_{II}}(C_{YII}-C_\infty)}{1-\mathrm{erf}\left(\frac{\beta}{\sqrt{D_{II}}}\right)}\exp\left(-\frac{\beta^2}{D_{II}}\right) = 0. \tag{2-31}$$

When β is calculated numerically using the above equation, Eq. (2-28) traces the movement of the interface. However, in practice, non-parabolic boundary motion will always arise when finite geometries and arbitrarily specified initial conditions are applied [Sekerka et al, 1975]. Numerical modelling is particularly effective when analyzing such situations [Crusius et al, 1992].

2.4.2.2. Numerical Solutions

Front-tracking methods are commonly applied when solving moving interface problems, with the position of the moving interface computed at each time step. Among them, the fixed-grid method is most basic and easiest to use. Another method -- the variable space grid method, first proposed by Murray and Landis, is very popular when modelling metallurgical processes [Crusius et al, 1992]. For example, Heckel and his co-workers [Tanzilli and Heckel, 1971; Lanam and Heckel, 1971; and Hickl and Heckel, 1975], in 1970's, examined many moving interface problems, e.g., solution treatment of α/β brass diffusion couples and aluminization of nickel alloys using the variable grid method. In addition, other approaches such as the enthalpy method and the isotherm migration method have been also applied to metallurgical problems [Crank, 1984].

Using the fixed space grid method, we can derive the numerical solution of a simple differential equation such as Eqs. (2-21) and (2-22) for points far from the moving interface. The interface will in general be between two grid points at any given time. However, special

formulae are needed to cope with terms such as $\frac{\partial T}{\partial y}$ and $\frac{\partial^2 T}{\partial y^2}$, as well as with the partial differential equation itself, in the neighborhood of the moving interface [Crank, 1984].

Consider the problem of ice melting as an example. It is assumed that, at any time t, the moving interface is located between two neighboring grid points, $n\Delta y$ and $(n+1)\Delta y$ (see Fig. 2-9). Using Lagrangian interpolation formulae, the discrete form of the derivatives will be [Crank, 1984]:

$$\left(\frac{\partial^2 T_I}{\partial y^2}\right)_{y=k\Delta x} = \frac{2}{(\Delta y)^2}\left\{\frac{T_{n-1}}{1+p} - \frac{T_n}{p} + \frac{T_m}{p(1+p)}\right\}, \tag{2-32}$$

$$\left(\frac{\partial T_I}{\partial y}\right)_{y=Y} = \frac{1}{\Delta y}\left\{\frac{pT_{n-1}}{1+p} - \frac{(1+p)T_n}{p} + \frac{(1+2p)T_m}{p(1+p)}\right\}. \tag{2-33}$$

for $y < Y(t)$, and

$$\left(\frac{\partial^2 T_{II}}{\partial y^2}\right)_{y=k\Delta x} = \frac{2}{(\Delta y)^2}\left\{\frac{T_m}{(1-p)(2-p)} - \frac{T_{n+1}}{(1-p)} + \frac{T_{n+2}}{(2-p)}\right\}, \tag{2-34}$$

$$\left(\frac{\partial T_{II}}{\partial y}\right)_{y=Y} = \frac{1}{\Delta y}\left\{\frac{(2p-3)T_m}{(1-p)(2-p)} + \frac{(2-p)T_{n+1}}{(1-p)} - \frac{(1-p)T_{n+2}}{(2-p)}\right\}, \tag{2-35}$$

for $y > Y(t)$. However, Eqs. (2-32) and (2-33) have singularities at $p = 0$ in Eq. (2-32) and $p = 1$ in Eq. (2-33). Difficulties with the above treatment will be compounded when implicit finite difference formulae are used. For example, Crank [1984] pointed out that, since the moving

interface is not known at the new time, some iteration procedure is usually inevitable.

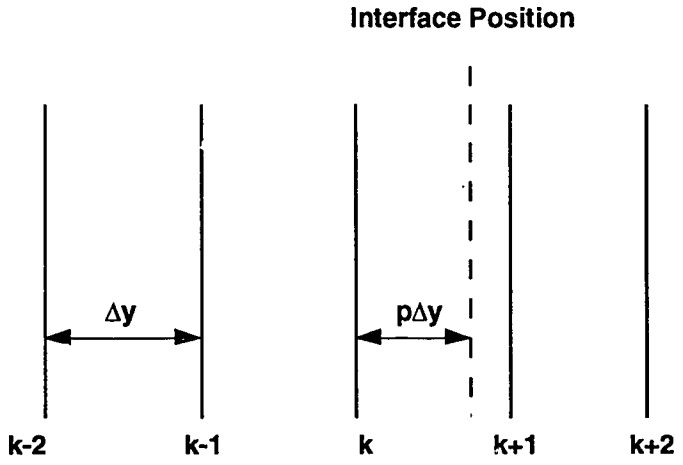

Fig. 2-9 Fixed-grid method (after Crank, 1984).

In the Murray and Landis method, the number of space intervals in each phase is constant throughout (Fig. 2-10). It is assumed that the water region ($y < Y(t) = \varepsilon$) is divided into r equally-sized space increments of thickness, $\Delta y_1 = \varepsilon/r$, that increase in size as the interface progresses. Similarly, the ice region ($y>\varepsilon$) is also divided into N-r equally-spaced intervals of thickness, $\Delta y_2 = (E-\varepsilon)/(N-r)$, which shrink with time. This situation is illustrated in Fig. 2-10 for the space case of N=2r=8 network intervals.

The Murray and Landis method focuses attention on the substantial temperature-time derivative of each internal point, given by,

$$\left(\frac{dT_I}{dt}\right)_j=\left(\frac{\partial T_I}{\partial y}\right)_j\frac{dy}{dt}+\left(\frac{\partial T_I}{\partial t}\right)_j, \qquad (2\text{-}36)$$

where the rate of travel of each point is related to the interface velocity in the water by,

$$\left(\frac{dy/dt}{y}\right)_j=\frac{d\varepsilon/dt}{\varepsilon}, \qquad (2\text{-}37)$$

for a uniform water grid spacing.

Combination of Eq. (2-36) with Eq. (2-37) leads to:

$$c_I\rho_I\left(\frac{dT_I}{dt}\right)_j=c_I\rho_I\frac{y_j}{\varepsilon}\left(\frac{\partial T_I}{\partial y}\right)_j\frac{d\varepsilon}{dt}+K_I\left(\frac{\partial^2 T_I}{\partial y^2}\right)_j, \qquad (2\text{-}38)$$

in the water region (for the network points j=1,2...(r-1)). The corresponding equation in the ice region is:

$$c_{II}\rho_{II}\left(\frac{dT_{II}}{dt}\right)_j=c_{II}\rho_{II}\frac{E-y_j}{E-\varepsilon}\left(\frac{\partial T_{II}}{\partial y}\right)_j\frac{d\varepsilon}{dt}+K_{II}\left(\frac{\partial^2 T_{II}}{\partial y^2}\right)_j, \qquad (2\text{-}39)$$

for j=r+1, r+2,..., N-1. At the interface point ε, these equations are

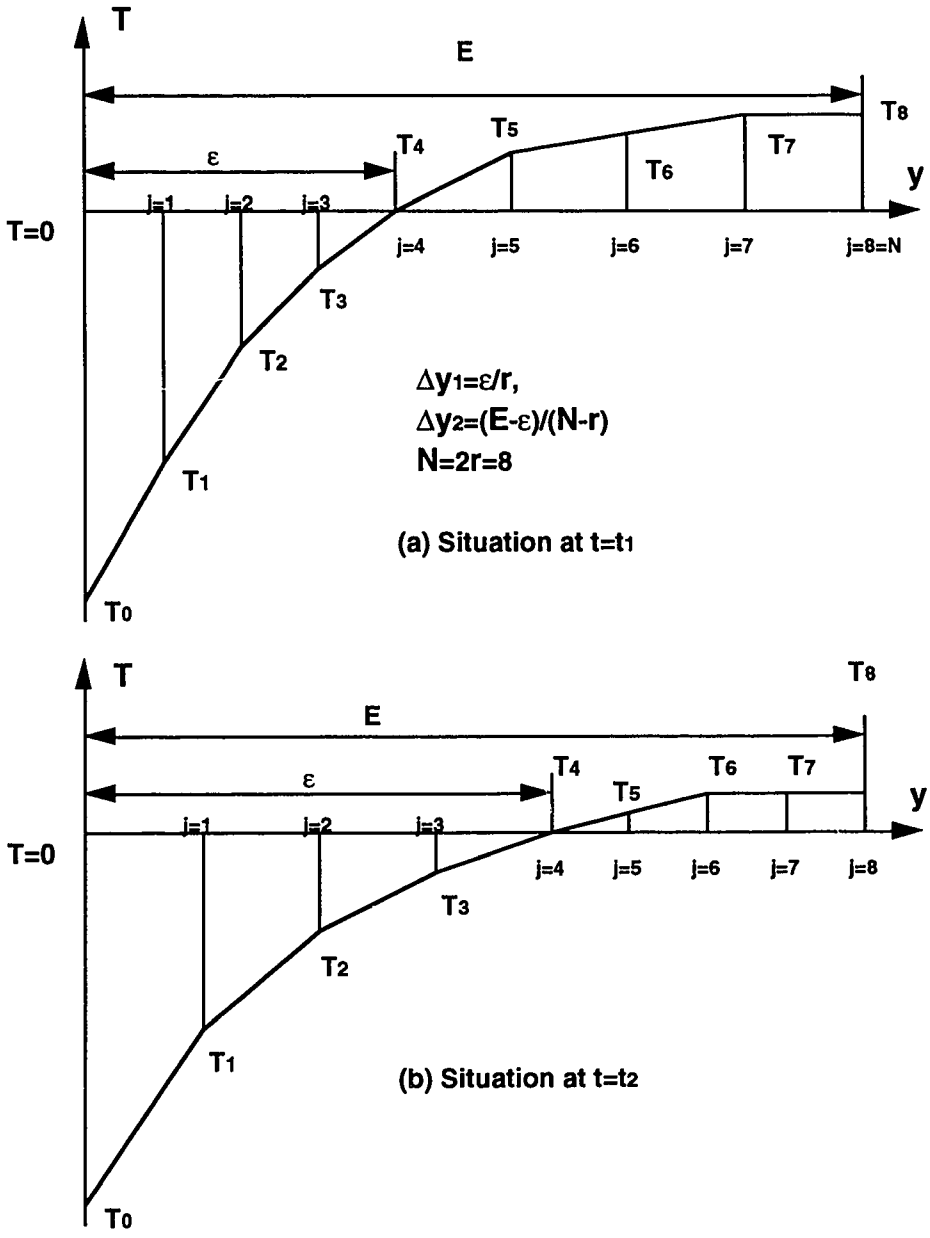

Fig. 2-10 Variable space-grid method (after Murray and Landis, 1959).

again coupled via Eq. (2-20), i.e.,

$$L\rho\frac{d\varepsilon}{dt}=K_I r\frac{T_{r-2}-4T_{r-1}}{2\varepsilon}+K_{II}(N-r)\frac{T_{r+2}-4T_{r+1}}{2(E-\varepsilon)}. \qquad (2\text{-}40)$$

2.4.2.3. Two or Three-Dimensional Moving Interface Problems

The complexity of moving interface problems for more than one space dimension, increases by several orders of magnitude [Fox, 1975]. In a monumental study, Lazaridis [1970] used an explicit finite-difference approximation with a fixed grid to solve two-phase solidification problems in both two- and three-space dimensions. He outlined the derivation of his equations for the two-dimensional case only and referred to his thesis [1969] for details and for the development of the three-dimensional relationships. The main problem occurred when the moving interface was very close to a grid point. Localized quadratic temperature profiles were used to avoid these singularity problems. Lazaridis' manipulation is very complicated indeed, in spite of the fact that he only considered explicit finite-difference methods [Fox, 1975].

The interface (Stefan) condition during melting and solidification problems can be expressed, in three-dimensional space, based on the energy balance at the interface [Carlaw and Jaeger, 1959],

$$T_I(x,y,z,t)=T_{II}(x,y,z,t)=T_m=0, \qquad (2\text{-}41)$$

and,

$$K_{II}\frac{\partial T_{II}}{\partial n} - K_I\frac{\partial T_I}{\partial n} = L\rho v_n, \qquad (2\text{-}42)$$

where n is outward normal to the interface (i.e. into the liquid), and v_n is velocity of the interface in the normal direction. The interface position is defined by the equation,

$$f(x,y,z,t)=0. \qquad (2\text{-}43)$$

A more usable form of Eq. (2-42) was derived by Patel [1968] as,

$$\left\{1+\left(\frac{ds}{dx}\right)^2+\left(\frac{ds}{dy}\right)^2\right\}\left\{K_{II}\left(\frac{\partial T_{II}}{\partial z}\right) - K_I\left(\frac{\partial T_I}{\partial z}\right)\right\} = L\rho\frac{ds}{dt}, \quad z=s(x,y,t) \qquad (2\text{-}44)$$

This relationship is explicitly linked with the derivatives of the moving interface f(x,y,z,t)=0, written as z=s(x,y,t).

2.4.3. Summary

Numerical methods are more suitable than analytical methods when handling practical moving interface problems. Using Murray and Landis's [1959] variable space grid method, the grid increment changes when the interface moves and the number of space intervals in each phase is constant. It appears that this method is not satisfactory in the situations where one phase changes markedly in dimensions. For example, the liquid phase changes from its maximum width to zero width during TLP-bonding and this situation will produce unsatisfactory calculation accuracy for the flux terms in Eq. (2-40)

(also see the analysis by Pabi [1979]). Using the fixed space grid method, the major problem occurs in applying the implicit finite difference scheme. Also special formulae are needed to deal with the singularity problems that occur in Eqs. (2-32)-(2-35).

2.5. Grain Boundary Diffusion

Since the process kinetics in two-phase diffusion-controlled problems are diffusion-controlled, all the factors affecting the diffusion process will affect process kinetics. It follows that the process kinetics of two-phase diffusion-controlled problems will be greatly affected when grain boundary diffusion enhances solute transfer.

A number of detailed reviews have been published concerning grain boundary diffusion, e.g., by Aust and Chalmers [1970] on the structure of grain boundaries and by Peterson [1983] on the mechanisms of grain boundary diffusion. Also, mathematical analyses of grain boundary diffusion have been discussed in the review paper by Gupta et al [1975]. As a result, only the literature directly appropriate to the present study will be reviewed.

2.5.1. Grain Boundary Diffusion Model and Basic Equations

The general approach in grain boundary diffusion involves use of the so-called uniform slab model. This was first proposed by Fisher [1951] and assumed that the grain boundary region is an isotropic slab of material of uniform thickness within which diffusion occurs

according to Fick's laws. The atomistic description of grain boundary diffusion is detailed in the paper by Benoist and Martin [1975]; this sheds some light on the physical meaning of the grain boundary thickness introduced in the slab model.

The grain boundary slab model has very simple geometry, where one isolated grain boundary (the bicrystal situation) or parallel grain boundaries (the polycrystal situation) is assumed perpendicular to the free surface (see Fig. 2-11). It is assumed that the concentration variation across the grain boundary slab (in the x-direction) can be neglected and the diffusivity along the grain boundary is much larger than the diffusivity in the lattice [Fisher, 1951 and Whipple, 1954]. The following mass balance equations are obtained,

$$\frac{\partial C}{\partial t} = D_l\left(\frac{\partial^2 C}{\partial x^2} + \frac{\partial^2 C}{\partial y^2}\right), \qquad |x| > \frac{\delta}{2} \tag{2-45}$$

in the bulk material, and ,

$$\frac{\partial C_{gb}}{\partial t} = D_{gb}\frac{\partial^2 C_{gb}}{\partial y^2} + \frac{2D_l}{\delta}\left(\frac{\partial C}{\partial x}\right)_{x=+\delta}, \qquad |x| < \frac{\delta}{2} \tag{2-46}$$

at the grain boundary region, where, C and C_{gb} are the solute concentrations, D_l and D_{gb} are the diffusion coefficients in the bulk material and in the grain boundary slab and δ is thickness of the grain boundary slab. Eq. (2-46) indicates that the change in the average concentration inside the grain boundary slab results from the divergence of the flux along the grain boundary (the first term) and

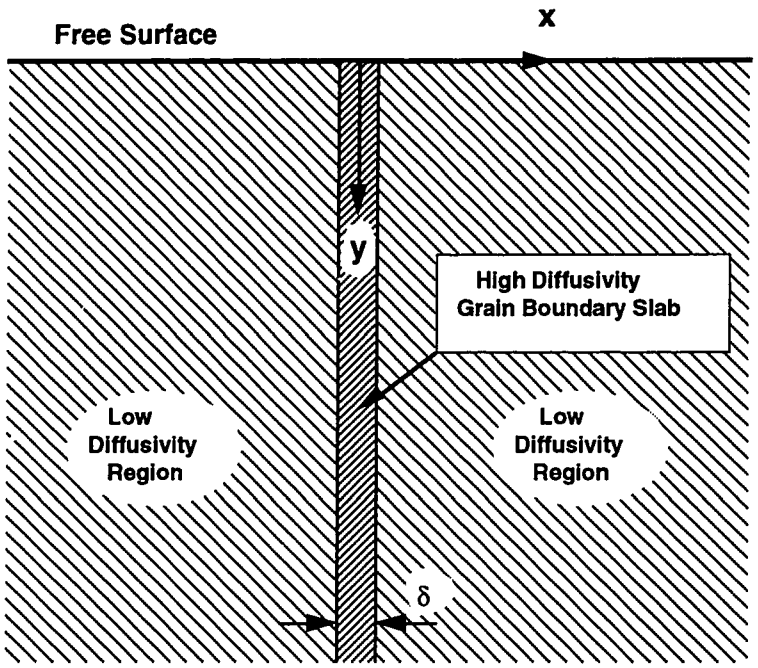

Fig. 2-11 Schematic showing a grain boundary slab of thickness δ (after Fisher, 1951).

from the exchange between the grain boundary and the lattice across the interface at $|x|= \frac{\delta}{2}$.

The continuity conditions at the interface between the lattice and the grain boundary require [Peterson, 1983],

$$C_{gb} = sC, \qquad |x|= \frac{\delta}{2} \tag{2-47}$$

where,

s=1, for self-diffusion in a pure material

$s=s_{eq}$, for dilute impurity diffusion and s_{eq} is the grain boundary segregation factor [Gibbs, 1966].

$s=C'_A/C_A$ for grain boundary self-diffusion in a binary alloy (i.e., A* (or B*) for diffusion in AB solid solution) [Bernardini and Martin, 1976].

Therefore, rewriting Eq. (2-46) using Eq. (2-47):

$$\frac{\partial C}{\partial t} = D_{gb}\frac{\partial^2 C}{\partial y^2} + \frac{2D_l}{s\delta}\left(\frac{\partial C}{\partial x}\right)_{x=+\delta}, \qquad |x| = \frac{\delta}{2} \tag{2-48}$$

2.5.2. Solutions for an Isolated Grain Boundary

The first analysis of combined lattice and grain boundary diffusion was carried out by Fisher [1951] for a semi-infinite sample with a slab of grain boundary and an infinite source (at constant surface concentration). The most serious approximation in Fisher's solution was that the concentration C_{gb} within the G.B. changed so slowly with time t that the term $\frac{\partial C_{gb}}{\partial t}$ could be set equal to zero. Whipple [1954] solved this problem exactly using a Fourier-Laplace transformation approach. Suzuoka [1961] later solved the case for an instantaneous source (a finite surface source) condition utilizing Whipple's transformations to evaluate the complex inversion integral.

Although, in principle, the Whipple and Suzuoka analyses provide exact continuum model solutions, in practice many investigators continue to use Fisher's analysis because it is simpler to apply. Later,

papers by Le Claire [1963], Cannon and Stark [1969], and Suzuoka [1964] have clearly established the superiority of the Whipple and Suzuoka's solutions. They have also demonstrated the use of simple and accurate techniques for extracting the grain boundary diffusion coefiicient from experimental data. According to Le Claire [1963], the grain boundary diffusivity can be evaluated using the expression

$$sD_{gb}\delta=\left(\frac{\partial ln\ \bar{C}}{\partial y^{6/5}}\right)\left(\frac{4D_l}{t}\right)^{1/2}\left(\frac{\partial ln\ \bar{C}}{\partial[\eta(s\beta)^{-1/2}]^{6/5}}\right)^{5/3}, \qquad (2\text{-}49)$$

where, $\bar{C}$ is the concentration of the diffusant found using the sectioning method for determining the diffusivities, $\eta=\frac{y}{\sqrt{D_l t}}$ and $\beta=\frac{\delta}{2\sqrt{D_l t}}\left(\frac{D_{gb}}{D_l}-1\right)$. Levine and MacCallum [1960] have shown by numerical calculation that when $\beta>30$, the quantity $\frac{\partial ln\ \bar{C}}{\partial[\eta(s\beta)^{-1/2}]^{6/5}}$ is very nearly independent of $\eta(s\beta)^{-1/2}$ and converges to 0.78 (for an infinite source) and $0.72(s\beta)^{0.008}$ (for an instantaneous source), according to Le Claire [1963] and Suzuoka [1964]. This means that the shape of the overall concentration profile $\bar{C}(y,t)$ is almost independent of the source condition provided that β is sufficiently large.

The analyses of G.B. diffusion in semi-infinite bicrystals have been extended to the situation where the grain boundary moves in the direction parallel to the surface. [Glaeser and Evans, 1988, Mishin and Razumovskii,1992]. These results indicate that grain boundary migration affects the apparent grain boundary diffusion coefficient values derived when the results of diffusion experiments are evaluated

using conventional (stationary) grain boundary diffusion models. This conclusion is important when considering the problem whether the diffusivity along the moving grain boundaries is higher than that of the stationary grain boundaries [Hillert and Purdy, 1978; Smidoda et al, 1978; Gust et al, 1982 and Balluffi, 1982]. Mishin and Razumovskii [1992] indicated qualitatively that moving grain boundaries intensively absorb the diffusant and spread it in a relatively thin layer near the surface. This effect may greatly affect the process kinetics of two-phase diffusion problems.

2.5.3. Grain Boundary Diffusion in Polycrystals

Harrison [1961] defined three classes of grain boundary diffusion kinetics in polycrystalline materials; these depend on the relationship between the lattice diffusion distance ($\sqrt{D_l t}$) and the grain size (d) of the material considered (see Fig. 2-12). In Type A kinetics, the lattice diffusion distance is much larger than the grain size, diffusion fields at neighboring grain boundary regions overlap and each diffusing particle has entered, migrated or left a large number of grain boundaries. Based on generalized "random walk" considerations, Hart [1957] demonstrated the existence of an apparent diffusion coefficient, D_{app}, during Type A behavior. This apparent diffusion coefficient combines the lattice diffusivity with a term fD_{gb}, that accounts for the fraction of sites, f, associated with the grain boundaries:

$$D_{app} = D_l \left(1 + f \frac{D_{gb}}{D_l}\right) \qquad (2\text{-}50)$$

where D_l and D_{gb} are the diffusion coefficients in the bulk material and at the grain boundaries. Campbell [1974] analyzed grain boundary diffusion using Laplace-Fourier transformations for diffusion from an instantaneous source through multiple parallel grain boundaries and qualitatively related the resulting concentration profiles with the grain boundary spacing. His results showed that when the bulk penetration distance was much larger than the grain boundary spacing ($\sqrt{Dt}>>d$), the average concentration profile was typical of a homogeneous medium with a grain boundary diffusion coefficient equal to the apparent diffusion coefficient. Based on these results, Campbell [1974] suggested that Hart's relation was not an appropriate solution for Type A diffusion problems.

In Type B kinetics, the lattice diffusion distance is much less than the grain size and each grain boundary is assumed to be isolated. This is identical with the semi-infinite bicrystal situation modelled by Fisher [1951], Whipple [1954] and Suzuoka [1961]. An examination of the overall kinetics during an exchange experiment confirmed that there is no single apparent diffusion coefficient in Type B kinetics and the amount of material removed from the crystal at time t is proportional to $t^{3/4}$ [Lidiard and Tharmalingam, 1959].

In Type C behavior, there is negligible lattice diffusion, diffusion occurs only within the grain boundary region and different apparent diffusion coefficients may be calculated depending on the type of

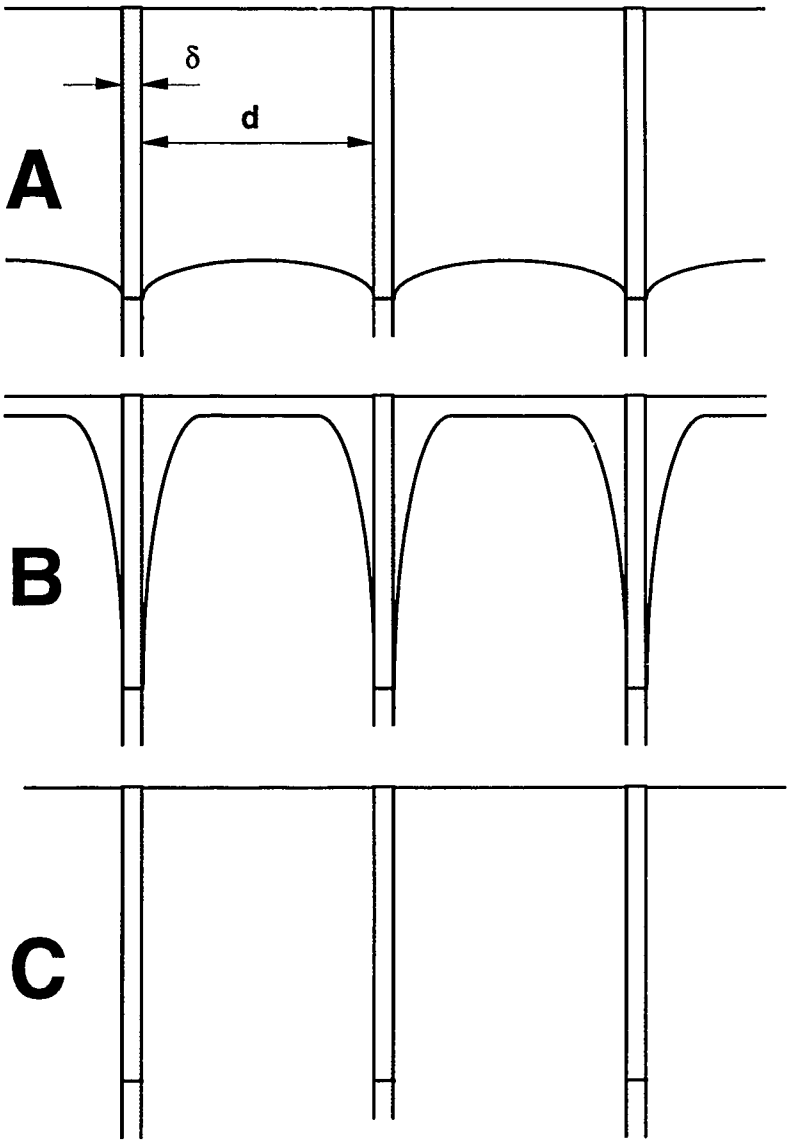

Fig. 2-12 Schematic representation of A-, B- and C-diffusion Kinetics. The vertical lines indicate grain boundaries and the curved lines are isoconcentration contours. The diffusion source coincides with the horizontal lines in each case (after Gupta et al, 1975).

experiment that is carried out [Harrison, 1961].

Cahn and Balluffi [1979] extended Harrison's classification of diffusion kinetics to allow for grain boundary migration. Fig. 2-13 defines diffusion in a number of regimes (V is the grain boundary migrating velocity) -- SID (stationary boundaries, isolated boundary diffusion, diffusion occurs in lattice), SIN (stationary boundaries, isolated boundary diffusion, no diffusion occurs in lattice), MID (migrating boundaries, isolated boundary diffusion, diffusion occurs in lattice), MIN (migrating boundaries, isolated boundary diffusion, no diffusion occurs in lattice) and SOMM (stationary or migrating boundaries, multiple boundary diffusion). Type A diffusion behavior occurs when $\sqrt{D_l t}$ or Vt exceeds the grain size, d. The Type B regime divides into distinct regimes depending on the velocity of the grain boundary. The Type C regime remains unchanged. Cermak [1990], using the finite element method, evaluated the dependence of the mean concentration of diffusant on the penetration depth. Near-surface enrichment of solute was also confirmed in Cermak's analysis, as Mishin et al [1992] had calculated. As pointed out early, this tendency will decrease the apparent diffusion coefficient D_{gb} value obtained using LeClaire's analysis. There is no difference between the apparent diffusion coefficient, D_{gb}, and the true diffusion coefficient values when $\sqrt{D_l t} > Vt$ [Cermak, 1990].

In practice, it is not always possible to maintain a semi-infinite thickness condition in comparison with the diffusant penetration

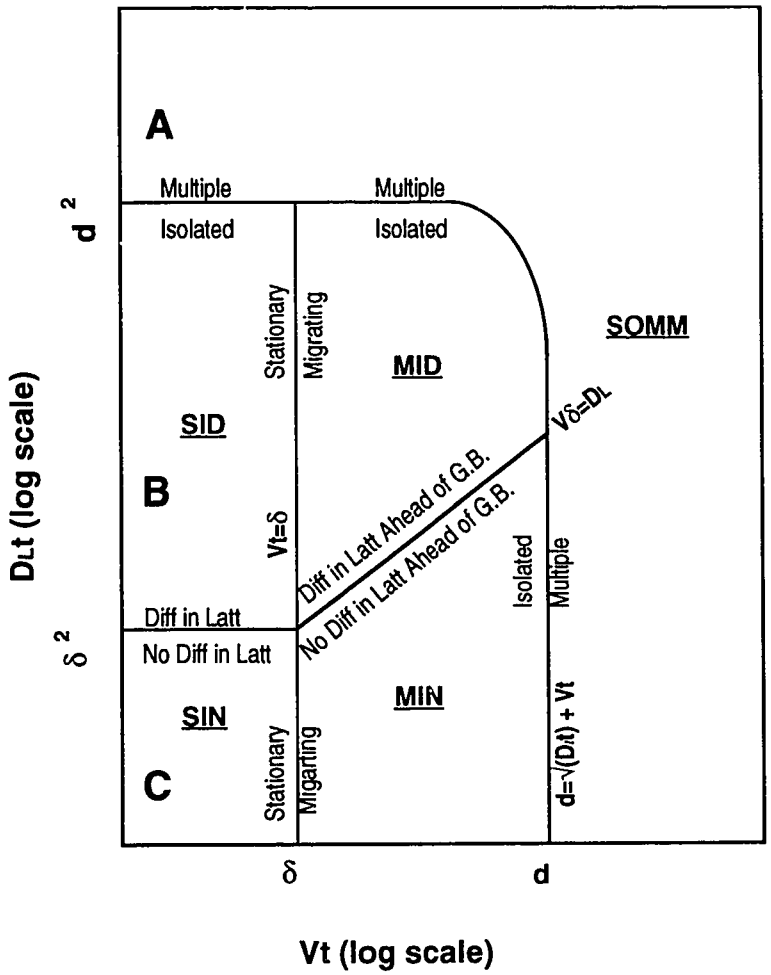

Fig. 2-13 Regimes of diffusional mass transport behavior expected for a polycrystal containing stationary or migrating boundaries (after Cahn and Balluffi,1979).

distance. Gilmer and Farrel [1976a, b] have shown that a correction must be made to account for the finite thickness of thin film

specimens. Physically, this means the diffusion field will be affected by the diffusion from the other surface of the thin film.

2.5.4. Summary

Grain boundary regions provide high diffusivity paths and grain boundary migration means that atoms have more chance to enter such regions. Consequently, both increased diffusivity at grain boundaries and grain boundary migration will affect the process kinetics during two-phase diffusion-controlled transformation. From the foregoing discussion, it is clear that the mathematical analyses of grain boundary diffusion differ depending on the grain size, the sample thickness, the velocity of grain boundary migration, and the contribution of lattice diffusion which is dictated by the processing temperature. Also, in practical situations, diffusion occurs over a wide range of time intervals, from very short to long holding periods. Consequently, when a two-phase diffusion-controlled problem is studied in a continuous manner, there will be a transition from initial Type C kinetics, through Type B behavior to Type A kinetics. It follows that analytical methods are incapable of handling practical situations. Numerical methods represent a more practical way of handling such problems, because they can readily accommodate a wide variety of boundary conditions and particularly, the transition regions between the Type C, B and A kinetic regimes.

2.6. Grain Boundary Grooving

It has been suggested that increasing interfacial area as a result of grain boundary grooving will enhance diffusion and consequently affect the process kinetics during two-phase diffusion-controlled transformation [Tuah-Poku et al, 1988 and Kokawa et al, 1992]. Modelling of the interface profile evolution and interface migration caused by grain boundary grooving are discussed below.

2.6.1 Dihedral Angle and Grain Boundary Grooving

Smith [1948] showed that when three different interfaces meet in a randomly-oriented polyphase alloy, they will take up positions in accordance with a simple surface tension equilibrium. The ratio of the sines of the angles between any two interfaces depend on the ratio of the interfacial free energies. In a two-phase alloy there will be grain intersections where two crystals of the same phase meet a different phase: this will produce two interphase boundaries (that are identical if orientation effects are neglected) and one single phase grain boundary (see Fig. 2-14). When this occurs the equilibrium angle (also called the *dihedral angle*) of the included phase is:

$$\theta = 2 \cos^{-1} \frac{\gamma_{\alpha\alpha}}{2\,\gamma_{\alpha\beta}}, \qquad (2\text{-}51)$$

where $\gamma_{\alpha\alpha}$ and $\gamma_{\alpha\beta}$ are the interfacial free energies of the monophase and duplex boundaries, respectively. The interfacial free energy depends on the crystallographic orientation in both solid-liquid and solid-solid systems [Basterfield, Miller and Weatherly, 1970]. Herring [1951]

generalized this interface equilibrium by considering interfaces that have direction-dependent energies and consequently torque terms.

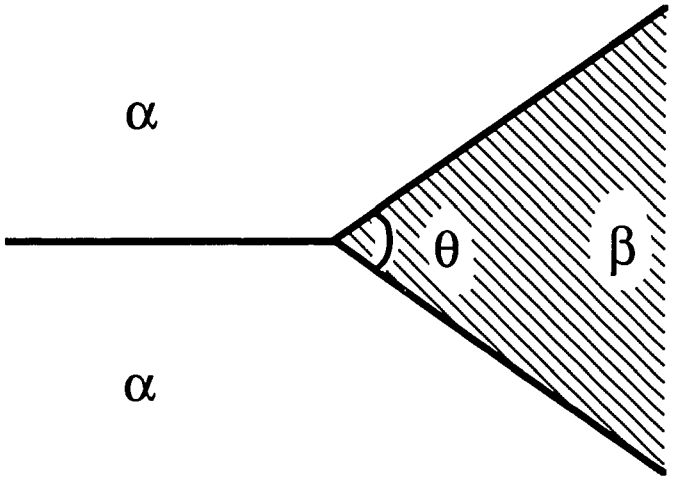

Fig. 2-14 Schematic showing dihedral angle or equilibrium angle (after Smith, 1949).

It follows that an initially flat interphase boundary will tend to form a groove at the line of intersection with a grain boundary (to establish the relation in Eq. (2-51)). The curvature of the groove profile will vary from point to point, and this will produce a difference in chemical potential along the interface. This gradient in chemical potential will drive atoms from a point of higher chemical potential to one of lower chemical potential so that the groove will deepen and widen with time [Mullins, 1957].

2.6.2. Mullins' Theory

Mullins theoretically analyzed the kinetics of grain boundary grooving when a bicrystal solid contacted a saturated fluid phase (liquid or gas) at sufficiently high temperature. Grooving occurred as a result of surface diffusion, volume diffusion in the fluid phase and evaporation-condensation [Mullins, 1957 and 1960]. In Mullins' model, the initial fluid-solid interface was flat, and the grain boundary region intersected the interface at right-angles (see Fig. 2-15). The principal assumptions in his analysis comprised,

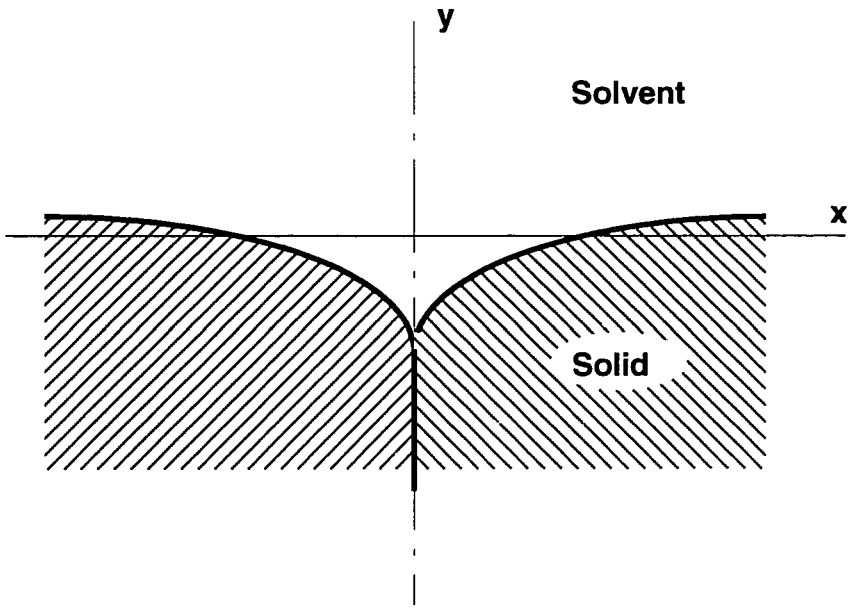

Fig. 2-15 Schematic of a grain boundary groove (after Mullins, 1959).

(1) the fluid-solid interfacial energy was independent of crystallographic orientation,
(2) the Gibbs-Thomson equation determined the relation between fluid-solid interfacial curvature and chemical potential,
(3) quasi-steady-state volume diffusion occurred in the fluid,
(4) the slope of the interface changed little from the initial interfac configuration, and
(5) there was negligible convection in the fluid.

In a gas-solid system, grain boundary grooving occurred due to a combination of interface diffusion and evaporation-condensation. In a liquid-solid system, grain boundary grooving occurred mainly due to volume diffusion in the saturated fluid.

2.6.2.1. Grooving as a Result of Volume Diffusion

Based on assumption (3), the concentration of solid element C(x,y,t) in the liquid satisiies the relation [Mullins, 1960]:

$$\nabla^2 C(x,y,t)=0. \tag{2-52}$$

Assumption (4) means that the interface can be represented as the plane y=0. From assumption (2), therefore, the boundary condition at the interface is given by the relation:

$$C(x,y,t)=C_0\left\{1+\frac{\gamma_{int}\Omega}{RT}K(x,t)\right\}, \tag{2-53}$$

where, C_0 is the concentration of solid element in the solvent phase in equilibrium with the flat interface, Ω is the atomic volume of the solid atom, γ_{int} is the interfacial energy of the solid surface, and K is the curvature of the interface (the concentrations of C and C_0 are expressed as the number of atoms per unit volume). The curvature K is given as:

$$K = \frac{\dfrac{\partial^2 Y}{\partial x^2}}{\left\{1 + \left(\dfrac{\partial Y}{\partial x}\right)^2\right\}^{3/2}}. \qquad (2\text{-}54)$$

Because of assumption (4) above, $\frac{\partial Y}{\partial x} << 1$ and K can be approximated by

$$K = \frac{\partial^2 Y}{\partial x^2}. \qquad (2\text{-}55)$$

Mullins [1960] evaluated the concentration distribution of C(x,y,t) by solving Eq.(2-52) using the boundary condition shown in Eq.(2-53).

If interdiffusion in the solid is negligible, the rate of migration of a segment of the interface depends on volume diffusion only in the solvent phase, namely,

$$\frac{\partial Y}{\partial t} = D\Omega\left(\frac{\partial C}{\partial y}\right)_{y=0}, \qquad (2\text{-}56)$$

where Y(x,t) is the y-coordinate at the interface and D is the interdiffusion coefficient in the liquid phase. Mullins differentiated Eq. (2-56) twice with respect to x to express this equation in terms of interface curvature,

$$\frac{\partial K}{\partial t} = D\Omega \frac{\partial^2}{\partial x^2}\left[\left(\frac{\partial C}{\partial y}\right)_{y=0}\right]. \qquad (2\text{-}57)$$

Substituting the concentration distribution C(x,y,t) that satisfies the boundary condition in Eq. (2-53) produces an integrodifferential equation for K(x,t). This equation was solved analytically, assuming that the the interface had a fixed slope at x=0, given by

$$\left(\frac{\partial Y}{\partial x}\right)_{x=0} = -\cos\theta. \qquad (2\text{-}58)$$

The dihedral angle is determined by the the well-known equation for the balance between the grain boundary energy γ_{gb} and the interfacial energy γ_{int} (also see §2.6.1.),

$$\theta = 2\cos^{-1}\frac{\gamma_{gb}}{2\gamma_{int}}. \qquad (2\text{-}59)$$

Based on these calculations, Mullins found that the groove profile had a fixed shape and linear dimensions that were proportional to $t^{1/3}$.

2.6.2.2. Grooving as a Result of Surface Diffusion

If surface diffusion is the only process that operates, the chemical potential along the interface depends on the interface curvature [Mullins, 1957], i.e.,

$$\mu(K)=K\gamma_{int}\Omega. \tag{2-60}$$

This chemical potential gradient will produce a drift of interface atoms with an average velocity given by the Nernst-Einstein relation:

$$V= - \frac{D}{kT}\frac{\partial \mu}{\partial s}=- \frac{D\gamma_{sur}\Omega}{kT}\frac{\partial K}{\partial s}, \tag{2-61}$$

where D is the coefficient of interface diffusion and s the arc length along the groove profile. The surface current J of atoms is the product of V by the atoms per unit area ν,

$$J=- \frac{D\gamma_{sur}\Omega\nu}{kT}\frac{\partial K}{\partial s}. \tag{2-62}$$

If the surface divergence of -J is evaluated, this represents the increase in the number of atoms per unit area per unit time. This can be converted to the speed of movement r_n of the interface element along its normal away from its center of curvature, by multiplying by Ω,

$$r_n= \frac{D\gamma_{int}\Omega^2\nu}{kT}\frac{\partial^2 K}{\partial s^2}. \tag{2-63}$$

This equation can be expressed in terms of y(x,t) by substituting for r and K according to the expressions,

$$r_n = \left\{1+\left(\frac{\partial Y}{\partial t}\right)^2\right\}^{-1/2} \frac{\partial Y}{\partial t'} \tag{2-64}$$

and $\frac{\partial}{\partial s} = \frac{\partial x}{\partial s}\frac{\partial}{\partial x}$. The result is,

$$\frac{\partial Y}{\partial t} = \frac{D\gamma_{int}\Omega^2\nu}{kT}\frac{\partial}{\partial x}\left\{(1+y'^2)^{-1/2}\frac{\partial}{\partial x}\left[\frac{y''}{(1+y'^2)^{3/2}}\right]\right\} \tag{2-65}$$

Using the small slope approximation, Eq. (2-65) becomes,

$$\frac{\partial Y}{\partial t} = \frac{D\gamma_{int}\Omega^2\nu}{kT} y''''. \tag{2-66}$$

The solution of the above equation produces the same conclusion as that when the volume diffusion is the only operating mechanism, except that the linear dimension is proportional to $t^{1/4}$. In the same paper [Mullins, 1957], it is also shown that the linear dimension is proportional to $t^{1/2}$, when the groove forms only under the action of an evaporation-condensation mechanism.

Clearly, Mullins' theories are extensions of Herring's [1950] early work which demonstrated by dimensional analysis that the quasi-steady state change in the dimensions of a small particle during sintering were proportional to t, $t^{1/2}$,$t^{1/3}$ and $t^{1/4}$ respectively for

viscous flow, evaporation-condensation, volume diffusion and surface diffusion mechanisms. Gjostein [1961] and Robertson [1965] examined grain boundary grooving in a copper/liquid lead system and confirmed Mullins' predictions. Similar results were produced when researching in chromium, molybdenum, and tungsten alloyed with rhenium [Allen, 1966].

Later, Mullins [1958] discussed the effect of thermal grooving on grain boundary motion and indicated that thermal grooves could pin grain boundaries at the surface and prevent their migration. However, Allen's [1982] analysis confirmed that this occurs only when the rate of grain boundary migration is slow. When the grain boundary migrates quickly, the grain boundary and its groove can move together along the surface.

2.6.3. Recent Developments

Ho and Weatherly [1975] applied Mullins' theory for interface migration by surface diffusion to the case of annealing an Al-$CuAl_2$ eutectic alloy. They measured the rate of migration of a triple junction formed between a grain boundary in Al and the Al-$CuAl_2$ interface. This is a solid-solid analogue of grain boundary grooving in solid-fluid systems. Since their experiment results accurately matched Mullins' predictions, this means that interface diffusion has a dominant effect on the evolution of the "groove". Ho and Weatherly [1975] also developed a theoretical model for interface migration by simultaneous interface and volume diffusion.

Robertson [1971] extended Mullins' analysis of grain boundary grooving by surface diffusion to the case where the groove slope ranged from 0 to 4 and Mullins' small slope approximation was not valid. His results showed that the groove width is within five percent of the small-slope groove width for all calculated groove root slopes but the groove depth departs by more than ten percent from the small-slope depth for groove root slopes greater than about 0.7. Hardy et al [1991], recently, generalized Mullins' theory for grain boundary grooving as a result of volume diffusion to the entire range of dihedral angles, by using a boundary integral formulation of the associated free boundary problem.

Mullins' analyses have focussed exclusively on the semi-infinite case, where groove profiles at different grain boundaries do not interact; this is only valid in very large grain-sized materials. Hackeny and Ojard [1988] examined grain boundary grooving by evaporation or by surface diffusion in a finite system and found that the shape of the groove profile predicted using an infinite geometry solution was closely approximated in the early stages of groove formation. However, the groove profile attained a constant surface curvature after long holding times.

In Mullins' work [1957,1960], each transport process operated separately. However, in practice, a number of different factors will affect grain boundary grooving. Srinivasan and Trived [1973] developed

a theory for the growth of a grain boundary groove under the concomitant action of surface and volume diffusion mechanisms. They assumed that the surface diffusion mechanism predominated for short holding times, although the volume diffusion contribution to the transport of matter was not insignificant. On the other hand, the groove profile was completely determined by the volume diffusion mechanism for long holding times. The results of their model could be used to derive both the surface and volume diffusion coefficients from the experimental results.

Some other work worth reporting involves Binh et al's [1976] theoretical and experimental research on grain boundary groove evolution by surface self-diffusion on a planar surface and on a wire. In case of a wire, they found that (1) there was non-steady state evolution of the groove profile, and (2) the mean groove angle was not constant, and varied with time. They assumed that the difficult-to-observe equilibrium angle remained constant. The "observable mean groove angle" is the slope angle that is measured at the bottom of the groove and this value will depend on the resolution of the measuring equipment.

2.6.4. Influence of Grain Boundary Diffusion

All the above theoretical investigations on grain boundary grooving are based on the assumption that the grain boundary does not play an important role in materials transport. Vogel and Ratke [1991], in their recent paper, combined volume diffusion in the melt and grain

boundary diffusion into one mathematical model to explain the deep, channel-like grooves formed at the grain boundary intersections with the solid-liquid interface (during isothermal annealing of Al-bicrystal couples in contact with an In-Al melt). Their model is an extension of Mullins' theory for grain boundary grooving via volume diffusion, with the addition of grain boundary diffusion. There are problems with their approach.

(1) When calculating the solute concentration in the liquid phase due to the grain boundary diffusion, they did not consider that the indium depletion in the liquid phase near the grain boundary caused the migration of the solid-liquid interface. Since the concentrations of the liquid and solid phases are in equilibrium and indium lowers the liquidus temperature of the aluminium solid, the solid-liquid interface will migrate in the direction of the bulk liquid.

(2) They assumed that there was negligible diffusional flow in the solid, and this contradicts their initial assumption (that grain boundary diffusion was substantial).

(3) Their calculation violated the thermodynamic equilibrium condition at the solid-liquid interface; also, they extended the small slope approximation in Mullins' theory beyond its application limit.

It follows that the proposed explanations regarding the instability in the groove profile are doubtful. In this connection, the wetting transition phenomenon that the contact angle (dihedral angle) at the site of grain boundary intersection with the solid-liquid interface approaches zero when the temperature exceeds a critical

value is explained by the fact that the interfacial energy decreases faster than the grain boundary energy [Straumal et al, 1992]

2.6.5. Summary

The driving force for interface migration, according to classical grooving theory, comes from the interfacial curvature. It follows that a flat interface that has no intersection with a grain boundary will not migrate. This is quite a different situation from moving interface problems in two-phase diffusion-controlled processes. The driving force for the interface migration in two-phase diffusion-controlled problems results from the concentration gradient in each phase and the interface will migrate even when the interface is flat and there is no grain boundary intersection (in single crystal situations). The materials transport mechanisms during two-phase diffusion-controlled processes include volume diffusion in each phase, interfacial diffusion and grain boundary diffusion.

Extremely complicated analytical solutions have been derived to understand grain boundary grooving. These derivations are difficult to apply in complex situations, where several diffusion mechanisms operate and where finite geometries apply. As a result, a new numerical model is required for the interface migration under the combined driving forces of concentration and interfacial curvature gradients.

2.7. Modelling of TLP-bonding

Mathematical modelling of process kinetics during Transient Liquid Phase (TLP) bonding is an effective way of selecting optimized joining parameters (filler metal composition and thickness, bonding temperature and holding time) prior to actual bonding trials.

2.7.1. Analytical Solutions

Various attempts have been made to model TLP-bonding. These approaches have generally been based on deriving analytical solutions for each individual stage of the bonding process. It has been tacitly assumed that the results of any stage do not affect the operating condition in any subsequent stage of the TLP-bonding process.

2.7.1.1. Heating Stage

Eq. (2-14) was used by Niemann & Garrett [1974] to calculate the loss of the copper from a Cu electroplated layer (the filler metal) during the heating cycle from room temperature to the bonding temperature during TLP-bonding of an Al-B composite material,

$$x\rho_c = 1.1284\ \rho_a(C_{\alpha s}-C_M)\sqrt{D_S t}\,. \qquad (2\text{-}67)$$

where, x is thickness of coating lost through diffusion, ρ_c is the density of copper, D_S is the diffusion coefficient of Cu in Al, t is time, $C_{\alpha S}$ is solubility of Cu in aluminium, ρ_a is the density of the alloy and C_M is the initial copper concentration in aluminium. The calculation was carried out assuming constant $C_{\alpha s}$ and D values. However, both the diffusion coefficient and solid solubility limit increase with

temperature. Because of this, Macdonald & Eagar [1992] indicated that an effective diffusion coefficient, based on the work of Shewmon [1975], should be used. In fact, this diffusion problem can be easily solved using numerical techniques (see the paper by Li, Zhou and North, 1993).

2.7.1.2. Dissolution Stage

No analytical solution is available for stage II-1 (base metal dissolution during the heating cycle from the melting point of the filler metal to the bonding temperature (see §2-1) since the solute concentrations, $C_{L\alpha}$ and $C_{\alpha L}$, at the interface vary with temperature. Also, few analytical solutions exist indicating the process kinetics during stage II-2 of TLP-bonding (isothermal base metal dissolution).

Nakao et al [1988] developed a dissolution parameter when joining Ni superalloy base metal using Ni-B-Cr filler metal using the Nernst-Brunner equation:

$$C=C_{sat}\left\{1-\exp\left(-K\frac{A\,t}{V}\right)\right\}, \qquad (2\text{-}68)$$

where C and C_{sat} are the solute concentrations in the liquid and at saturation, K is the dissolution rate, V is the volume of the liquid and A is the area of the solid-liquid interface. However, Nakagawa et al [1992] argued that the Nernst-Brunner's assumption of a thin boundary layer and a large bulk liquid region is hardly applicable during TLP-

bonding. They also pointed out that solute diffusion in the base metal was neglected in Nakao et al's approach.

Lesoult [1976], according to Tuah-Poku et al [1988], used a square-root law solution to estimate the time for interlayer melting during TLP-bonding (for a binary eutectic alloy TLP-bonded using a single element filler metal). However, the assumption that the width of the liquid zone equals the width of the interlayer (when melting of the interlayer is completed) is not really what occurs, as Macdonald & Eagar [1992] pointed out. In fact, the base metal will dissolve when the interlayer melts (see §2.1 of this thesis). In this connection, Liu et al [1991] developed a model that accounts for base metal melt-back when the interlayer dissolves. They used a general error function solution to describe the solute distribution in the liquid zone, when modelling stage II-2a (the dissolution stage when three metallurgical phases exist, see Section 2-1). They also assumed no solute diffusion in the base metal. However, these assumptions are questionable. The error function solution is really only applicable for infinite or semi-infinite mediums, and the liquid zone is very thin in comparison with the solute diffusion rate in the liquid during TLP-bonding. Also, solute diffusion in the base metal might affect the process kinetics during stage II [Tual-Poku, 1988]. Liu et al [1991] listed some governing equations and the initial and boundary conditions for stage II-2b, and did point out that those equations must be solved numerically.

In summary, analytical methods are difficult to apply during modelling of the dissolution stage during TLP-bonding. Later in this section, it will be shown that numerical methods are extremely effective when solving such problems.

2.7.1.3. Isothermal Solidification

The solute distribution in the liquid can be considered uniform during the isothermal solidification stage in TLP-bonding [Nakagawa et al, 1991], and therefore, solute diffusion in the liquid can be ignored. In addition, the solid region can be assumed to be semi-infinite because solute diffusion in the solid is slow. It follows that the isothermal solidification stage during TLP-bonding can be analytically modelled, as a single-phase diffusion-controlled moving interface problem (see Fig. 2-16).

Lynch et al [1959] first linked interface movement with the mass balance at the liquid-solid interface, but failed to provide an analytical solution for the problem. Tuah-Poku et al [1983] proposed a method of estimating the completion time for the isothermal solidification stage. In their treatment, the problem was simplified to a half semi-infinite base metal with a surface on which the solute concentration was maintained at $C_{\alpha L}$. Consequently, an error function solution can be employed to describe the solute distribution in the base metal (also, see §2.2 in this thesis):

$$C(y,t) = C_{\alpha L} + C_{\alpha L}\,\mathrm{erf}\left(\frac{y}{\sqrt{4Dt}}\right) \qquad (2\text{-}69)$$

where $C_{\alpha L}$ is the solute concentration in solid at the interface. Using

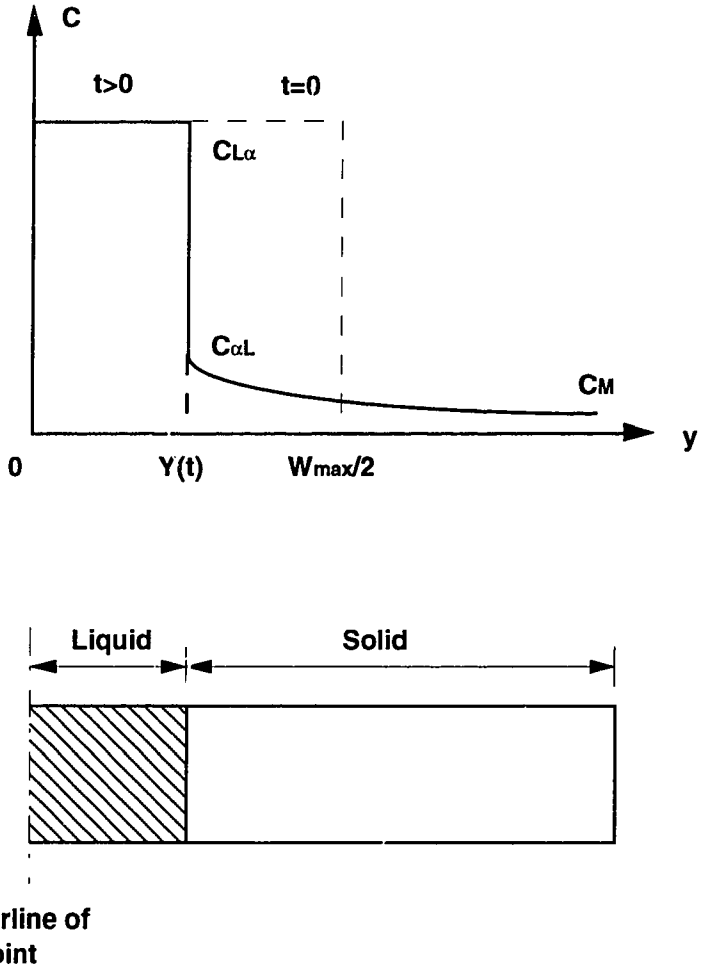

Fig. 2-16 Concentration profile along the specimen length during the isothermal solidification stage.

the procedure introduced in §2.2 of this thesis, the total solute amount M_t, which has entered the base metal at time t, can be calculated by,

$$M_t = 2C_{\alpha L}\sqrt{\frac{Dt}{\pi}}. \tag{2-70}$$

If the amount of solute diffused into the base metal during the heating and dissolution stages is ignored, the total amount of solute diffused into the base metal equals the original solute content (of the filler metal), i.e.,

$$C_F W_0 = 4C_{\alpha L}\sqrt{\frac{Dt}{\pi}}. \tag{2-71}$$

The completion time for isothermal solidification can then be calculated using the relation,

$$t_S = \frac{\pi}{16D_S}\left(\frac{C_F W_0}{C_{\alpha L}}\right)^2. \tag{2-72}$$

A similar treatment of this problem was reported by Onzawa et al. [1990].

Ikawa et al [1979] and Nakao et al [1989] used similar error function solutions to derive the solute distribution in the base metal and took account of the mass balance equation at the solid-liquid interface in order to obtain an analytical solution for the isothermal

solidification stage of TLP-bonding. The following discussion provides an outline of their derivation, with some small modifications that allow for similar concentration units as in the present thesis. The solute distribution in the base metal is described by the relation,

$$C(y,t) = C_{\alpha L} + C_{\alpha L}\,\mathrm{erf}\left(\frac{y-Y(t)}{\sqrt{4Dt}}\right), \tag{2-73}$$

and the mass balance at the solid-liquid interface is,

$$(C_{L\alpha}-C_{\alpha L})\frac{dY}{dt} = D_S\left(\frac{\partial C_S(y,t)}{\partial y}\right)_{y=Y(t)}$$

$$= -\frac{C_{\alpha L}}{\sqrt{\pi D t}}. \tag{2-74}$$

By integrating the above equation, an expression for the displacement of the interface as a function of time at the bonding temperature is,

$$W(t)=W_{max}-\frac{4C_{\alpha L}}{(C_{L\alpha}-C_{\alpha L})}\sqrt{\frac{D_S t}{\pi}}. \tag{2-75}$$

When W(t)=0, the completion time for the isothermal solidification stage is given as,

$$t_S = \frac{\pi}{16D_s}\left(\frac{C_{L\alpha}-C_{\alpha L}}{C_{L\alpha}}\frac{C_F W_0}{C_{\alpha L}}\right)^2. \tag{2-76}$$

Comparing Eq. (2-72) with Eq.(2-76), there is one more

term, $\frac{C_{L\alpha}-C_{\alpha L}}{C_{L\alpha}}$, in Eq. (2-76). If $C_{\alpha L} << C_{L\alpha}$, the two equations are identical and this happens to be the conditions under which the error function solution can be applied in the base metal (see Eq. (2-69) and more details in Appendix I).

A more rigorous treatment has been presented by Lesoult [1979]; his derivation is basically identical to that described by Danckwerts [1950] when he derived a general solution for unsteady-state linear heat conduction or diffusion. A general error function solution is assumed in the solid phase,

$$C_S(y,t) = A_1 + A_2 \operatorname{erf}\left(\frac{y}{2\sqrt{D_S t}}\right). \qquad (2\text{-}77)$$

where A_1 and A_2 are constants determined by the specific boundary conditions. At the moving interface,

$$C_S(Y,t) = A_1 + A_2 \operatorname{erf}\left(\frac{Y}{2\sqrt{D_S t}}\right) = C_{\alpha L}. \qquad (2\text{-}78)$$

Since Eq. (2-78) has to be satisfied for all values of t, Y must be proportional to $\sqrt{t}$, i.e.,

$$Y=-K\sqrt{4Dt}, \qquad (2\text{-}79)$$

The mass balance at the interface produces,

$$(C_{L\alpha}-C_{\alpha L})\frac{dY(t)}{dt} = D_S\left(\frac{\partial C_S(y,t)}{\partial y}\right)_{y=Y(t)}. \quad (2\text{-}80)$$

Solving Eqs. (2-77) to (2-80), we can derive,

$$\frac{K(1+erfK)\sqrt{\pi}}{\exp(-K^2)} = \frac{C_{\alpha L}-C_M}{C_{L\alpha}-C_{\alpha L}}. \quad (2\text{-}81)$$

By substituting $\beta=-K\sqrt{D_S}$, $C_{-\infty} = C_{L\alpha}$, and $C_\infty = C_M$ in Eq. (2-31) (in Section 2.4), an identical equation can be derived. Similar solutions were derived by Sakamoto et al [1989] and Ramirez and Liu [1992]. In Lesoult [1979] and Liu et al's [1991] derivations, the term $\exp(-K^2)$ is above the fraction in Eq. (2-81). This may be due to a misprint.

Therefore, the completion time for isothermal solidification can be calculated from,

$$t_S = \frac{W_{max}^2}{16K^2D_S}. \quad (2\text{-}82)$$

where, W_{max} is the maximum liquid width that is calculated using the mass balance method [Tuah-Poku, et al, 1988]

Le Bance and Morel [1990] used an identical derivation procedure to obtain a solution that accounted for boron consumption by boride formation (when a boron-containing filler metal was used during TLP-bonding of a nickel-based superalloy [Gale and Wallach, 1991]).

2.7.1.4. Homogenization Stage

Eq. (2-9) was used by Ikawa and Nakao [1979] to model the homogenization stage,

$$C(y,t)=C_M+\frac{1}{2}(C_F-C_M)\left\{\mathrm{erf}\left(\frac{y+\frac{W_{max}}{2}}{\sqrt{4D_St}}\right)-\mathrm{erf}\left(\frac{y-\frac{W_{max}}{2}}{\sqrt{4D_St}}\right)\right\}. \quad (2\text{-}83)$$

The solute concentration attains its maximum value at the centerline of the specimen (when y=0), namely,

$$C_{max}=C(0,t)=C_M+(C_F-C_M)\,\mathrm{erf}\left(\frac{W_{max}}{4\sqrt{D_St}}\right). \quad (2\text{-}84)$$

Kang [1988] and Nakao et al [1991] confirmed a good agreement between the calculated results (from Eq. (2-84)) and experimental results (based on the redistribution of Cr during homogenization of different nickel superalloy base metals TLP-bonded using a Ni-Cr-B filler metal). It is worth noting that there was a small deviation between the analytical calculation and experimental measurement in the early stages of homogenization.

2.7.2. Numerical Simulation

The only numerical modelling investigation to-date was carried out by Nakagawa et al [1991]. They examined dissolution behavior during TLP-bonding of Ni using Ni-P and Ni-Cr-P filler metal. This

research confirmed the importance of filler metal thickness and of heating rate between the filler metal melting temperature and the bonding temperature on the base metal dissolution process. The explicit finite difference method was employed to solve the diffusion equations in the solid and in the liquid. However, a stepwise ("mechanical") mass balance method was used to determine solid-liquid interface movement. This method cannot determine the exact interface position, which can be very important, e.g., when calculating the curvature of the interface during two-dimensional modelling of TLP-bonding. A superior method involves use of a mathematical equation such as Eq.(2-30) to track the liquid-solid interface. Another problem with Nakagawa et al's approach is the extremely long calculation time required when the entire TLP-bonding process is modelled using the explicit finite difference method. As a result, much more work is needed during numerical modelling of TLP-bonding.

2.7.3. Effect of Grain Boundaries on Process Kinetics

Tuah-Poku et al [1988] compared their analytically calculated and experimental completion times for isothermal solidification during TLP-bonding of Ag using Cu filler metal and found a marked difference between these results. They suggested that this difference might be due to liquid penetration at grain boundaries in the base metal. Such liquid penetration increases the solid-liquid interfacial area for diffusion. Kokawa et al [1991] also observed that the rate of isothermal solidification was faster when fine-grained nickel was TLP-bonded (compared to that when coarse-grained nickel was joined

using Ni-P filler metal). An analysis of electron channelling patterns derived from completed joints confirmed that liquid penetration was greatest at random high angle grain boundaries in the base metal. There was little liquid penetration at ordered grain boundaries including small angle and twin boundaries.

2.7.4. Summary

This review has confirmed that almost all the modelling work to-date on TLP-bonding has involved analytical methods. However, all analytical approaches have treated the joining process as a number of discrete stages and this is not what actually occurs during the TLP-bonding process. For example, the completion time required for solute homogenization will depend on the solute distribution immediately following completion of the isothermal solidification stage. Similarly, the solute distribution in the base metal at the end of the dissolution period will markedly affect movement of the solid-liquid interface during the initial stage of isothermal solidification. In addition, at each stage, the error function solution and a parabolic law are employed in the analytical calculations, and these may be considered only as approximate solutions. Also, the analytical solutions for TLP-bonding must be carefully evaluated, e.g., under what conditions can Eq. (2-72) be used to estimate the completion time of isothermal solidification. Numerical modelling has the key advantage that it can treat base metal dissolution, liquid phase isothermal solidification and solute homogenization as sequential processes. Also, numerical modelling can be readily applied to 2- or 3-dimensional joining

situations, and when the fabricated components have complicated shapes.

Chapter 3

TLP-bonding Experimentation

This chapter describes the experimentation carried out during TLP-bonding of single crystal and polycrystalline pure nickel base metals using Ni-19at.% P eutectic filler metal. The results obtained from the single crystal nickel experiments will be directly compared with the output of the one-dimensional numerical calculation presented in the next chapter. A comparison of the experimental results produced during TLP-bonding of single crystal and polycrystalline nickel base metals also provides a direct indication concerning the effect of grain boundary regions on the isothermal solidification process. This aspect is particularly important with regard to the development of two-dimensional numerical models for TLP-bonding, since little research has been carried out on the influence of base metal grain boundary regions on the process kinetics. In effect, the experimental results produced during TLP-bonding of base metals with different grain sizes provide the baseline information required for numerical model development in the subsequent chapters of this thesis.

3.1. Experiment Set-up

3.1.1. Materials

High purity and commercially-pure nickel base metal were employed during TLP-bonding. Pure nickel base metal was available as single crystal, coarse-grained and fine-grained material. The chemical compositions of the different nickel base metals are shown in Table 3-1. In the case of single crystal nickel, the (100) orientation of the face-centered-cubic lattice was always aligned perpendicular to the joint interface during TLP-bonding. The coarse-grained nickel base metal was Ohno-casted [Ohno, 1989] and had a grain size of approximately 3.4 mm. The fine-grained nickel base metals had average grain sizes of 33 μm and 40 μm for high purity and low purity respectively. The single crystal and fine-grained nickel base metals were employed in the as-received condition, while the coarse-grained base material was annealed at 1150 °C for 24 hours in vacuum prior to TLP-bonding.

The test specimen dimensions were 12 mm diameter x 3 mm thickness (for the single crystal nickel base metal) and 12 mm diameter x 5 mm thickness (for coarse-grained and fine-grained nickel base metals). 25 μm thick Ni-19at.% P filler metal was employed during all TLP-bonding experiments.

3.1.2. Vacuum Furnace

All TLP-bonding experiments were completed in a specially-designed, oil-quenchable vacuum furnace (see Fig. 3-1). This furnace was vertically configured so that the individual test specimens could be quenched into an oil bath while under vacuum. The distribution of

Table 3-1 Compositions of different nickel base metals (concentration in ppm)

	Nominal Purity (wt.%)	Al	As	Co	Cr	Cu	Fe	Mg	Mn	S	Si	Ti
Single Crystal	99.999	7	<0.5	<2	19	5	26	2	-	<1	4	<2
Coarse Grain	99.99	57	<1.1	115	110	40	310	2	6	<1	36	<2
Fine Grain, High Purity	99.99	6	3.8	170	10	8	19	3	<1	<1	10	4
Fine Grain, Low Purity	99.5	300	23	500	<4	62	520	154	1590	34	130	550

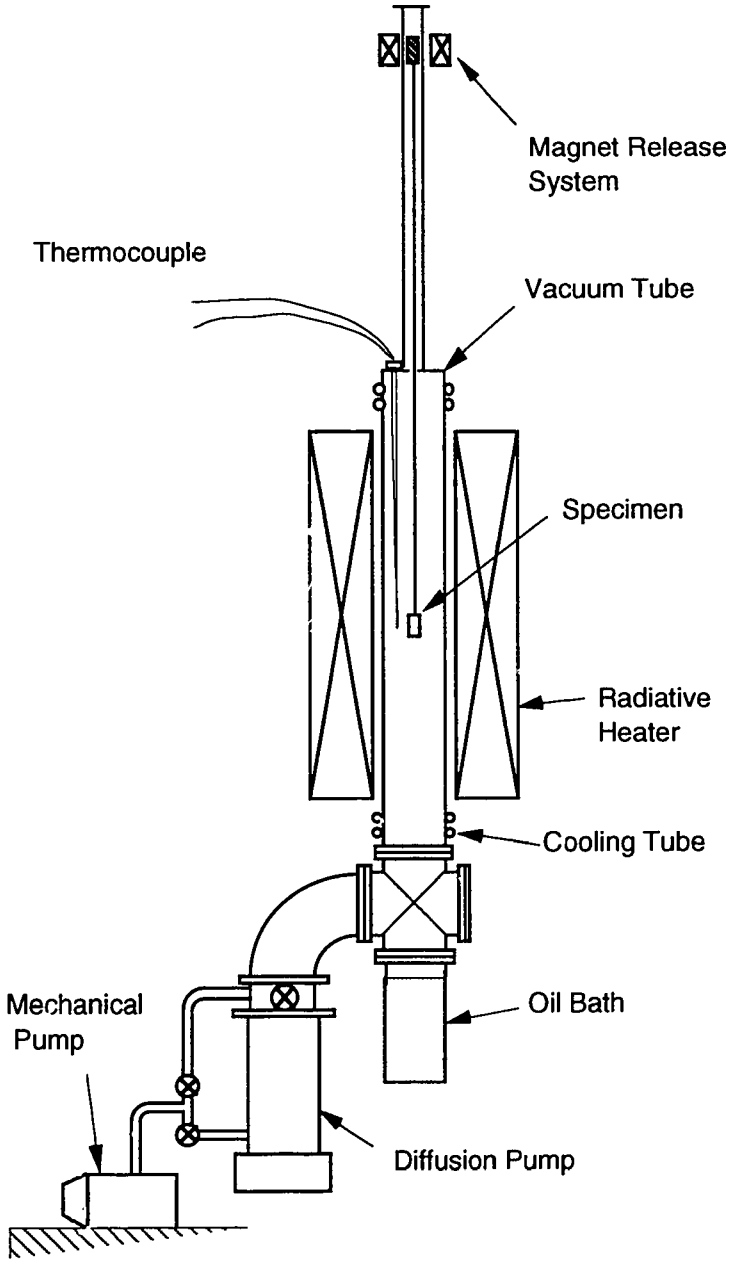

Fig. 3-1 Schematic of the specially-designed, oil-quenchable vacuum furnace.

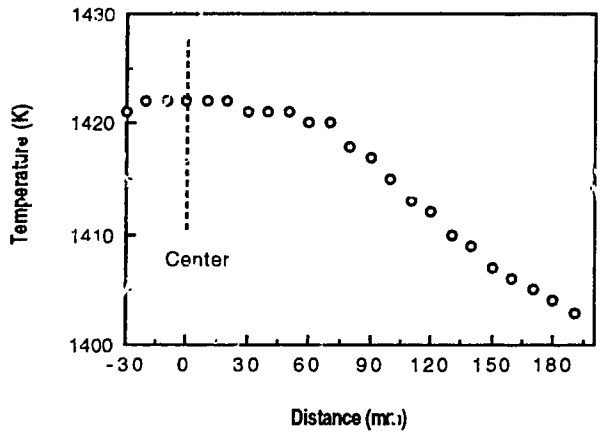

Fig. 3-2 Temperature distribution along the length of the vacuum tube in the furnace

temperature along the length of the vacuum tube is shown in Fig. 3-2. This confirmed that a 100 mm long uniform-temperature zone existed at the tube center. Since the inside diameter of the vacuum tube was 40 mm, it is considered that the temperature across the tube radius is uniformly distributed. The heating cycle employed during all TLP-bonding experiments is shown in Fig. 3-3. The average heating rate was around 2.5 K/s between the filler metal melting point (1153 K) and the bonding temperature (1423 K). The bonding temperature was 1423 K throughout and this temperature was maintained within ±5 K during the holding period. In all tests, the vacuum was maintained at about 10^{-5} Torr.

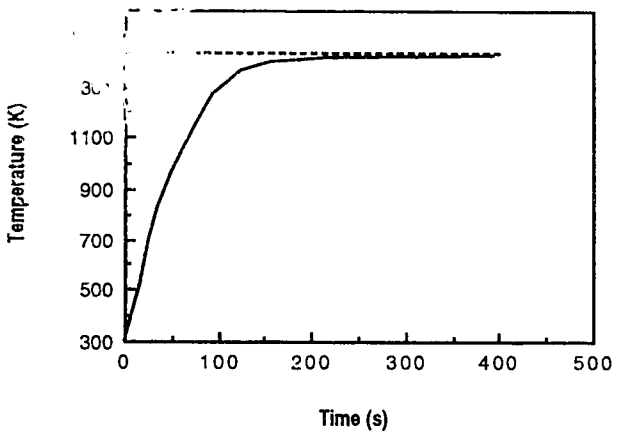

Fig. 3-3 The heating cycle during TLP-bonding.

3.1.3. Experimental procedure

The surfaces of the nickel samples were polished using #1200 grade emery paper to remove the deformed surface layer produced by specimen machining operation and to make the contacting surfaces smoother. All test specimens were then ultrasonically cleaned using acetone immediately prior to spot welding. The filler metal was inserted at the joint interface, and the assembly was spot-welded using a nickel clamping fixture that maintained a constant gap width at the joint interface. In addition, the two spot welds present at the joint interface promoted intimate contact between the filler and base materials (see Fig. 3-4). Escape of liquid filler metal during the brazing operation was prevented by painting alumina-based stop-off material at the joint periphery. The test assembly was suspended on a

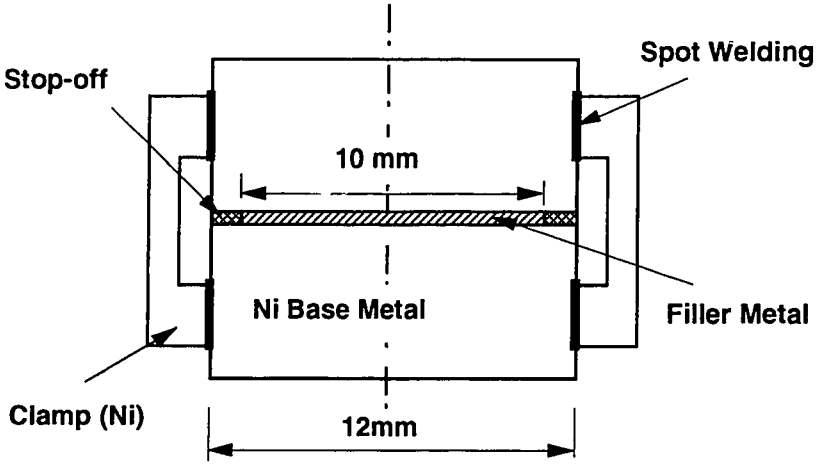

Fig. 3-4 Configuration of the TLP-bonding assembly.

wire and was then pulled to the uniform-temperature zone and then dropped into the oil bath after a given holding time.

All test samples were examined using a combination of optical and scanning electron microscopy (SEM). The test samples were etched as follows: in a solution of 1 part concentrated nitric acid + 1 part glacial acetic acid when observing the bonded region, and in a solution of 1 part concentrated nitric acid + 2 parts concentrated hydrochloric acid + 3 parts glycerin for grain size measurement.

The average width of the eutectic structure in the bonded region was measured by evaluating the cross-sectional area of the eutectic

structure at a magnification of 500 times. The eutectic width was evaluated over a distance of 5 mm at the mid-section of the TLP-bonded test specimens while the base metal grain size was measured immediately adjacent to the bonded interface over the whole length of the joint interface and in the base metal region.

3.2. Results

The process kinetics during TLP-bonding were evaluated directly by measuring the eutectic width in joints produced at different holding times (see Fig. 3-5 and Table 3-2). It should be noted that only the isothermal solidification stage is illustrated in the Fig. 3-5, since the time required for dissolution is very short and is particularly difficult to measure [Tuah-Poku et al, 1988]. The eutectic width decreased

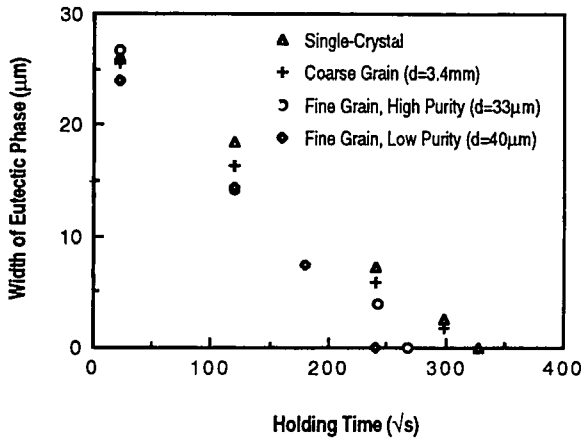

Fig. 3-5 TLP-bonding of nickel base metals with different grain sizes (d is the mean grain size prior to TLP- bonding).

Table 3-2 Experimental results indicating the change in width of eutectic phase with increasing holding time during TLP-bonding of nickel base metal

Holding Time (s)	Single Crystal	Coarse Grain	Fine Grain, High Purity	Fine Grain, Low Purity
48	26.2	25.5	26.6	23.9
14,400	18.5	16.3	14.3	14.4
32,400	-	-	-	7.34
57,600	7.22	5.91	3.89	≈0
72,000	-	-	≈0	0
90,000	4.66	1.77	0	-
129,600	≈0	-	-	-
176,400	-	0	-	-

linearly with the square-root of bonding time during TLP-bonding of all nickel base metals. The rate of isothermal solidification of the coarse-grained Ohno-casted nickel samples was slightly faster than that of the single crystal nickel samples, while the rate of isothermal solidification of fine-grained nickel samples was much faster. It follows that grain boundary regions can speed up the process kinetics during isothermal solidification.

Figs. 3-6 to 3-8 show the oil-quenched bonded region microstructures produced using the different nickel base metals. A planar liquid-solid interface is apparent in TLP-bonded single-crystal

nickel base metal. However, liquid penetration occurred in the joints produced in polycrystal nickel base metal and the liquid-solid interface was non-planar (see Figs. 3-6 to 3-8).

The amount of grain growth during TLP-bonding is shown in Table 3-3. There was negligible variation in grain size during the TLP-bonding of the coarse-grained nickel base metal; the average grain size throughout the joining process was about 3.4 mm. However, extensive grain growth occurred in TLP-bonded fine-grained base metal. The overall grain size of high purity nickel base metal was only slightly smaller than that of low purity nickel base metal and therefore the test results can be use to compare the influence of base metal purity on process kinetics. It can be concluded that the low purity joints have faster process kinetics (a faster rate of isothermal solidification). It is also interesting to note the difference in grain sizes observed in regions close to and far from the solid-liquid interface (see Table 3-3). It is possible that grain boundary groove retarded grain boundary migration in regions close to the solid-liquid interface [Mullins, 1958 and Allen, 1982].

3.3. Discussion: Factors Affecting Process Kinetics

TLP-bonding is a diffusion-controlled process and any factor that affects the diffusion process will alter the process kinetics during the joining operation. In the one-dimensional (single crystal base metal) situation, solute transport occurs via volume diffusion in the solid and

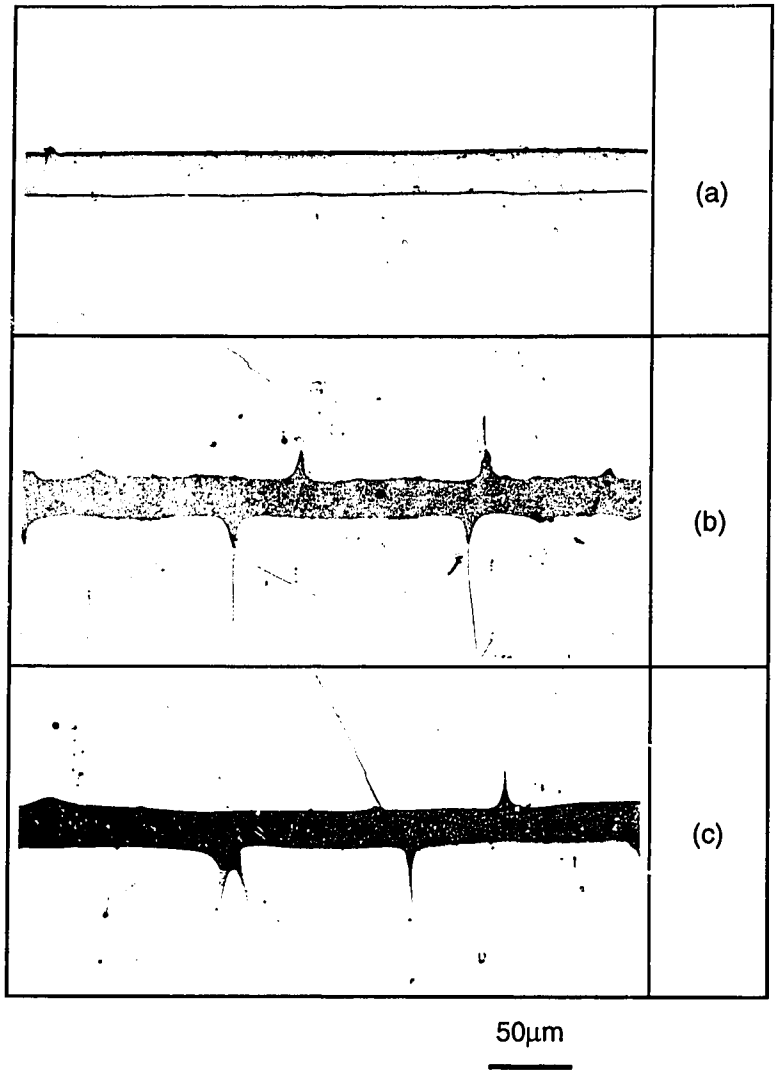

Fig. 3-6 Opticai microstructures of the joint region following TLP-bonding at 1423 K for 8 minutes using different nickel base metals: (a) single-crystals; (b) fine-grained, high purity and (c) fine-grained, lcw purity.

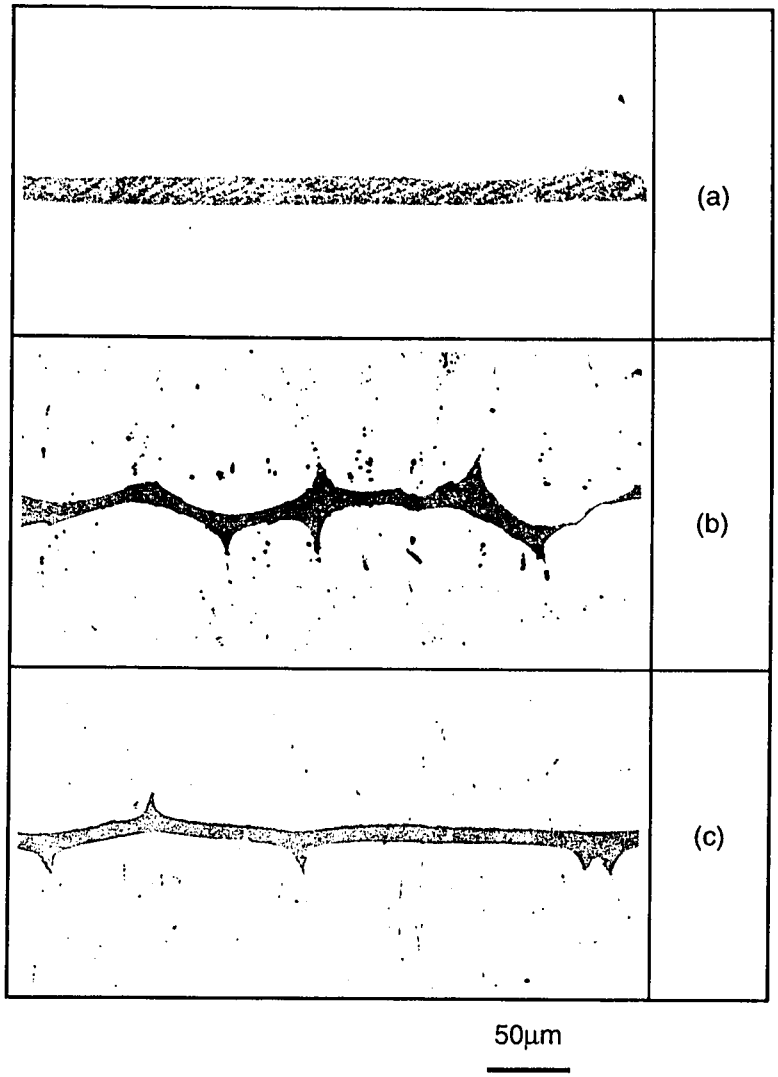

Fig. 3-7 Optical microstructures of the joint region following TLP-bonding at 1423 K for 4 hours using different nickel base metals: (a) single-crystals; (b) fine-grained, high purity and (c) fine-grained, low purity.

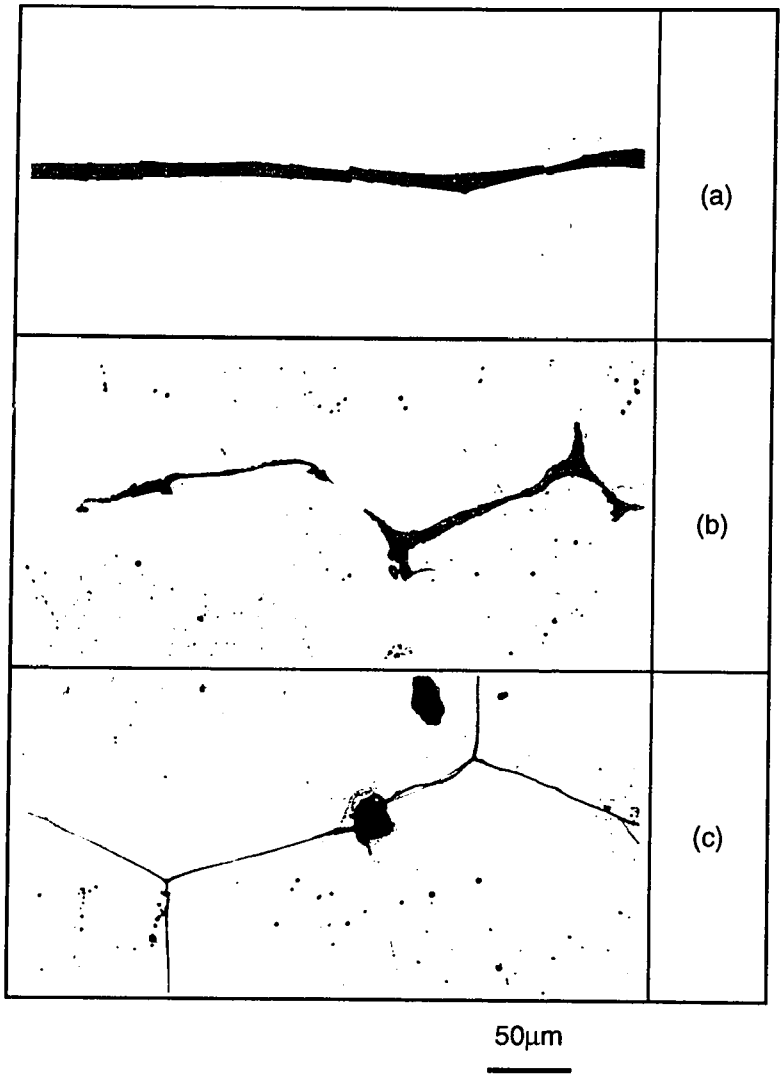

Fig. 3-8 Optical microstructures of the joint region following TLP-bonding at 1423 K for 16 hours using different nickel base metals: (a) single-crystals; (b) fine-grained, high purity and (c) fine-grained, low purity.

Table 3-3 Change in grain size during TLP-bonding

Holding Time (s)	Coarse Grained Nickel	Fine Grain, Low Purity Nickel (in bulk base metal)	Fine Grain, High Purity Nickel	
			in bulk base metal	near the solid-liquid interface
48	2.9mm	-	285μm	90μm
14,400	4.2mm	476μm	431μm	129μm
57,600	3.0mm	593μm	463μm	212μm
90,000	3.1mm	680μm	525μm	297μm

in the liquid. However, solute transport in polycrystalline base metal depends on a number of aspects (see Fig. 3-9):

(1) The polycrystalline base metal contains grain boundary regions where the diffusivity is much higher than in the bulk region [e.g., Peterson, 1983].

(2) The curved liquid-solid interface promotes interfacial diffusion which is faster than that in the bulk base metal [Mulins, 1957].

(3) TLP-bonding is basically a homogenization process in which solute continuously diffuses from the liquid zone into the base metal solid. It follows that increasing of the solid-liquid interfacial area (as a result of liquid penetration and grain boundary grooving) will provide a larger transport area for solute diffusion across the interface [Kokawa et al, 1992].

(4) Grain boundary migration (as a result of grain growth during TLP-bonding) will mean that solute has more chance of visiting grain boundaries; this will affect solute diffusion and therefore process kinetics.

(5) Other factors, such as grain boundary segregation, will directly affect the grain boundary free energy, and solute diffusivity.

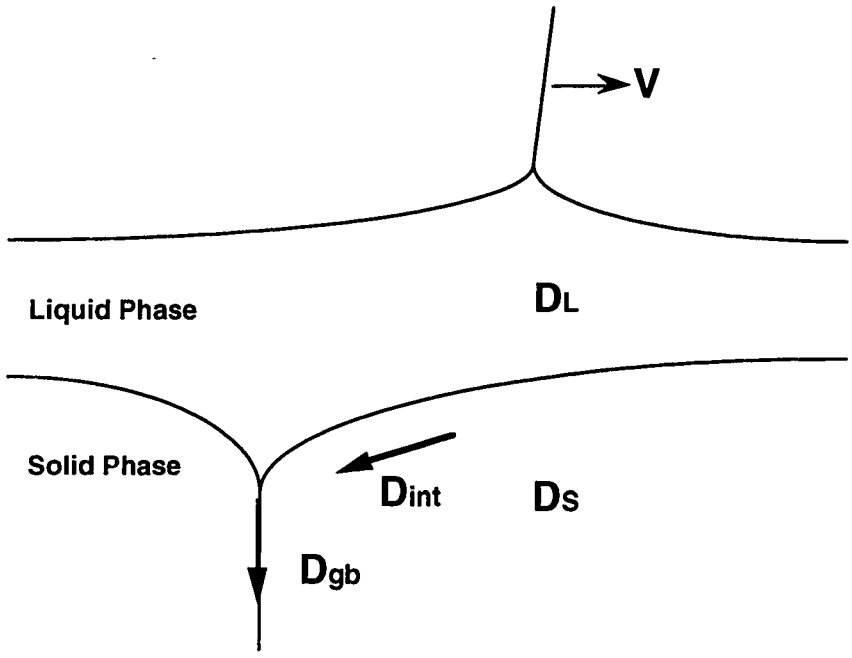

Fig. 3-9 Schematic showing the factors in the two-dimensional model of TLP-bonding. D_L, D_S, D_{gb} and D_{int} are the diffusion coefficients in the liquid, the solid, grain boundary regions and liquid-solid interface regions respectively.

It follows that the effect of grain boundary regions on the process kinetics during TLP-bonding must depend on the solution of a two or three-dimensional, diffusion-controlled moving interface problem.

3.4. Summary

The influence of base metal grain size on the isothermal solidification process kinetics during TLP-bonding of nickel using Ni-19at.% P filler metal was examined. The eutectic width decreased linearly with the square-root of the holding time for all nickel base metals examined, and the rate of isothermal solidification increased in the following order: single crystal, coarse-grained and fine-grained nickel. It follows that the grain boundary regions can speed up the overall solute transport rate. The presence of impurities in the base metal also increase the rate of isothermal solidification.

It is suggested that the differing performance observed when bonding single crystal and polycrystalline materials can be explained due to grain boundary related factors influencing process kinetics. The following chapters will describe the numerical models that explain the effect of grain boundaries on the process kinetics during TLP-bonding and other two-phase diffusion-controlled processes.

Chapter 4

One-Dimensional Modelling of Process Kinetics

In this chapter, a general one-dimensional numerical model is developed, which considers two-phase diffusion at a moving interface, with the aim of increasing the calculation efficiency and accuracy. The validity of the model will be verified by comparing the calculated results with direct experimental test results. The numerical model output will also be compared with some analytical solutions. Finally this numerical model will be applied to examine the TLP-bonding process and the requirements for parameter optimization during TLP-bonding will be discussed in detail.

4.1. Computer Simulation

4.1.1. Physical model

Fig. 4-1 shows a schematic illustration of the diffusion-controlled, two-phase moving interface problems that exist during solution treatment of an α/β brass diffusion couple and during TLP-bonding (see §2.1). Fig. 4-1(a) indicates a planar interface situation where constant size zones of solute-rich, second-phase (β brass) are dispersed uniformly throughout the matrix (α brass). When this assembly is held at the solution temperature, the second-phase grows and then dissolves [Heckel et al, 1975]. Fig. 4-1(b) illustrates the

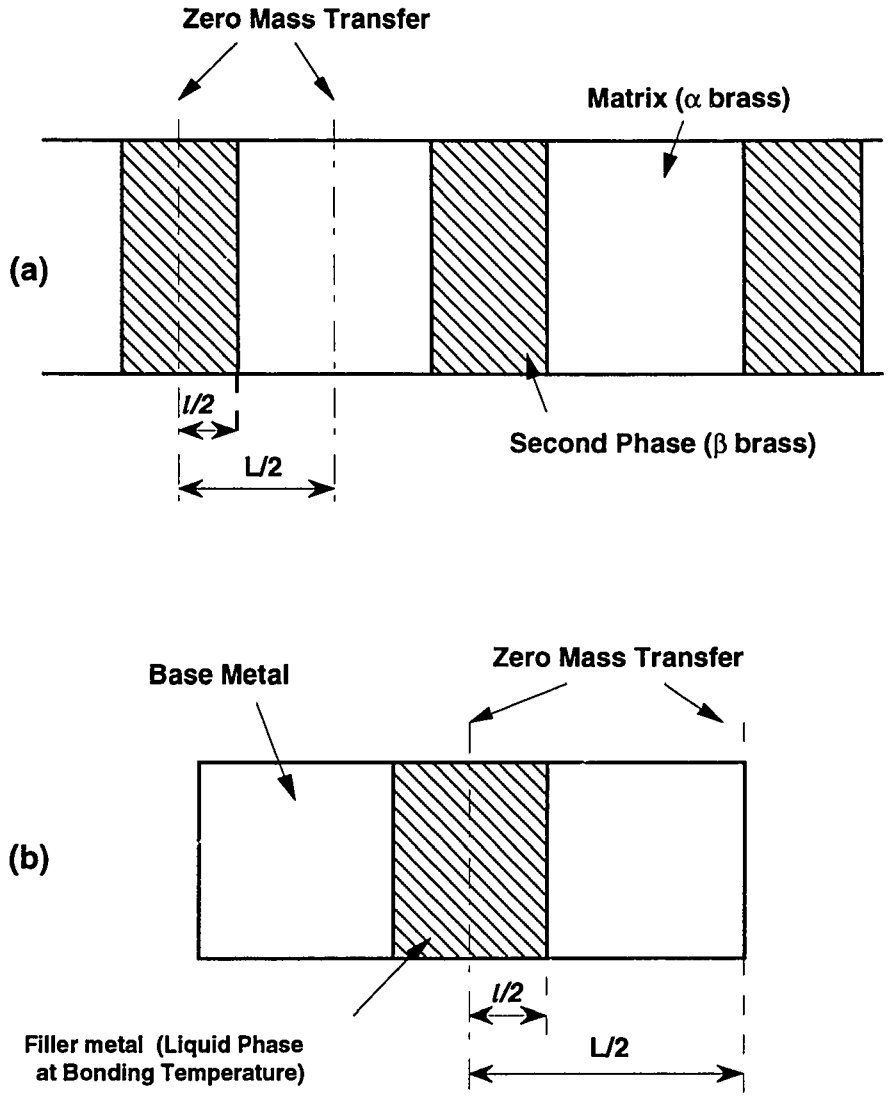

Fig. 4-1 Schematic illustrating modelling of (a) α/β brass solution treatment (after Heckel et al, 1972); (b) TLP-bonding of nickel.

situation during TLP-bonding, when the liquid phase grows and then disappears at the bonding temperature. As pointed out early, both processes are diffusion-controlled and involve moving interfaces.

The basic assumptions during numerical modelling are:

(1) The moving interface remains planar throughout the processing period; this is the exact case when only single crystal base metals are involved.

(2) The diffusion coefficient, molar volume and activity coefficient of the solute are independent of composition. The molar volumes of the different phases are also equal;

(3) Local equilibrium exists at the moving interface;

(4) There is negligible liquid flow due to convection and stirring (in the liquid phase) and there is no effect of latent heat on the temperature distribution and on movement of the solid-liquid interface when a liquid phase is involved.

4.1.2. Problem Formulation

Fig. 4-2 shows the solute concentration profile, C(y,t), and the moving interface location, Y(t). The second phase region is located at $0 \le y \le Y(t)$ and the matrix region is located at $Y(t) \le x \le \frac{L}{2}$. The width of the second phase is $W(t) = 2\ Y(t)$. The governing equations which determine the solute diffusion field are:

$$\frac{\partial C_I(y,t)}{\partial t} = D_I \frac{\partial^2 C_I(y,t)}{\partial y^2}, \qquad 0 \le y \le Y(t) \qquad (4\text{-}1)$$

$$\frac{\partial C_{II}(y,t)}{\partial t} = D_{II}\frac{\partial^2 C_{II}(y,t)}{\partial y^2}, \qquad Y(t) \le y \le \frac{L}{2} \tag{4-2}$$

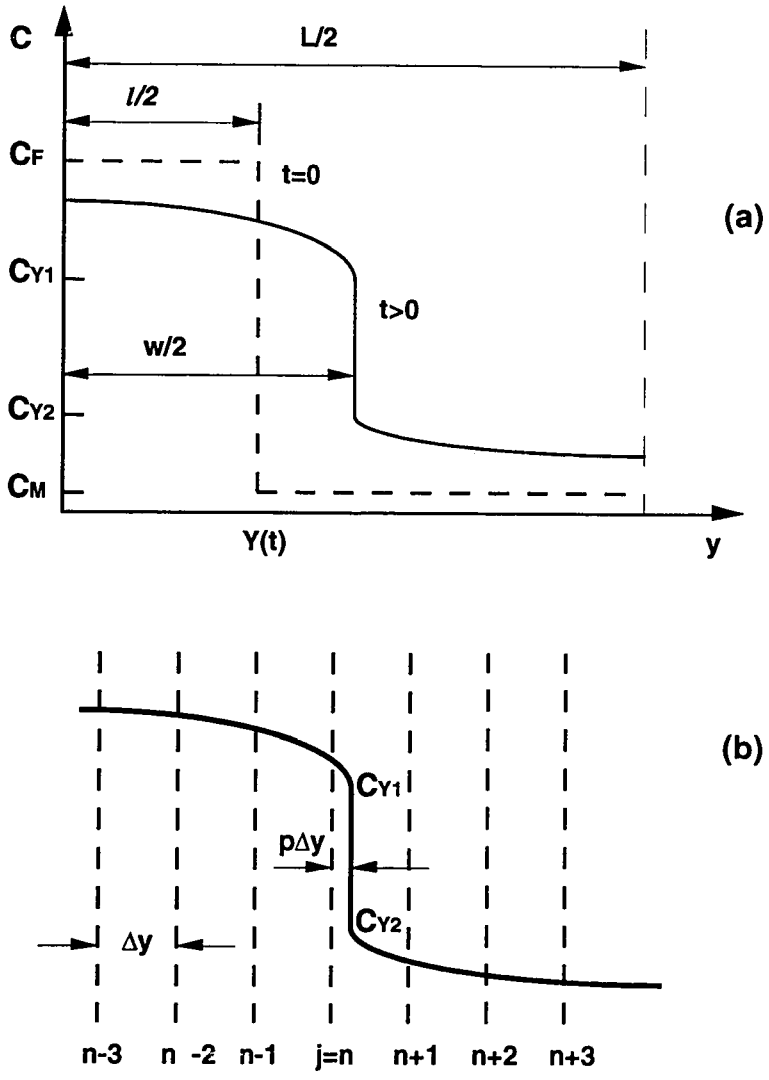

Fig. 4-2 (a) Concentration profiles produced by interface movement. (b) The numerical method employed to analyze interface movement.

These are subject to the following boundary conditions:

$$\left(\frac{\partial C_I(y,t)}{\partial y}\right)_{y=0}=0, \tag{4-3}$$

and

$$\left(\frac{\partial C_{II}(y,t)}{\partial y}\right)_{y=L/2}=0. \tag{4-4}$$

The initial conditions are:

$$C_I(y,0) = C_F, \qquad 0 \le y \le l/2 \tag{4-5}$$

and

$$C_{II}(y,0) = C_M. \qquad l/2 \le y \le L/2 \tag{4-6}$$

At the moving interface,

$$C_I(Y(t),t) = C_{YI}, \tag{4-7}$$

and

$$C_{II}(Y(t),t) = C_{YII}. \tag{4-8}$$

and because of the conservation of mass at the moving interface, interface movement is determined by the relationship:

$$(C_{YI}-C_{YII})\frac{dY(t)}{dt} = J_I-J_{II}$$
$$=-\left(D_I\frac{\partial C_I(y,t)}{\partial y}\right)_{y=Y(t)}+\left(D_{II}\frac{\partial C_{II}(y,t)}{\partial y}\right)_{y=Y(t)}, \tag{4-9}$$

where J_I is the flux in Phase I at the interface and J_{II} is the flux in Phase II at the interface.

4.1.3. Numerical Analysis

The approach taken involves using the finite difference approximation to obtain discrete forms of differential equations (4-1), (4-2) and (4-9), with finite boundary and initial conditions. An implicit finite difference method is employed when approximating Eqs. (4-1) and (4-2) in order to decrease the calculation time; this overcomes the stability restriction on the maximum time step. Many investigators [Tanzilli,1968; Heckel,1972; Pabi,1979; Lanam,1971; Karlsson; Nakagawa,1991 and Battle and Peklke, 1990] have solved Eq. (4-9) using the explicit method. However, the accuracy of the solution decreases when large time steps are employed. In the present thesis, Eq. (4-9) is solved using an implicit method. As a result, a fully implicit scheme has been developed to handle the diffusion controlled, moving interface problem.

4.1.3.1. Approximating the Diffusion Equations

The space domain is divided into H equally-spaced intervals of length $\Delta y = \frac{L}{2H}$, namely, $y_j = (j-1)\Delta y$, $j = 1, 2, 3, \cdots\cdots, H+1$. The interface lies between the nodes $j = n$ and $n+1$, and $p = \{Y(t) - (n-1)\Delta y\}/\Delta y$, where $0 \leq p \leq 1$ and $n = 1, 2, 3, \cdots\cdots$ (see Fig. 4-2(b)). The time step varies with the interface velocity at a constant interface displacement $\Delta t = \frac{E\Delta y}{\frac{dY}{dt}}$,

where E is a constant. Since the interface moves very quickly during the initial period of the processes and then slows down, this treatment ensures that the time step will be small enough (in the initial stage) so that the calculation accuracy will be acceptable. The finite difference expressions for Eqs. (4-1) and (4-2) are:

$$\frac{C_j^{t+\Delta t}-C_j^t}{\Delta t} = D\frac{\theta(\delta^2C)_j^{t+\Delta t}+(1-\theta)(\delta^2C)_j^t}{(\Delta y)^2} \qquad (4\text{-}10)$$

where θ is a weighted constant and $(\delta^2C)_j = C_{j+1}-2C_j+C_{j-1}$, for the nodes j = 2,3, ·····, H; except for the nodes near the moving interface. Using the zero flux boundary conditions in Eqs. (4-3) and (4-4), at the boundary nodes j = 1 and H+1, one can obtain,

$$(\delta^2C)_1 = 2(C_2-C_1) \qquad (4\text{-}11)$$

$$(\delta^2C)_{H+1} = 2(C_H-C_{H+1}) \qquad (4\text{-}12)$$

Near the moving interface [Crank, 1984]:

$$(\delta^2C)_n = 2\left\{\frac{C_{n-1}}{1+p} - \frac{C_n}{p} + \frac{C_{YI}}{p(1+p)}\right\}, \qquad (4\text{-}13)$$

$$(\delta^2C)_{n+1} = 2\left\{\frac{C_{YII}}{(1-p)(2-p)} - \frac{C_{n+1}}{(1-p)} + \frac{C_{n+2}}{(2-p)}\right\}, \qquad (4\text{-}14)$$

Eqs. (4-10)-(4-14) comprise two sets of relations, one (from j = 1 to k) for the second-phase region, and the other (from j = n+1 to H) for the base metal region. However, Eqs. (4-13) and (4-14) have

singularities at p = 0 in Eq. (4-13) and p = 1 in Eq. (4-14). This singular behavior is handled using the following approach. When $p < \frac{1}{2}$, the equation set extends from j = 1 to n-1 for the second phase region, and C_n can be calculated using a finite difference expression (assuming that the concentration on both sides of the moving interface are described by quadratic relations):

$$(\delta^2 C)_{n-1} = 2\left\{\frac{C_{n-2}}{2+p} - \frac{C_{n-1}}{1+p} + \frac{C_{YI}}{(1+p)(2+p)}\right\} \tag{4-15}$$

$$C_n = -\frac{pC_{n-2}}{2+p} + \frac{2pC_{n-1}}{1+p} + \frac{2C_{YI}}{(1+p)(2+p)} \tag{4-16}$$

When $p > \frac{1}{2}$, the equation set extends from j = n+2 to H for the base metal region:

$$(\delta^2 C)_{n+2} = 2\left\{\frac{C_{YII}}{(2-p)(3-p)} - \frac{C_{n+1}}{(2-p)} + \frac{C_{n+3}}{(3-p)}\right\} \tag{4-17}$$

and C_{k+1} is given as:

$$C_{n+1} = \frac{2C_{YII}}{(2-p)(3-p)} + \frac{2(1-p)C_{n+2}}{(2-p)} - \frac{(1-p)C_{n+3}}{(3-p)} \tag{4-18}$$

The solution of Eq. (4-10) is unconditionally stable and convergent when $\frac{1}{2} \le \theta \le 1$. However, for $0 \le \theta < \frac{1}{2}$, we must employ the relation [Richtmyer, 1957]:

$$\frac{D\Delta t}{(\Delta y)^2} \leq \frac{1}{2(1-2\theta)}. \qquad (4\text{-}19)$$

This stability restriction on the maximum time step requires an enormous number of calculation cycles during problem solution. In the present thesis, the θ value is taken as $\frac{1}{2} - \frac{(\Delta y)^2}{12D\Delta t}$, where θ is taken as 0 for all values of $\theta < 0$ at the initiation of the process, when the velocity of the moving interface is very fast and the time step must be small. This special scheme has a truncation error of $O(\Delta t^2 + \Delta y^4)$ [Richtmyer, 1957]. This is smaller than that when $\theta = 0$ (for an explicit scheme), $\theta = 1$ (for an implicit scheme) and even $\theta = 0.5$ (using the Crank-Nicolson scheme [Crank, 1975]). The solution is also stable. Another advantage of the implicit scheme is that there are no stability restrictions concerning time step selection. This means that the calculation time can be decreased without affecting the solution stability.

4.1.3.2. Approximating the Moving Interface

Rearranging Eq. (4-9) provides:

$$\frac{dY(t)}{dt} = \frac{1}{(C_{YI}-C_{YII})}\left\{-\left(D_I\frac{\partial C_I(y,t)}{\partial y}\right)_{y=Y(t)} + \left(D_{II}\frac{\partial C_{II}(y,t)}{\partial y}\right)_{y=Y(t)}\right\}$$

$$= f(Y(t),t). \qquad (4\text{-}20)$$

The modified Euler method (implicit scheme) is applied to solve Eq. (4-20), namely,

$$Y^{(0)}(t+\Delta t)=Y(t)+\Delta t\ f(Y(t),t), \tag{4-21}$$

and

$$Y^{(k+1)}(t+\Delta t)=Y(t)+\frac{\Delta t}{2}\ \{f\{Y(t),t)+f(Y^{(k)}(t+\Delta t),t+\Delta t)\}, \tag{4-22}$$

where k= 0,1,2,....., and the iteration at each time step is performed until·

$$\left|\frac{Y^{(k+1)}(t+\Delta t)-Y^{(k)}(t+\Delta t)}{Y^{(k)}(t+\Delta t)}\right| < 10^{-6}. \tag{4-23}$$

This implicit scheme for Eq. (4-20) improves the the calculation accuracy, since the error is $O(\Delta t^3)$ [Gerald and Wheatly, 1989] and much larger time steps are therefore permissible.

The treatment applied to Eqs. (4-13) and (4-14) can be used to approximate the derivatives in Eq. (4-20). When $p > \frac{1}{2}$,

$$\left(\frac{\partial C_I}{\partial y}\right)_{y=Y}=\frac{1}{\Delta y}\left\{\frac{pC_{n-1}}{1+p}-\frac{(1+p)C_n}{p}+\frac{(1+2p)C_{YI}}{p(1+p)}\right\}, \tag{4-24}$$

and

$$\left(\frac{\partial C_{II}}{\partial y}\right)_{y=Y}=\frac{1}{\Delta y}\left\{\frac{(2p-5)C_{YII}}{(2-p)(3-p)}+\frac{(3-p)C_{n+2}}{(2-p)}-\frac{(2-p)C_{n+3}}{(3-p)}\right\}. \tag{4-25}$$

and when $p < \frac{1}{2}$,

$$\left(\frac{\partial C_I}{\partial y}\right)_{y=Y} = \frac{1}{\Delta y}\left\{\frac{(1+p)C_{n-2}}{2+p} - \frac{(2+p)C_{n-1}}{1+p} + \frac{(3+2p)C_{YI}}{(1+p)(2+p)}\right\}, \qquad (4\text{-}26)$$

and

$$\left(\frac{\partial C_{II}}{\partial y}\right)_{y=Y} = \frac{1}{\Delta y}\left\{\frac{(2p-3)C_{YII}}{(1-p)(2-p)} + \frac{(2-p)C_{n+1}}{1-p} - \frac{(2-p)C_{n+2}}{(2-p)}\right\}. \qquad (4\text{-}27)$$

4.1.3.3. Initiating the Solution

Since the numerical solution cannot be initiated directly using the initial conditions (in Eqs. (4-5) and (4-6)), an approximate analytical solution for a very small time step is used as the starting point for the finite difference scheme, i.e.,

$$Y(\Delta t) = \frac{1}{2}l + 2\beta\sqrt{\Delta t}. \qquad (4\text{-}28)$$

In Eq. (4-28), β is calculated using Eq. (2-31) in Chapter 2 and is a constant that depends on the material properties (on the solute diffusivity and solubility values).

The numerical computation proceeds as follows:

(i) The initial movement of the interface is calculated using Eq. (4-28).

(ii) The new solute concentration distribution at each nodal point, after the initial interface movement, is calculated using the discrete forms of Eqs. (4-1) and (4-2).

(iii) The new moving interface position is calculated starting from the previous position, using the discrete form of Eq. (4-9).

(iv) The redistribution of solute from the previous concentration at each nodal point is calculated using the discrete forms of Eqs. (4-1) and (4-2)

(v) Steps (iii) and (iv) are repeated until the process is completed.

4.2. Testing the Model

The normalized thickness of the second-phase (W/*l*) is plotted as a function of dimensionless time (Dt/l^2) in Fig. 4-3 to Fig. 4-5. The optimum calculation conditions which produced satisfactory results were evaluated using a trial and error procedure. Different mesh size and E values were selected and tested until no major changes in output results were produced, when finer Δx and E values were substituted. The effectiveness of these computations was evaluated by comparing the calculated values with the experimental results produced during solution treatment of α and β brass, and during TLP-bonding of single-crystal nickel. The input values employed in these calculations are listed in Table 4-1. The phosphorus diffusion coefficient in liquid nickel is not available and is assumed to be 500 $\mu m^2/s$ (most diffusion coefficients in liquid metals range from 100-1000 $\mu m^2/s$ [Welty et al, 1984]). The input data for the α/β brass diffusion couple are the same

Table 4-1 Input parameters for numerical calculations

Figure Referred	Composition System	C_M (at.%)	C_{YII} (at.%)	C_{YI} (at.%)	C_F (at.%)	D_{II} ($\mu m^2/s$)	D_I ($\mu m^2/s$)	$2l$ (μm)	2L (μm)	Δy (μm)	E
Fig. 4-3	Ni-P	0	0.166 *	10.223 *	19	18 **	500	25	6025	1	0.01
Fig. 4-4	α/β-brass ***	29.1	32.5	36.9	39.4	5	100	381	1134	10	0.1
Fig. 4-5a	hypothetical ****	0	40	90	100	0.0603	0.0603	0.44	1.321	0.01	0.1
Fig. 4-5b	hypothetical ****	0	10	60	100	0.0603	0.0603	0.44	18.033	0.01	0.1
Fig. 4-5c	hypothetical ****	0	10	90	100	0.0603	0.0603	0.44	18.033	0.01	0.1

Data From

* Nash [1992]
** NaKao et al [1991]
*** Heckel et al [1975]
**** Pabi [1990]

as those used by Heckel et al [1972]. The inputs for Fig. 4-5 were designed by Pabi [1979] to test the applicability of different numerical models.

4.2.1. Comparison of Numerically Calculated Results with Experimental Values

4.2.1.1. TLP-Bonding of Nickel Single-Crystal

Fig. 4-3 compares the output of the computer model with the experimental results produced during TLP-bonding of single-crystal nickel base metal. It is apparent that the computed results are in good agreement with the experimental values, bearing in mind the difficulties in obtaining an accurate diffusion coefficient value for

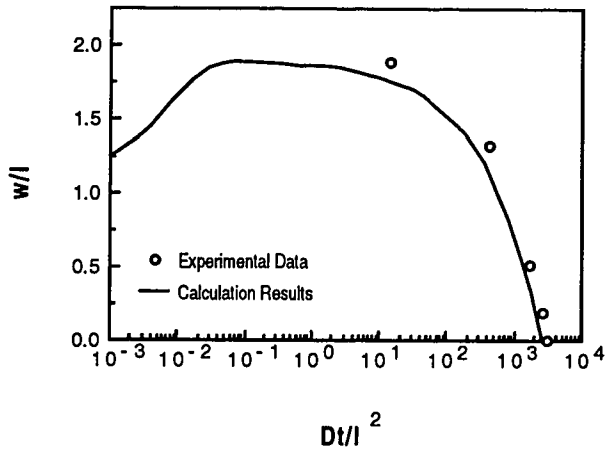

Fig. 4-3 Comparison of the calculated and experimental results during TLP-bonding of single-crystal nickel.

phosphorus in the liquid phase, and the error caused by the assumption that the phosphorus diffusion coefficients are independent of composition. It is important to point out that the excellent correspondence between calculated and experimental results occurs only when a single-crystal nickel base metal is employed during TLP-bonding. During modelling, it was assumed that there would be no effect of grain boundary regions on movement of the solid-liquid interface. When fine-grained nickel base metal is employed during TLP-bonding, there is a marked effect of grain boundaries on the rate of isothermal solidification (the rate of isothermal solidification increases when the grain size of the base metal decreases, also see §3.2). This aspect will be discussed in later chapters of this thesis.

4.2.1.2. Solution Treatment of α and β Brass Diffusion Couples

Fig. 4-4 compares the output of the numerical model with Heckel et al's [1975] experimental results and the model calculations produced by Tanzilli and Heckel [1968] and by Pabi [1979]. The TH (Tanzilli and Heckel) model indicates a larger amount of transient growth compared with the experimental results, and does not accurately correspond with experimental results during the final stage of the solution process. In this connection, Heckel et al [1972] added a dotted line to their calculated curve to account for this discrepancy (see Fig. 4-4). Pabi's model [1979] indicates faster solution kinetics late in the solution process in comparison with the experimental results. The output of the model developed in the present thesis has a better fit with the experimental results than the TH model or Pabi's models, althoughsome

deviation still exists late in the solution process. This difference between calculated and experimental test results may be attributed to errors in ascribing solubility and diffusion coefficient values, and to experiment errors during data collection.

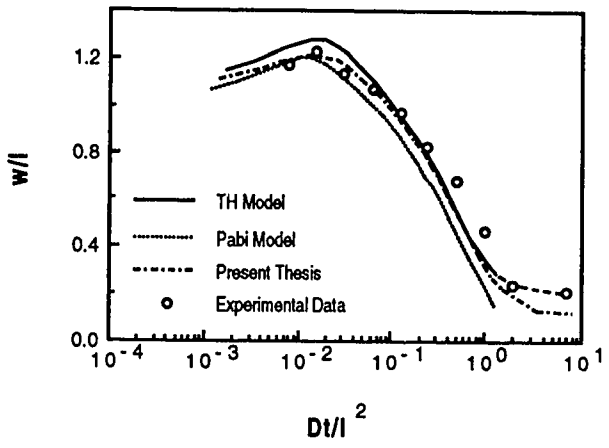

Fig. 4-4 Comparison of the calculated and experimental results during solution treatment of thin, multilayer α/β brass diffusion couples (using the experimental results indicated by Heckel et al, 1972).

4.2.2. Effectiveness of the Model Developed in This Thesis

4.2.2.1. Efficiency

The cpu times involved during modelling were compared at $\theta = 0$ (in the explicit scheme) and $\theta = \frac{1}{2} - \frac{(\Delta y)^2}{12D\Delta t}$ (in the implicit scheme) using a Silicon Graphics IRIS 4.0.1 Mini-computer. The cpu times are

400 and 7.9 seconds respectively for Curve a in Fig. 4-5. In the explicit case, the time step is limited to 8.0×10^{-4} sec and around 7.0×10^{4} cycles are required to complete the calculations. Using the implicit method, the time steps range from 1.85×10^{-5} to 0.285 sec and around 400 cycles are needed to complete the calculations. Although this difference in cpu time does not appear great, it becomes extremely important when TLP-bonding is modelled. When TLP-bonding of nickel base metal is modelled, the fully implicit scheme requires 3 minutes of cpu time, the calculation time steps range from 8.6×10^{-4} to 70 sec, and the number of calculation cycles is around 3500. However, when the explicit scheme is used, the time step must be less than 10^{-3} sec, the total processing time is around 9.0×10^{5} sec and 10^{8} calculation cycles are required during numerical modelling. It follows that the numerical model developed in this thesis has high efficiency. The cpu times involved in the TH and Pabi's model calculations were necessarily long since the explicit method was employed during their numerical calculations.

4.2.2.2. Accuracy

Apart from directly comparing with the experimental results, the output of the different models can also be compared using the hypothetical input values suggested by Pabi [9], namely:

(1) when the interface flux into the matrix exceeds that from the dissolving phase, there is no second phase growth (this is Curve a in Fig. 4-5);

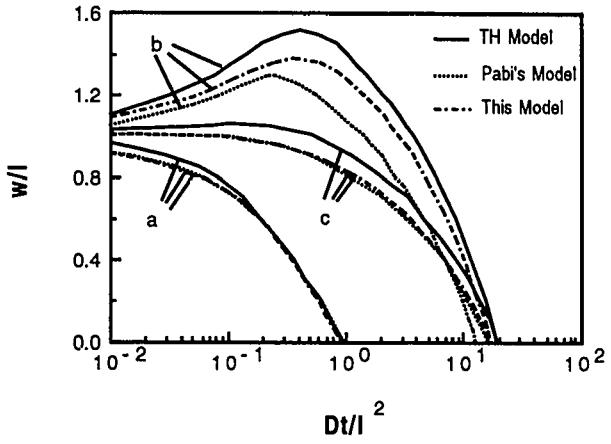

Fig. 4-5 Comparison of the output of the different computational models (TH-Tanzilli and Heckel's model, 1971 and Pabi's model, 1979).

(2) when (D_{II}/D_I) and $(C_F-C_{YI})/(C_{YII}-C_M)$ are both unity, there is zero interface movement for a short time period and then the second phase dissolves monotonically (this is Curve c in Fig. 4-5);

(3) when the flux into the second-phase exceeds that into the matrix, the second phase grows and then dissolves (this is Curve b in Fig. 4-5).

The output of the model developed in this thesis closely corresponds with that produced using Pabi's model (for Curves a and c). However, the TH model indicates an erroneous transient growth in Curve c because of errors in the flux term calculation in Eq. (4-20). This occurred due to the unequal grid size in the different phases during numerical modelling (see §2.4). When transient second-phase

growth occurs (Curve b), the model developed in the present thesis produces a better prediction than the models produced by the Tanzilli and Heckel [1968] and by Pabi [1979]. (This is clearly apparent based on an examination of Fig. 4-4.)

4.3. Application of the Model during TLP-bonding

The numerical model has been used to examine TLP-bonding. The input values employed during the numerical calculations are presented in Table 4-2. A wide range of input values were employed to indicate the effect of joining parameters on the completion time for TLP-bonding. For example, the solute diffusion coefficient in the solid varies from 0.1 $\mu m^2/s$ to 10.0 $\mu m^2/s$, and the diffusion coefficient in the liquid varies from 100 $\mu m^2/s$ to 1000 $\mu m^2/s$ (the diffusion coefficients in the solid and in the liquid encompass much of the range of values indicated in the literature [Welty et al, 1984]).

4.3.1. Kinetic Modelling of TLP-bonding

(1) Solute Distribution

Figs. 4-6 to 4-8 show the change in solute concentration distribution during base metal dissolution, isothermal solidification and homogenization (assuming an infinite heating rate to the bonding temperature). When the dissolution process is complete (at t = 3.36s) the solute concentration in the liquid is almost uniform. In addition, apart from the initial period of isothermal solidification, there is virtually no solute concentration change in the liquid during the isothermal solidification stage in TLP-bonding.

Table 4-2 Input values for numerical modelling of TLP-bonding

Figure Referred	C_M (at.%)	C_{YII} (at.%)	C_{YI} (at.%)	C_F (at.%)	D_{II} ($\mu m^2/s$)	D_I ($\mu m^2/s$)	$2l$ (μm)	2L (μm)	Δy (μm)	E
Fig. 4-6 to 4-15	0.1	1	10	20	10	500	30	10000	1	0.01
Fig. 4-16	0.1	1	10	20	1	100-1000	30	10000	1	0.01
Fig. 4-17	0.1	1	10	20	0.1-10	100	30	10000	1	0.01
Fig. 4-18	0.1	1-3	10	20	10	500	30	10000	1	0.01

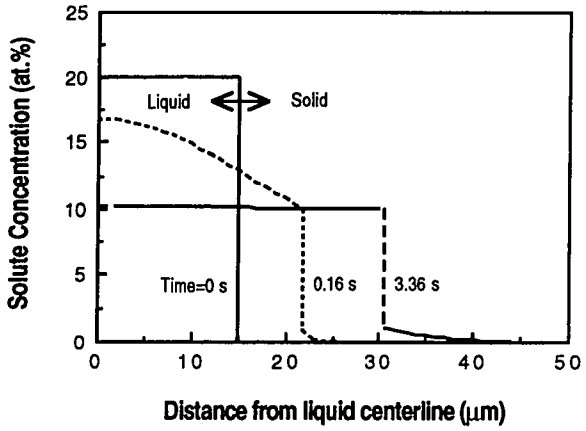

Fig. 4-6 Change in solute concentration profile during the base metal dissolution stage.

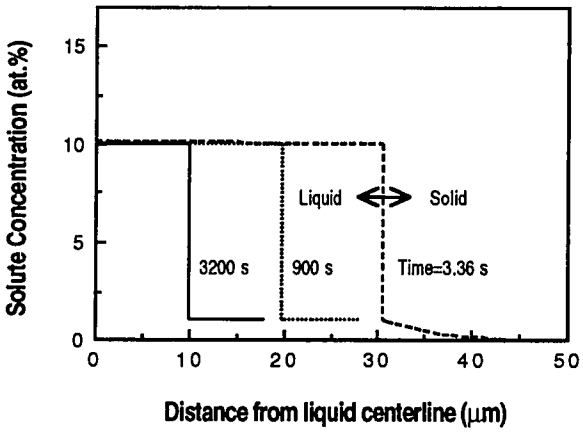

Fig. 4-7 Change in solute concentration profile during the isothermal solidification stage.

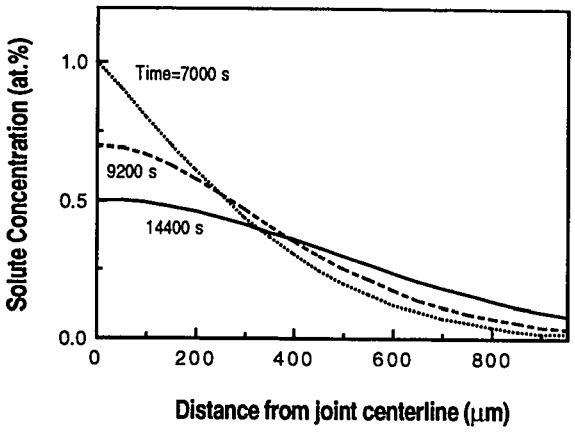

Fig. 4-8 Change in solute concentration profile during the homogenization stage.

(2) Movement of the Liquid-Solid Interface

Fig. 4-9 shows the change in liquid width with holding time during bonding (a logarithmic scale is used to show both of the dissolution and isothermal solidification stages). The details in Fig. 4-9 are simplified in Figs. 4-10 to 4-11 to confirm whether movement of the liquid-solid interface obeys the parabolic law during base metal dissolution and isothermal solidification. During base metal dissolution, movement of the liquid-solid interface does not obey the parabolic law. The deviation from linearity in Fig. 4-10 occurs since the solute distribution in the liquid is not uniform and interface movement is determined by the combined effects of flux delivery from the liquid and flux diffusion into the base metal (see Fig. 4-12).

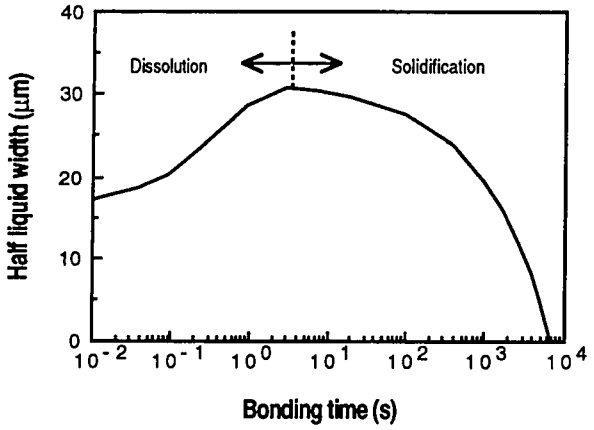

Fig. 4-9 Change in liquid width with bonding temperature during TLP-bonding.

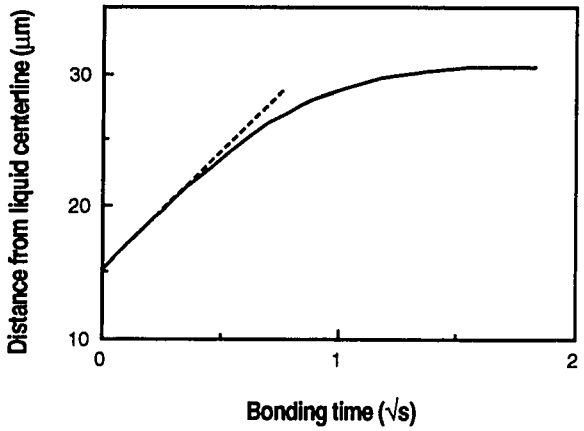

Fig. 4-10 Change in liquid width with bonding time during the dissolution stage.

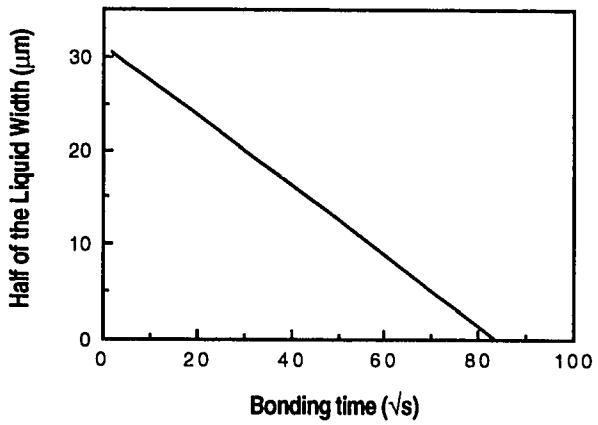

Fig. 4-11 Change in liquid width with bonding time during the isothermal solidification stage.

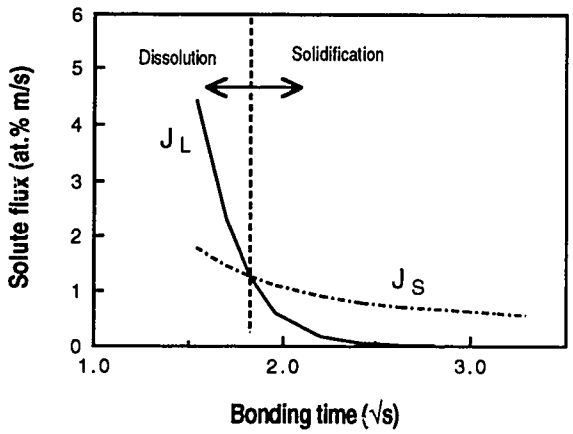

Fig. 4-12 Variation of the solute flux during the bonding period, J_L is the flux supplied by the liquid and J_S is the flux diffused into the base metal.

Later in the isothermal solidification process, however, the solute distribution in the liquid becomes uniform and the solute flux from the liquid is zero. Also, solute diffusion in the solid is very limited compared with the dimensions of base metal and consequently the situation can be treated as a semi-infinite case. At the initiation of the isothermal solidification stage, the solute flux from the liquid is not zero and this will produce a slight deviation from linearity (see Fig. 4-13).

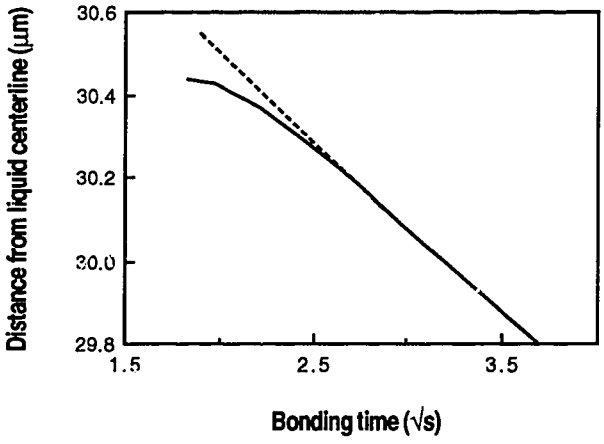

Fig. 4-13 Detailed analysis of the initial stage of isothermal solidification.

4.3.2. Comparison of Numerical Calculation with Analytical Solutions

(1) Isothermal Solidification

Many investigators have applied analytical methods to model the isothermal solidification and homogenization stages during TLP-bonding [Lesoult, 1976; Ikawa et al, 1979; Ikawa and Nakao, 1979; Tuah-Poku et al, 1988; Nakao et al, 1989 and Liu et al, 1991]. However, it is very difficult to obtain analytical solutions for the dissolution stage (see §2.7.1). In this section, the numerical output will be compared with the results of analytical solutions.

In the analytical solution for the isothermal solidification stage, it is assumed that movement of the solid-liquid interface (ΔX) obeys a parabolic law:

$$\Delta X=2\beta\sqrt{t} \tag{4-29}$$

where t is holding time during TLP-bonding and β can be calculated numerically using the following relation (see Appendix I):

$$(C_{L\alpha}-C_{\alpha L})\beta\sqrt{\pi} + \frac{\sqrt{D_S}(C_{\alpha L}-C_M)}{1-\mathrm{erf}(\frac{\beta}{\sqrt{D_S}})}\exp(-\frac{\beta^2}{D_S})=0 \tag{4-30}$$

Therefore, the solid-liquid interface movement is characterized by a constant β value which defines the rate of interface movement. The β parameter is a convenient monitor when the results of the analytical and numerical calculations are compared. In the numerical calculations, β is evaluated using the relation:

$$\beta = \frac{dY}{2d\sqrt{t}} = \sqrt{t}\,\frac{dY}{dt}. \qquad (4\text{-}31)$$

Fig. 4-14 shows the variation of the β parameter during base metal dissolution and subsequent isothermal solidification. β decreases progressively and approaches zero when base metal dissolution is

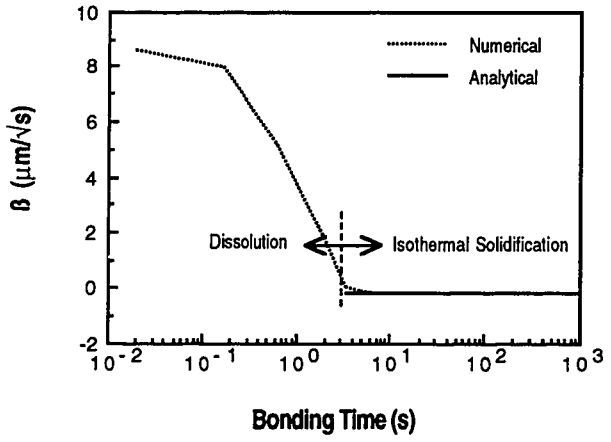

Fig. 4-14 Comparison between the numerical and analytical calculated β values.

nearly completed. β continues to decrease to a value of -0.185 $\mu m/\sqrt{s}$ and this value is identical with that produced using the analytical solution (Eq. (4-28)). It follows that the isothermal solidification stage during TLP-bonding can be readily estimated using an analytical

solution and that the completion time for isothermal solidification may be calculated using the relation:

$$t_s = \left(\frac{W_{max}}{4\beta}\right)^2 \tag{4-32}$$

where the maximum width of liquid phase, W_{max}, is calculated using the relation, $W_{max} = \frac{W_0 C_F}{C_{\gamma II}}$, if the diffusion during the dissolution stage is neglected. A relationship of this form (i.e., Eq. (4-32)) has been previously indicated by a number of investigators [Ikawa et al, 1979, Lesoult, 1979, Nakao et al, 1989, Sakamoto et al, 1989 and Liu et al, 1992]. In direct contrast, base metal dissolution depends on a non-parabolic relation and no single value of β value can characterize solid-liquid interface movement.

(2) Homogenization

Work will be described to examine if the thick layer solution (see §2.2.2) can be used to model the TLP-bonding process. In the thick layer solution, solute diffusion occurs wholly in the solid-state when the interlayer of thickness of 2h is inserted between two semi-infinite dimension specimens. The solute concentration attains its maximum value at the centerline of the specimen (when y=0) from Eq. (2-9), namely,

$$C_{max}=C(0,t)=C_M+ (C_0-C_M)\ erf\left(\frac{h}{4\sqrt{D_S t}}\right) \tag{4-33}$$

Assuming h is half the thickness of the filler metal and Co is the initial solute concentration in the filler metal, the calculation results using Eq. (4-33) are compared with the numerical calculated values in Fig. 4-15 (for the solute concentration at the specimen centerline during TLP-bonding). The numerical and analytical results are in close agreement during a portion of the homogenization cycle, although differences are apparent early and late in the processing cycle (see Fig. 4-15). It follows that the analytical solution could be used to model the homogenization stage during TLP-bonding. (The large difference between numerical and analytical solutions during base metal dissolution and isothermal solidification occurs because the analytical calculations assume that solute diffusion occurs wholly in solid-state and no liquid phase is formed.)

Ikawa and Nakao [1979] developed an analytical solution when they evaluated the homogenization during TLP-bonding of nickel-based superalloy material. In this case, the value of h was half the maximum liquid width at the end of the dissolution stage and C_0 equalled $C_{L\alpha}$. The advantage of the treatment used in this thesis is that there is no need to calculate the maximum liquid width using Eq. (4-33). Nakao et al [1990] found close agreement between the calculated and experimental values (for aluminium diffusion to the joint centerline). However, there was a clear difference between the experimentally-observed and calculated values early in the homogenization process. They suggested that this difference may have been caused by a critical assumption in their analytical calculations (that the aluminium

concentration at the bonded layer was uniform at the beginning of the homogenization period). Fig. 4-15 shows a similar deviation between the numerical and analytical results in the early stages of the homogenization stage. The deviation between the numerical and analytical results late in the homogenization stage in Fig. 4-15 is due to the semi-infinite test specimen assumption in the analytical calculations.

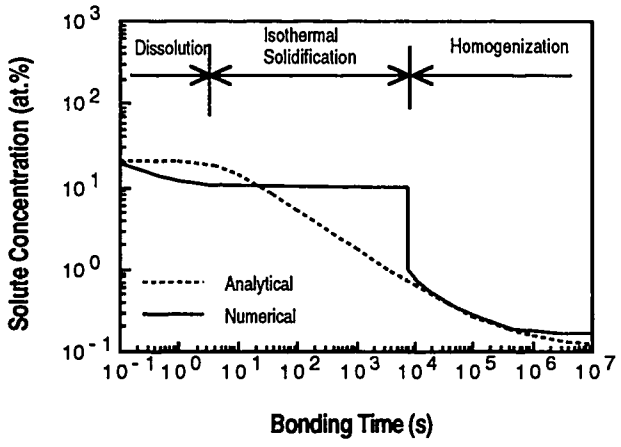

Fig. 4-15 Calculated changes in the solute concentration at the specimen centerline during TLP-bonding.

It may be concluded that the simple analytical solutions can be used to estimated the completion times for isothermal solidification and to estimate the solute concentration at the joint centerline. In analytical solutions, the error function is needed and Eq. (4-30) must

be solved numerically. It is worth noting that direct parameter input into the numerical program will allow prediction of the completion times for dissolution, isothermal solidification or homogenization (for any selected bonding temperature and filler metal/base metal combination). In effect, numerical modelling is particularly useful when complex joining situations are contemplated. This is shown in the following section.

4.3.3. Optimum Selection of Joining Parameters

Based on the close correspondence between the numerical calculations and the experimental results, the model output can be used to:

(1) predict the completion times required for dissolution, isothermal solidification and homogenization;

(2) predict the solute concentration distribution both in the solid phase and in the liquid phase throughout TLP-bonding; and

(3) select the optimum filler metal (chemistry, thickness) and bonding parameters (e.g., temperature) which will insure that the TLP-bonding operation will be completed within a reasonable time-frame.

It is well-understood that the filler metal must contain a melting point depressant which is soluble and has a high diffusivity in the base metal being joined. It is also easy to understand that the smaller the content of the melting point depressant, the faster the process will proceed, since the TLP-bonding depends directly on solute diffusion into the surrounding base metal (see §2-7). Figs. 4-16 and 4-

17 show the effect of varying the solute diffusion coefficients in the liquid and solid on the time required for completion of base metal dissolution, isothermal solidification and homogenization. In this thesis, the completion time required for the homogenization stage is arbitrarily defined as the time required to decrease the maximum solute concentration to <0.5 at.% at the specimen centerline. In practical TLP-bonding situations, the selected concentration value will be determined by the component manufacturing mechanical properties requirements.

The completion time required for base metal dissolution decreases when the solute diffusion coefficients in the solid and liquid phases are increased, with the solute diffusivity in the liquid having the most important effect. However, isothermal solidification and homogenization are only affected by the solute diffusivity in the base metal (the completion time for these stages decreases when the diffusion rate of the solute in the base metal increases). Since the completion time for base metal dissolution is very short compared to that required during isothermal solidification, these results indicate that TLP-bonding is principally-dependent on the solute diffusivity in the base metal.

It has been suggested that there will be an optimum bonding temperature during TLP-bonding, and that this will depend on the interplay of increasing solute diffusivity and decreasing the equilibrium solute concentration in solid (when the bonding

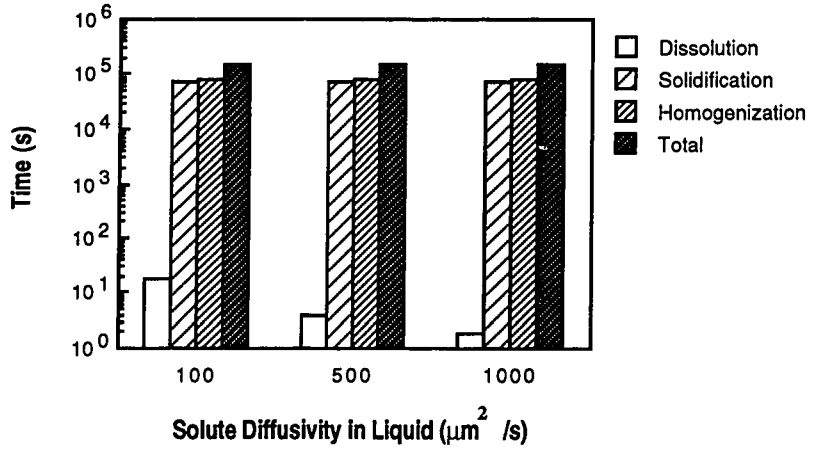

Fig. 4-16 Effect of solute diffusivity in the liquid on the completion times required for dissolution, isothermal solidification, and homogenization.

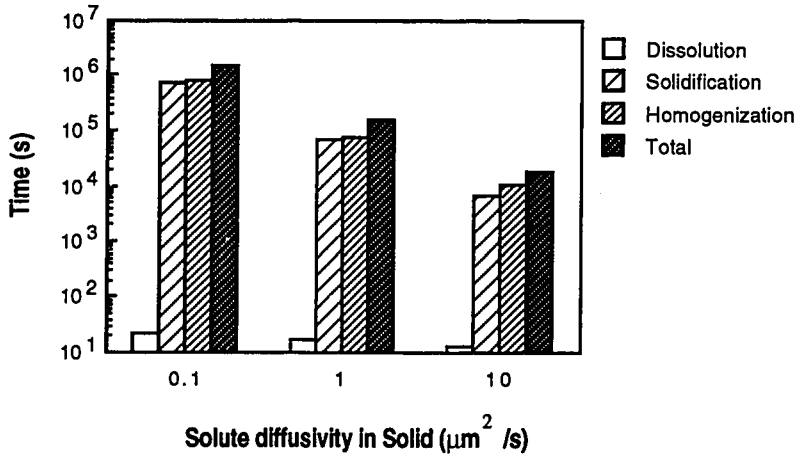

Fig. 4-17 Effect of solute diffusivity in the solid on the completion times required for dissolution, isothermal solidification, and homogenization.

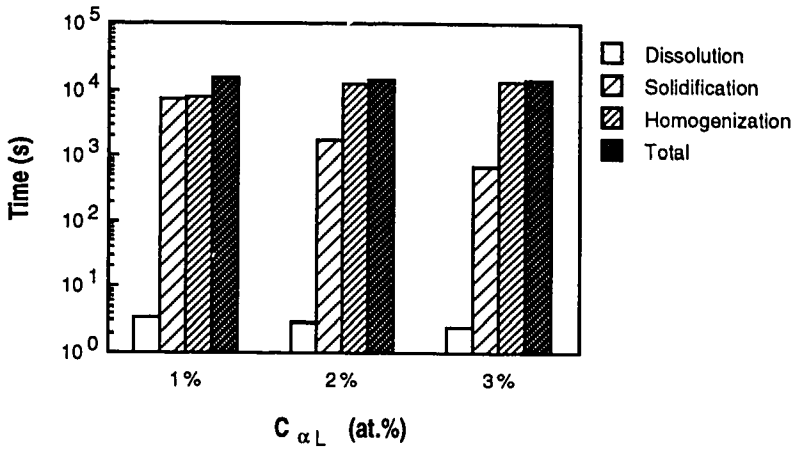

Fig. 4-18 Effect of the solidus composition at the bonding temperature, $C_{\alpha L}$, on the completion times required for dissolution, isothermal solidification, and homogenization.

temperature is increased) [Tuah-Poku et al, 1988]. However, this view is based wholly on a consideration of the isothermal solidification stage during TLP-bonding. The critical homogenization stage is not taken into account. Fig. 4-18 shows the influence of changes in the equilibrium solute content in solid at the bonding temperature, C_{YII}, on the completion times required for base metal dissolution, isothermal solidification and homogenization. C_{YII} may be varied by altering the solute content in the filler metal, or by changing the bonding temperature. Although increasing the C_{YII} value decreases the time required for completion of isothermal solidification, it also increases the time required for homogenization. In fact, the time required for

completion of the entire TLP-bonding cycle will not be affected by an increase in the $C_{\gamma II}$ (or $C_{\alpha L}$) value. This means the highest bonding temperature should be selected when the TLP-bonding process is to be optimized (since this will increase the rate of solute diffusion into the base metal).

4.4. Summary

A fast and accurate, fully implicit finite difference model has been developed that simulates diffusion-controlled, two-phase moving interface problems. The computed results are in good agreement with the experimental results produced during TLP-bonding of single-crystal nickel base metal using Ni-19at.%P filler metal, and during the solution treatment of thin, multilayer α and β brass diffusion couples. The model developed in this thesis produces results that compare well with the output of previous numerical models proposed by Tanzilli and Heckel [1968], and Pabi [1979].

The numerical model has been used to examine the liquid-solid interface migration during base metal dissolution and liquid phase isothermal solidification, and to simulate solute redistribution during homogenization. The main results comprise:

(1) The numerical model predicts the optimum joining parameters during TLP-bonding. The optimum conditions occur during TLP-bonding when the solute diffusivity in the liquid and solid phases increases, and when the highest bonding temperature is employed.

(2) Base metal dissolution cannot be represented using a parabolic law. However, the isothermal solidification stage can be readily estimated by assuming a linear relation between liquid-solid interface displacement and the square-root of the holding time at the bonding temperature. The values produced using numerical and analytical modelling are identical in this case. Also, an analytical solution can be used to estimate the solute concentration at the specimen centerline following a given holding period during the homogenization stage.

Chapter 5

Numerical Model: Effect of Grain Boundaries on Process Kinetics

In this chapter, a numerical model will be developed to examine the influence of grain boundary diffusion and grain boundary migration on the process kinetics during the two-phase diffusion-controlled transformations. The process kinetics are examined by considering the total amount diffused into the base metal, not by calculating the location of the moving interface.

5.1. Computer Simulation

5.1.1. Physical Model

5.1.1.1. The Amount of Solute Diffused

As mentioned in §2.1, the growth and/or dissolution of the unstable phase is the direct result of solute transfer across the interface between the unstable phase and the matrix. It follows that the total amount diffused across the interface at any given time may be used as a monitor of process kinetics. For example, during the isothermal solidification stage of TLP-bonding, the relation between the liquid width, W(t), and the amount diffused into the base metal, M(t), is given as (also see Fig. 5-1):

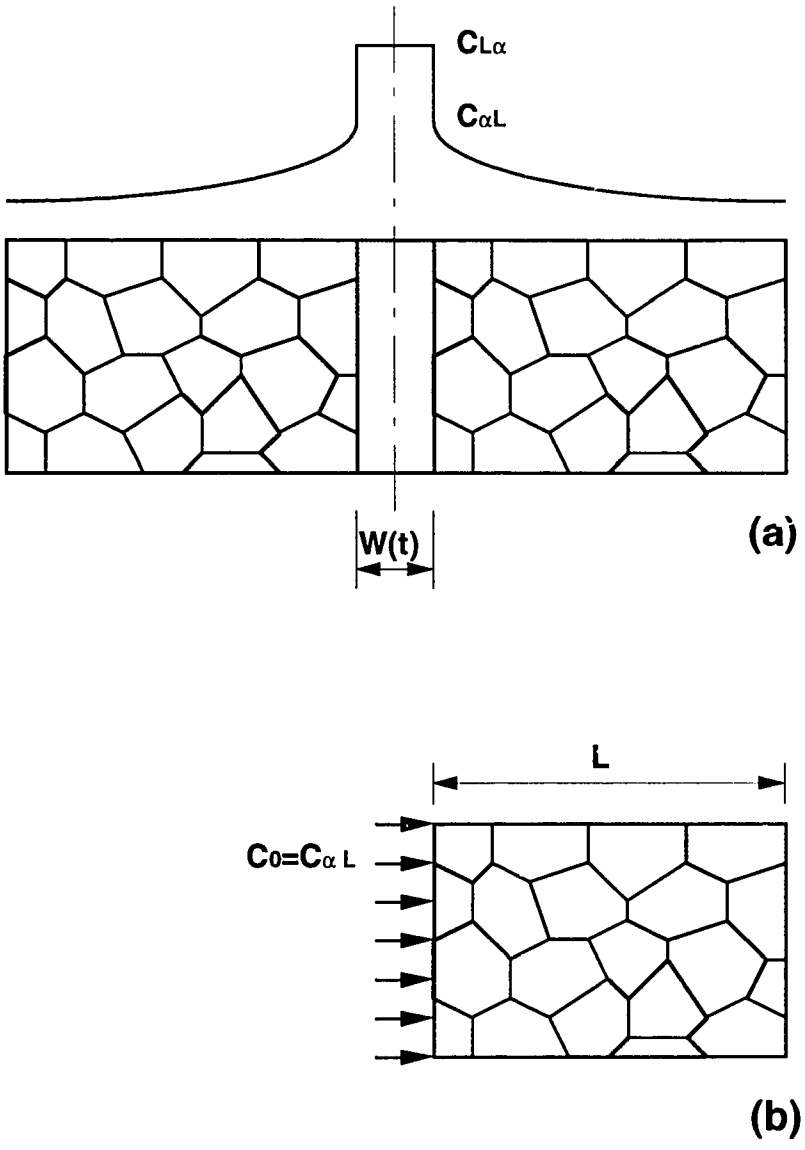

Fig. 5-1 Development of a grain boundary model for analyzing TLP-bonding (a) isothermal solidification stage; (b) the exchange experiment model.

$$\{W_{max}-W(t)\}C_{L\alpha}=2M(t) \qquad (5\text{-}1)$$

where W_{max} is the maximum liquid width and $C_{L\alpha}$ is the solute concentration in the liquid at the interface. It follows that the process kinetics during isothermal solidification might be effectively described by M(t), the amount of solute diffused, instead of W(t), the liquid width present during TLP-bonding. Of course, not every two-phase diffusion process has such a simple relation between the M(t) and W(t) as in Eq. (5-1). However, calculating the amount of solute diffused with processing time is indeed a useful indication of process kinetics. For this reason, the present chapter examines the factors which affect M(t).

5.1.1.2. The "Exchange Experiment" Model

If the second phase is ignored and the solute concentration on the new surface is maintained at the concentration of the interface when two phases are actually present, the model system changes to that in an "exchange experiment". In an exchange experiment, diffusion occurs from a surface at constant solute concentration into material that is free of diffusant [Lidiard and Tharmalingam, 1959]. For example, during isothermal solidification in TLP-bonding, liquid phase is not considered and it is simply assumed that the base metal has a free surface where the solute concentration is maintained at $C_0=C_{\alpha L}$ (see Fig. 5-1(b)). The numerical calculation evaluates the amount of solute diffused into the base metal from this surface and the joining process

terminates when the total amount of diffusing solute attains the initial solute content in the filler metal (with the assumption that any solute diffusion that occurs during the dissolution stage can be neglected). The advantage of this novel approach is that the problem becomes much simpler and we only have a one-phase diffusion process.

The computer model in this chapter evaluates the total amount of material which diffuses as a function of holding time during an 'exchange' experiment (see the model illustrated in Fig. 5-2). It is assumed that the grain boundary regions are perpendicular to the free

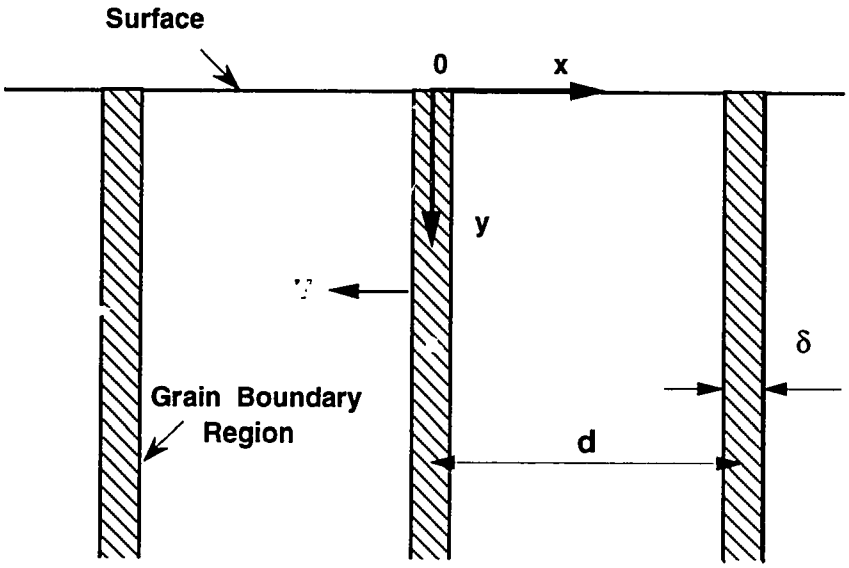

Fig. 5-2 Schematic of the grain boundary diffusion model.

surface, have thickness, δ, and are at a constant spacing, d. The grain boundaries move at a constant velocity, V, in a direction parallel to the free surface. The other key assumptions during modelling are:

(1) The diffusion coefficients, molar volumes, and activity coefficients involved are independent of composition change.

(2) The second phase is much smaller than the base metal; therefore, the changes in dimensions of the base metal are negligible.

(3) The moving interface has no effect on the distribution of the diffusing solute in the base metal. This applies during TLP-bonding, since the maximum difference of solute concentration in the base metal is much less than that at the interface (see Appendix I).

(4) No interaction occurs between the diffusing solute and the grain boundary regions.

5.1.2. Problem Formulation

Because of symmetry, only one unit containing a grain boundary is considered. The y-axis is along the moving grain boundary and the x-axis is parallel to the direction of grain boundary motion (see Fig. 5-2). The calculation region is defined by $\Omega \in \{x=-d/2,\ d/2;\ y=0,\ L/2\}$, where L/2 (=1 mm) is the specimen length. The governing equations for the change in diffusant concentration with holding time are [Fisher, 1951; Whipple, 1954; and Mishin and Razumovskii, 1992]:

$$\frac{\partial C}{\partial t} = D_l \left(\frac{\partial^2 C}{\partial x^2} + \frac{\partial^2 C}{\partial y^2} \right) - V \frac{\partial C}{\partial x}, \qquad |x| > \frac{\delta}{2} \qquad (5\text{-}2)$$

in the bulk material, and,

$$\frac{\partial C_{gb}}{\partial t} = D_{gb}\frac{\partial^2 C_{gb}}{\partial y^2} + \frac{D_l}{\delta}\left(\frac{\partial C}{\partial x}\right)_{x=+\delta/2} - \frac{D_l}{\delta}\left(\frac{\partial C}{\partial x}\right)_{x=-\delta/2}, \quad |x| < \frac{\delta}{2} \tag{5-3}$$

at the grain boundary region. In these equations, C and C_{gb} are the bulk material and grain boundary concentrations, D_l and D_{gb} are the diffusion coefficients in the bulk material and at the grain boundary, V is rate of grain boundary migration, and the grain boundary thickness, δ, is assumed to be 5.0×10^{-10} m. At the interface between the bulk materials and the grain boundary, $|x| = \frac{\delta}{2}$,

$$C_{gb} = kC. \tag{5-4}$$

The parameter, k, is a material constant [Peterson, 1983] and is taken to be unity in all calculations. From Eqs. (5-3) and (5-4):

$$\frac{\partial C}{\partial t} = D_{gb}\frac{\partial^2 C}{\partial y^2} + \frac{D_l}{k\delta}\left(\frac{\partial C}{\partial x}\right)_{x=+\delta/2} - \frac{D_l}{k\delta}\left(\frac{\partial C}{\partial x}\right)_{x=-\delta/2}, \qquad |x| = \frac{\delta}{2} \tag{5-5}$$

The initial and boundary conditions are:

$$C(x,y,0) = 0 \tag{5-6}$$

$$C(x,0,t) = C_0 \tag{5-7}$$

$$\left(\frac{\partial C}{\partial y}\right)_{y=L} = 0 \tag{5-8}$$

where C_0 is the concentration at the free surface.

The mean concentration at penetration depth, y, is given as:

$$\bar{C}(y,t) = \frac{1}{d}\int_{-d/2}^{d/2} C(x,y,t)dx \qquad (5\text{-}9)$$

and the total amount diffused within domain Ω is:

$$M(t)= \iint_{\Omega} C(x,y,t)dxdy \qquad (5\text{-}10)$$

5.1.3. Numerical Analysis

The diffusion equations described in the preceding section are solved numerically using an explicit finite difference method. The finite difference grid is shown in Fig. 5-3. The interval between lines parallel to the y-axis is Δx (=d/20). The intervals between the lines parallel to the x-axis are Δy=2μm when y < 8μm, Δy=5μm when 8μm < y < 28μm and Δy=50μm when y > 28μm. Using the forward-time, centred-space finite difference approximation, Eqs. (5-2) and (5-5) can be written as:

$$\frac{C_{i,j}^{t+\Delta t}-C_{i,j}^{t}}{\Delta t} = D_l\frac{C_{i+1,j}^{t}-2C_{i,j}^{t}+C_{i-1,j}^{t}}{(\Delta x)^2} + D_l\frac{C_{i,j+1}^{t}-2C_{i,j}^{t}+C_{i,j-1}^{t}}{(\Delta y)^2} + V\frac{C_{i+1,j}^{t}-C_{i-1,j}^{t}}{2\Delta x} \qquad (5\text{-}11)$$

$$\frac{C_{i,j}^{t+\Delta t}-C_{i,j}^{t}}{\Delta t} = D_{gb}\frac{C_{i,j+1}^{t}-2C_{i,j}^{t}+C_{i,j-1}^{t}}{(\Delta y)^2} + \frac{D_l}{k\delta}\frac{-3C_{i,j}^{t}+4C_{i+1,j}^{t}-C_{i+2,j}^{t}}{2\Delta x}$$

$$-\frac{D_l}{k\delta}\frac{3C_{i,j}^{t}-4C_{i-1,j}^{t}+C_{i-2,j}^{t}}{2\Delta x} \qquad (5\text{-}12)$$

5.1.3.1. Stability Criterion

Eq. (5-11) is a typical transport equation, and its stability analysis can be found in literature, e.g., in the paper by Noye [1982]. The calculation time step Δt_1 must be,

$$\Delta t_1 \leq \frac{(\Delta x)^2(\Delta y)^2}{2D_l[(\Delta x)^2+(\Delta y)^2]} \qquad (5\text{-}13)$$

The stability analysis of the grain boundary diffusion Eq. (5-12) requires:

$$\Delta t_2 \leq \frac{\delta\Delta x(\Delta y)^2}{2[\delta\Delta x D_{gb}+2(\Delta y)^2 D_l]} \qquad (5\text{-}14)$$

Further details are provided in Appendix II and the calculation time step is:

$$\Delta t \leq \min\{\Delta t_1 , \Delta t_2\}. \qquad (5\text{-}15)$$

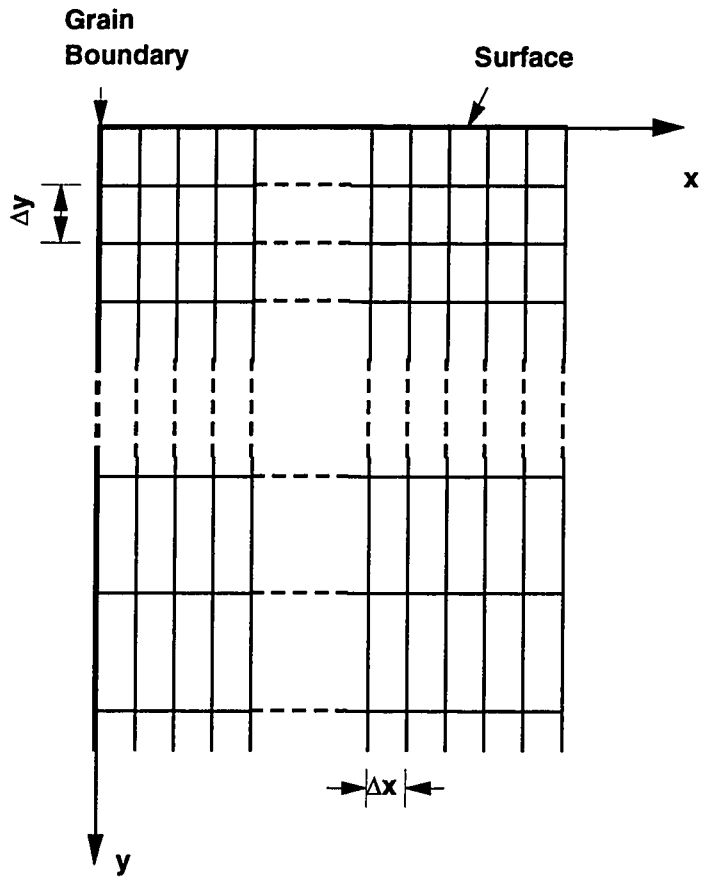

Fig. 5-3 Finite difference grid used in the grain boundary diffusion model.

5.1.3.2. Consistency Analysis

The analysis of the compatibility of finite difference Eq. (5-11) with respect to partial differential Eq. (5-2), confirms that Eq. (5-11) introduces a numerical diffusion term, $(\frac{1}{2} V^2 \Delta t) \frac{\partial^2 C}{\partial x^2}$ (A similar effect

is indicated in the paper by Noye [1982]). Because of this, the time step must be small enough so that this *fictitious* diffusion term is much less than the true diffusion coefficient value. When the time step satisfies the criterion given by Eq. (5-15), the fictitious diffusion coefficient ($\frac{1}{2} V^2 \Delta t$) is approximately $10^{-4} \sim 10^{-5}$ of the real diffusion coefficient, D_l.

A consistency analysis of the grain boundary diffusion equation indicates that the finite difference approximation (5-12) is consistent with the grain boundary diffusion equation (5-5) (for further information, see Appendix III).

5.2. Results and Discussion

5.2.1. Influence of Grain Boundary Diffusivity

Fig. 5-4 shows the effect of grain boundary diffusivity and of grain size on the ratio of M_p/M_s, where M_p is total amount diffused into a polycrystalline material and M_s the total amount diffused in a single-crystal case. The influence of the grain boundary regions depends on the grain size and on the D_{gb}/D_l ratio. At low temperatures ($T < 0.5\text{-}0.75T_m$, where T_m is the equilibrium melting temperature of the material in degrees Kelvin) the D_{gb}/D_l ratio is 10^5 or higher. The influence of grain boundaries on diffusional transport is much greater under these conditions. However, at high temperatures ($T > 0.75\ T_m$), the D_{gb}/D_l ratio is 10^3 or less and consequently Fig. 5-4 indicates that the contribution that results from grain boundary diffusion will be

much less. Fig. 5-4 also shows that the contribution due to grain boundary diffusion increases when the grain size becomes smaller.

5.2.2. Influence of Grain Boundary Migration

Fig. 5-5 shows the effect of grain boundary migration on the M_v/M_p ratio, where M_v is the total amount diffused into a polycrystalline material that has moving grain boundaries, and M_p is the total amount diffused into a polycrystalline material, when the grain boundaries are stationary. Grain boundary migration speeds up mass transfer during part of the holding period, and during this period more diffusion occurs when the grain size, the rate of the grain boundary migration and the D_{gb}/D_l ratio are increased.

Increased diffusion due to grain boundary migration can be explained by the build-up in diffusant material in the wake of the moving grain boundary (see Fig. 5-6). For short holding times (for small lattice diffusion distances), the migrating grain boundary has little influence on the concentration profile and consequently, there is negligible difference between total amount diffused in the migrating and stationary grain boundary situations. However, when the processing time increases, more diffusant is built up in the wake of the moving grain boundary and therefore, more material is diffused into the specimen. For long holding times (large diffusion distances), the

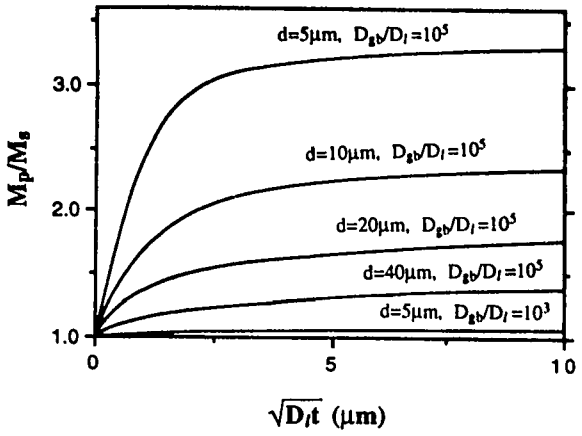

Fig. 5-4 The effect of grain size and of D_{gb}/D_l on the M_p/M_s ratio.

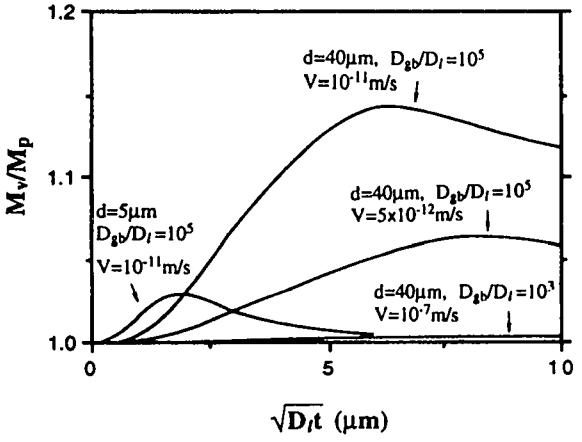

Fig. 5-5 The effect of grain boundary migration on the M_v/M_p ratio.

difference in the concentration profiles decreases continuously: the total amount diffused via migrating and stationary grain boundaries become the same at very long holding times.

The ratio M_v/M_p attains a maximum value when $\sqrt{D_i t} + Vt$ approaches the grain size, d (see Table 5-1). Cahn and Balluffi [1979] indicated that the boundary between Type B and Type A kinetics occurred when $\sqrt{D_i t} + Vt = d$. They did point out, however, that although their curves indicated a sharp transformation from Type A and Type B behavior, they should really be considered as transition regions.Both Mishin and Razumovskii [1992] and Cermak [1990] pointed out that migrating grain boundaries spread the diffusant in a relatively thin layer near the surface of the sample. Fig. 5-7 shows that the calculated diffusant distribution in the y-direction. It is apparent that migrating grain boundaries enrich the near-surface region in diffusant and deplete regions far from the surface. (In Figure 5-7, $\bar{C}_v$ is the mean diffusant concentration in a polycrystalline material with moving grain boundaries, and $\bar{C}$ is the mean diffusant concentration in a polycrystalline material that has stationary grain boundaries.)

5.2.3. Apparent Diffusion Coefficient

When the surface is maintained at constant concentration, C_0, anddiffusion takes place into material that is initially free of diffusant, the analytical solution for the amount diffused (M_s) into a semi-infinite, single crystal is [Crank, 1975]:

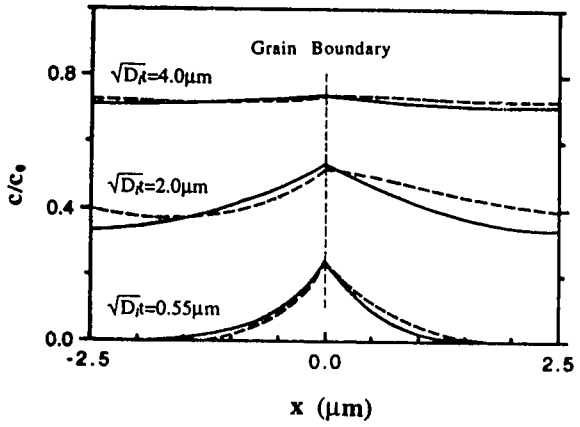

Fig. 5-6 Concentration profile along x-direction, at y = 6μm, when d = 5μm, $D_{gb}/D_l = 10^5$, and V = 10^{-11}m/s. The dashed line is for a migrating grain boundary and the solid line is for a stationary grain boundary.

Table 5-1 $\sqrt{D_l t}$ + Vt values where the M_V/M_P ratio reaches its maximum value

d (μm)	V (x10^{-12}m/s)	t (x10^{-5}s)	$\sqrt{Dt}$ + Vt (μm)
5	10	3.0	4.7
40	10	36.0	42.0
40	5	67.0	41.7

$$M_S = 2C_0\sqrt{\frac{D_l t}{\pi}} \qquad (5\text{-}16)$$

Assuming a single apparent diffusion coefficient (D_{app}), instead of individual lattice and grain boundary diffusion coefficients, the total amount diffused (M_p) in a polycrystalline material will be:

$$M_p = 2C_0\sqrt{\frac{D_{app}t}{\pi}} \tag{5-17}$$

Combining Eqs. (16) and (17):

$$D_{app} = D_l\left(\frac{M_p}{M_s}\right)^2 \tag{5-18}$$

From this relation, Fig. 5-4 indicates that, in a polycrystalline material, the D_{app}/D_l ratio increases when the holding time increases and then tends to a constant value at long processing times. Assuming that the diffusion process reaches a steady-state, when the lattice diffusion distance is much larger than the grain size, then [Porter and Eastering, 1992]:

$$D_{app} = D_l\left(1 + \frac{\delta}{d}\frac{D_{gb}}{D_l}\right) \tag{5-19}$$

This relation is very similar to Eq. (2-50) that Hart [1957] derived based on generalized "random walk" considerations. The numerical prediction for the D_{app}/D_l ratio can be calculated using the results in Fig. 5-4 and Eq. (5-18). Table 5-2 compares the numerical values

withthose produced using Eq. (5-19). It is apparent that Eq. (5-19) provides a satisfactory approximation for the apparent diffusion coefficient in polycrystalline material, when long processing times occur and $\sqrt{D_l t}$
exceeds d. This point is further illustrated in Fig. 5-8, where the numerical calculations are extended so that the lattice diffusion distance is 10 times larger than $\frac{d}{2}$ (L=1.5mm in this calculation). The results in Fig. 5-8 are quite different from those indicated by Campbell [1974], since the average concentration profile is that in a homogeneous medium, that has an apparent diffusion coefficient equal to the grain boundary diffusion coefficient. This difference between the results in this study and these of Campbell may be due to underlying assumptions in each case. A continuous source is used in the present study, while Campbell analyzed diffusion from an instantaneous source.

Both lattice diffusion coefficient, D_l, and grain boundary diffusion coefficient, D_{gb}, are used in numerical calculations using the two-dimensional model. If the model is modified to examine the one-dimensional case, a single lattice diffusion coefficient is required and this can be taken as the apparent diffusion coefficient (calculated using Eq. (5-19)). The solute concentration profiles in the one-dimensional and two-dimensional cases are be compared in Fig. 5-9 (the mean solute concentration at penetration depth, y, in two-

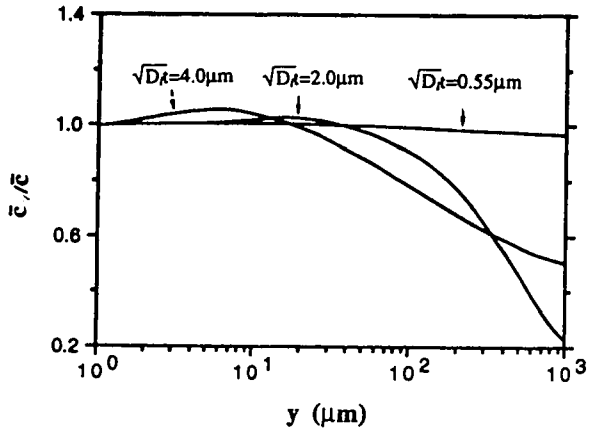

Fig. 5-7 The change in the $\bar{c}_v/\bar{c}$ ratio along the y-direction, when d = 5μm, $D_{gb}/D_l = 10^5$, and V = 10^{-11}m/s.

Table 5-2 D_{app}/D_l ratio values calculated when $D_{gb}/D_l = 10^5$

d (μm)	$\frac{\sqrt{Dt}}{d}$	$\frac{D_{app}}{D_l}$, by Eq. (5-18)	$\frac{D_{app}}{D_l}$, by Eq. (5-19)
5	2	10.89	11
10	1	5.48	6
20	0.5	3.04	3.5
40	0.25	1.91	2.25

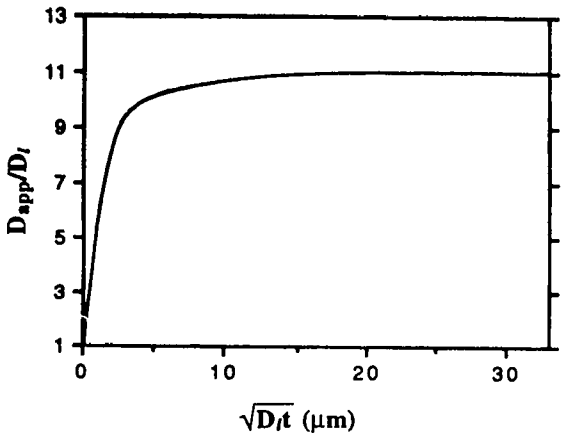

Fig. 5-8 The relation between the lattice diffusion distance $\sqrt{D_l t}$ and the D_{app}/D_l ratio, when d = 5μm and $D_{gb}/D_l = 10^5$.

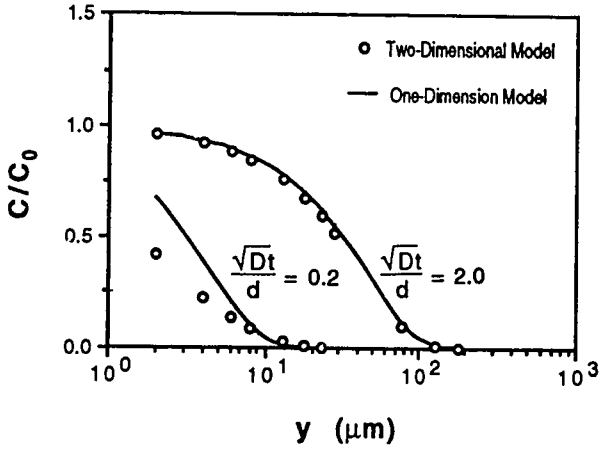

Fig. 5-9 The change in the $\bar{C}/C_0$ ratio along y-direction. In the grain boundary diffusion model, $\delta = 5x10^{-4}$μm, d = 5μm, $D_{gb}/D_l = 10^5$; in the one-dimensional model, $D=D_{app}= D_l(1+ \frac{\delta}{d}\frac{D_{gb}}{D_l})$.

dimensional model is given by Eq. (5-9)). Both results are identical when the diffusion distance is twice the grain size, d. This provides the further evidence that an apparent diffusion coefficient exists which combines the effects of the lattice diffusion coefficient and the grain boundary diffusion coefficient.

The difference in the total amount diffused in the migrating and stationary grain boundary situations decreases when $\sqrt{D_i t}$ +Vt is much larger than d. In this situation, the apparent diffusion coefficient can also be calculated using Eq. (5-19), as Cahn and Balluffi [1979] suggested.

5.2.4. Influence of Grain Boundary Regions on the Isothermal Solidification during TLP-bonding

As pointed out in Section 2.7., the completion time for isothermal solidification during TLP-bonding can be estimated using the relation (see Appendix I for further details):

$$t = \left(\frac{C_F W_0}{C_{\alpha L}}\right)^2 \frac{\pi}{16 D_S} \qquad (5\text{-}20)$$

where C_F is solute concentration in the filler metal, W_0 is the initial width of the filler metal and D_S is the solute diffusion coefficient in the solid. Based on the results described in this chapter, Eq. (5-20) can be modified to take grain boundary diffusion into account,

$$t = \left(\frac{C_F W_0}{C_{\alpha L}}\right)^2 \frac{\pi}{16 D_{app}} \qquad (5\text{-}21)$$

where D_{app} is the apparent diffusion coefficient. This equation can be used to calculate the completion time for isothermal solidification during TLP-bonding if the D_{app} is known, or to calculate D_{app} if the completion time for isothermal solidification is experimentally measured.

5.3. Summary

A numerical model was developed that indicates in a continuous manner the effect of increased diffusivity at grain boundary regions, and of grain boundary migration on the total amount of solute diffused and hence, on the process kinetics during two-phase diffusion-controlled problems. The principal conclusions are:

1. The influence of grain boundary regions on the total amount of solute diffused depends on the grain size, and the ratio of grain boundary diffusion coefficient and lattice diffusion coefficient, D_{gb}/D_l. When the D_{gb}/D_l ratio is high (for temperatures in the range, $T < 0.5\text{-}0.75T_m$), the influence of grain size on the total amount diffused is marked and decreasing the grain size increases the total amount diffused. When the D_{gb}/D_l ratio is low, i.e., 1000 or less (at high processing temperatures in the range, $T > 0.75T_m$), the influence of grain size on the total amount diffused is small.

2. The apparent diffusion coefficients in Type B and Type A kinetic regimes, and in the transition regime between Type B and Type A behavior, are calculated using the numerical model.

3. When $\sqrt{D_l t}$ is larger than the grain size, d, the numerical calculations support Hart's analysis [1957], that an apparent diffusion coefficient exists. This apparent diffusion coefficient can be approximated using the relation, $D_{app} = D_l\left(1 + \frac{\delta}{d}\frac{D_{gb}}{D_l}\right)$.

4. Grain boundary migration increases the total amount diffused during only part of the holding period. During this period, the total amount diffused increases, when the grain size, the D_{gb}/D_l ratio, and the rate of grain boundary migration increase. For short processing times, grain boundary migration has negligible effect on the total amount diffused and, for long holding times, the total amount diffused is also similar in stationary and migrating grain boundary situations.

Chapter 6

Numerical Model for Grain Boundary Grooving

In this chapter, a numerical model will be developed for the evolution of grain boundary grooves during two-phase diffusion-controlled transformation. This model includes the following factors: the concentration gradient in each phase, the excess chemical potential resulting from both the balance between the grain boundary free energy and the interfacial free energy, and from the gradient of interfacial curvature.

6.1. Computer Simulation

A quantitative description of grain boundary grooving depends on finding the solution to a two-dimensional, diffusion-controlled, non-steady-state moving interface problem. No published work has dealt with such a problem, for the boundary conditions that apply in the present thesis.

6.1.1. Physical Model

In practical situations, grain boundary regions in the base metal are not planar, they intersect the interphase interface at different angles and at different intervals. However, this situation is extremely difficult to model due to its complexity. In the present thesis, a

simple and symmetrical model is assumed where grain boundaries are planar and parallel with each other, and intersect the interface at right angles at constant intervals (see Fig. 6-1). The solute distribution and the interface position can be obtained by solving the diffusion

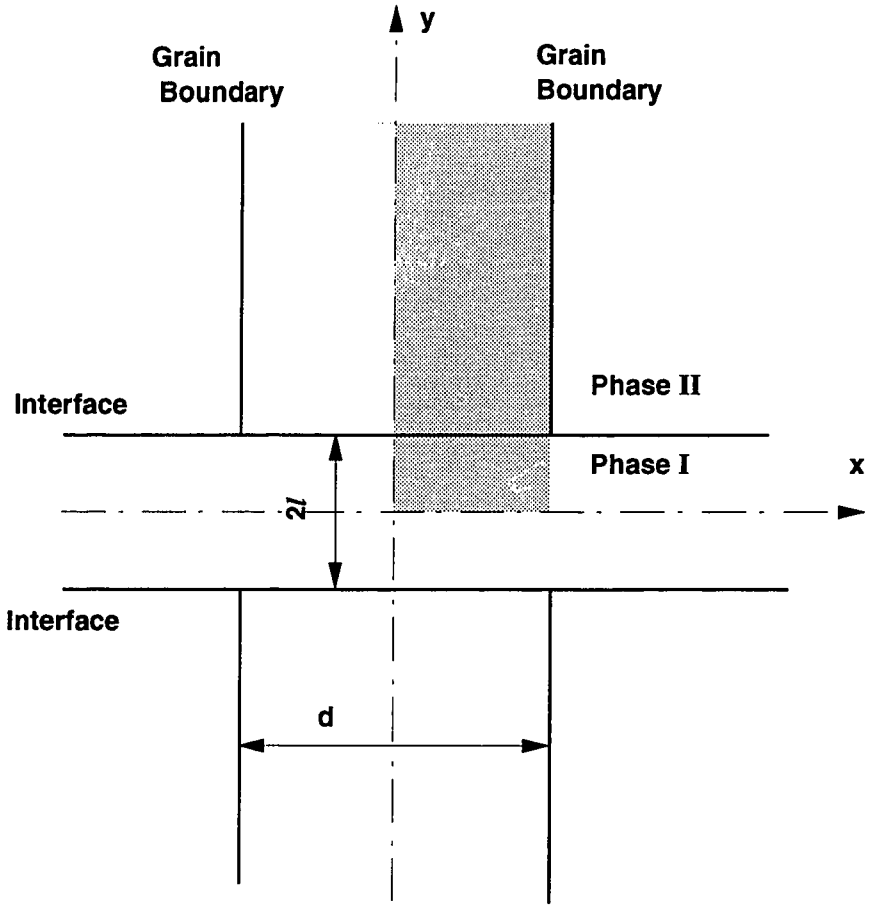

Fig. 6-1 Schematic of the model indicating grain boundary groove formation.

equations in the shadowed region in Fig. 6-1 with suitable initial and boundary conditions. In Fig. 6-1, no grain boundaries are assumed in the second phase (Phase I), which is an exact situation when Phase I is a fluid.

Grain boundary grooving in two-phase diffusion-controlled problems depends on the following driving forces, transport mechanisms and effects:

(1) Driving forces: the concentration gradient and the excess chemical potential resulting from the balance between the grain boundary free energy and the interfacial free energy at grain boundary triple junctions, and from the gradient of interfacial curvature;

(2) Transport mechanisms: volume diffusion in each phase, interfacial diffusion and grain boundary diffusion;

(3) Other factors: grain boundary segregation and the melting point difference between the grain boundary and the bulk region.

Because of such complexity, it is very difficult to take all the above factors into account. As a first approximation, the transport mechanism involves only volume diffusion in both phases and the driving force includes all three different gradients indicated above.

The following assumptions are made to simplify the mathematical calculations:

(1) The diffusion coefficient, molar volume and activity coefficient of the solute are independent of composition. The molar volume of the both phases are identical;

(2) In liquid-solid situation, flow of the liquid phase as a result of the convection and stirring is negligible, and hence, the flow of solute and solvent elements required for the migration of the liquid-solid interface depend only on interdiffusion;

(3) Local equilibrium exists at the interface, and therefore the compositions of each phases on the interface can be derived using the relevant equilibrium phase diagram;

(4) No intermediate phase is formed;

(5) The Kirkendall effect is negligible.

6.1.2. Problem Formulation

The change of the solute concentration in both phases at points far from the interface and from the grain boundary can be described as follows:

$$\frac{\partial C_I}{\partial t} = D_I \nabla^2 C_I \qquad (6\text{-}1)$$

$$\frac{\partial C_{II}}{\partial t} = D_{II} \nabla^2 C_{II} \qquad (6\text{-}2)$$

where C_I and C_{II} are the solute concentrations, and D_I and D_{II} are the solute diffusion coefficients in Phase I and Phase II respectively.

Migration of the interface can be described using the following relation:

$$(C_{YI}-C_{YII})\,\mathbf{V} = -D_I\frac{\partial C_I}{\partial \mathbf{n}} + D_{II}\frac{\partial C_{II}}{\partial \mathbf{n}}, \tag{6-3}$$

where **V** is the velocity of the interface in the direction normal to the interface, C_{YI} and C_{YII} are the solute concentrations at the interface in phase I and phase II, and $(\partial/\partial\mathbf{n})$ is the directional differential normal to the interface. According to Patel's analysis [1968], Eq. (6-3) can be transformed to:

$$(C_{YI}-C_{YII})\frac{dY}{dt} = \left\{-D_I\left(\frac{\partial C_I}{\partial y}\right)_{y=Y} + D_{II}\left(\frac{\partial C_{II}}{\partial y}\right)_{y=Y}\right\}\left\{1+\left(\frac{\partial Y}{\partial x}\right)^2\right\}, \tag{6-4}$$

where Y(x,t) is the y-coordinate at the interface. This equation provides the velocity of the interface in the y-direction. Therefore, using this equation, we can calculate the migration of the interface along grid lines parallel to the y-axis. This approach is taken in the finite difference analysis described below.

The boundary and initial conditions are:

$$\left(\frac{\partial C_I}{\partial y}\right)_{y=0}=0, \tag{6-5}$$

$$\left(\frac{\partial C_I}{\partial x}\right)_{x=0}=\left(\frac{\partial C_I}{\partial x}\right)_{x=0}=0, \tag{6-6}$$

$$C_{II}(x,y,t) = 0, \qquad \text{at } y=L/2 \tag{6-7}$$

$$C_I(x,y,0) = 0, \qquad \text{at } y \geq l \tag{6-8}$$

$$C_I(x,y,t) = C_F, \qquad \text{at } l \geq y \geq 0 \tag{6-9}$$

$$Y(x,0) = l/2, \tag{6-10}$$

where l and C_F are the thickness and initial concentration of phase I.

6.1.2.1. The Excess Chemical Potential Resulting from the Balance between the Grain Boundary Energy and the Interfacial Energy

Suppose that a grain boundary intersects an interface at point O and the intersecting point shifts from O to O' by ΔY as shown in Fig. 6-2. The change in free energy caused by this shift of the intersecting point is given by [Swalin, 1962 and Woodruff, 1973]:

$$\Delta\gamma \approx (-\gamma_{gb} + 2\,\gamma_{int}\cos\theta)\Delta Y, \tag{6-11}$$

where γ_{gb} is the grain boundary energy and γ_{int} is the interfacial energy (the orientation dependence of γ_{int} is assumed to be negligible). This treatment is different from the classical approaches where an equilibrium dihedral angle is assumed at the grain boundary triple junction at all times (see Section 2.6.). The advantages of this treatment comprise: (1) it treats the formation of the grain boundary groove as a dynamic process; (2) Eq. (6-11) can handle the situation when γ_{gb} is larger than 2 γ_{int} [Woodruff, 1973]. The thickness of the

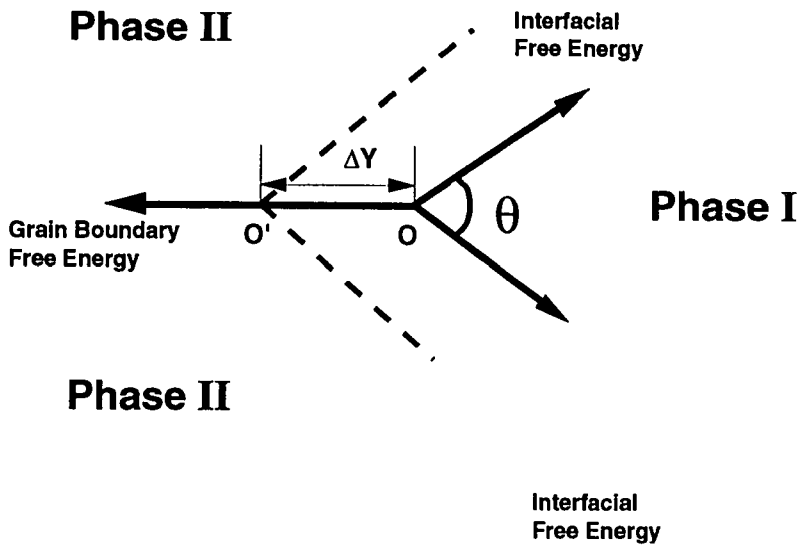

Fig. 6-2 Schematic of the balance between grain boundary free energy and interfacial free energy at the grain boundary triple junction.

specimen in the direction perpendicular to the plane of the page is assumed to be unit length.

From Eq. (6-11), the solute at the intersecting point O has an excess chemical potential $\Delta\mu$, compared with the solute in the bulk, according to,

$$\Delta\mu = \frac{\Delta\gamma}{\Delta n} = (-\gamma_{gb} + 2\gamma_{int}\cos\theta)\frac{\Delta Y}{\Delta n}$$

$$= (-\gamma_{gb} + 2\gamma_{int}\cos\theta)\frac{\Omega}{(C_{L\alpha}-C_{\alpha L})\delta} \qquad (6\text{-}12)$$

where Δn (mol) is the amount of solute required to shift the intersecting point from O to O', Ω is the molar volume of the liquid and solid phases, and δ is the width over which the chemical potential of the solute is influenced by the grain boundary. In the present calculations, d is taken to be equal to the grid size, ε, in the x-direction.

In order to account for the effects of chemical potential $\Delta\mu$ on interdiffusion, equivalent concentrations were introduced at the intersecting points C_I^e and C_{II}^e, given by the following equations:

$$C_I^e = C_I \exp\left(\frac{\Delta\mu}{RT}\right) \approx C_I\left(1+\frac{\Delta\mu}{RT}\right), \qquad (6\text{-}14)$$

$$C_{II}^e = C_{II} \exp\left(\frac{\Delta\mu}{RT}\right) \approx C_{II}\left(1+\frac{\Delta\mu}{RT}\right). \qquad (6\text{-}15)$$

6.1.2.2. The Excess Chemical Potential Resulting from Interfacial Curvature

The interfacial curvature also influences the chemical potential of solute atoms. The solute atoms at the liquid-solid interface having curvature K have a chemical potential greater than that of the solute atoms in bulk [Swalin, 1962]:

$$\Delta\mu = \frac{K\gamma_{int}\Omega}{(C_{YI}-C_{YII})}, \tag{6-16}$$

where γ_{int} is the interfacial free energy per unit area, Ω the atomic volume, and,

$$K=\frac{\dfrac{\partial^2 Y}{\partial x^2}}{\left\{1+\left(\dfrac{\partial Y}{\partial x}\right)^2\right\}^{3/2}}. \tag{6-17}$$

A positive value of K corresponds to a concave interface. The influence of chemical potential on interdiffusion is taken into account by introducing equivalent concentrations C_I^e and C_{II}^e given by

$$C_I^e = C_I \exp\left(\frac{\Delta\mu}{RT}\right) \approx C_I\left(1+\frac{\Delta\mu}{RT}\right), \tag{6-18}$$

$$C_{II}^e = C_{II} \exp\left(\frac{\Delta\mu}{RT}\right) \approx C_{II}\left(1+\frac{\Delta\mu}{RT}\right). \tag{6-19}$$

6.1.3. Numerical Analysis

In this chapter, the diffusion equations described in the preceding section are solved numerically using the explicit finite difference method. In the finite difference analysis, a network of lines pass through the shadowed area in Fig. 6-1 (also see Fig. 6-3). The interval between lines parallel to the y-axis is $\Delta\varepsilon$ (=2μm). The intervals between the lines parallel to the x-axis are ξ=5μm for $l \geq y \geq 0$ and

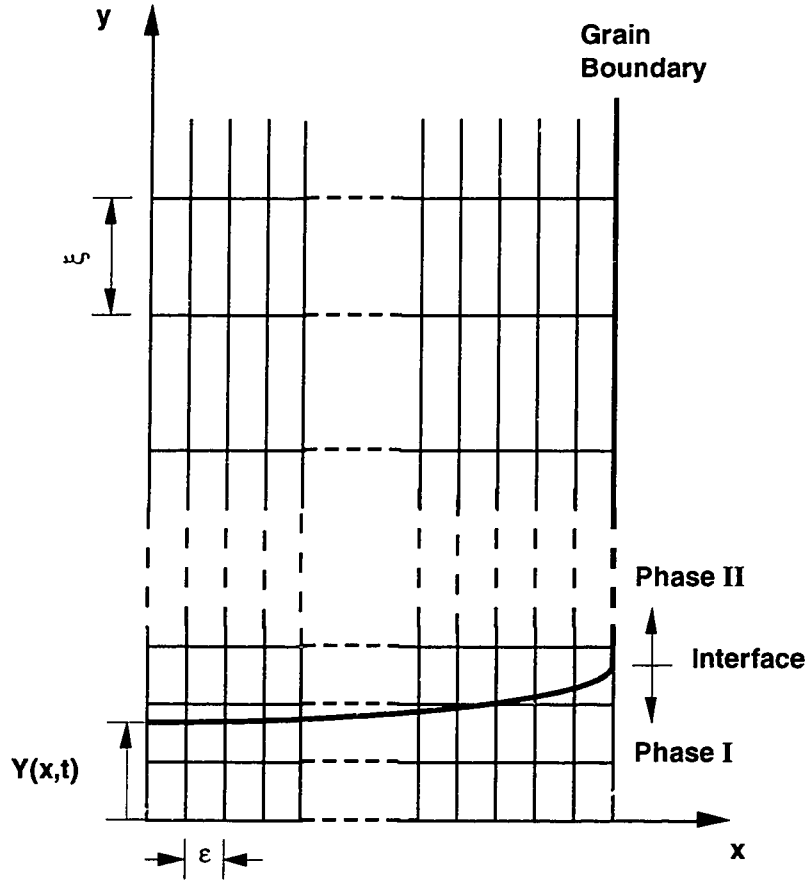

Fig. 6-3 Finite difference grid used in the grain boundary grooving model.

$\Delta y=25\mu m$ for $y \geq l$. The solute concentration at points far from the interface are calculated using the standard explicit finite difference expression [Crank, 1975] for Eqs. (6-1) and (6-2):

$$\frac{C_{i,j}^{t+\Delta t}-C_{i,j}^{t}}{\Delta t}=D\frac{C_{i+1,j}^{t}-2C_{i,j}^{t}+C_{i-1,j}^{t}}{(\Delta x)^2}+D\frac{C_{i,j+1}^{t}-2C_{i,j}^{t}+C_{i,j-1}^{t}}{(\Delta y)^2}, \qquad (6\text{-}20)$$

where $D=D_I$ and D_{II}. This finite difference equation is consistent to the Eqs. (6-1) and (6-2). and its solution is conditionally stable [Noye, 1982].

Special formulae are required when calculating solute concentration near the interface. For example, we need to calculate the solute concentration at point p near the interface in Phase I (see Fig. 6-4). Since the interface displacement is expressed in y-direction (see Eq. 6-4), the interface location will be determined by the positions along the grid lines in the y-direction (e.g. points a, b, d and e in Fig. 6-4). The neighboring grid points of point p are b, c, f and g (g and f are points far away from the interface, b and c are the points at the interface). The solute concentration $C_p(m,n)$ at point p is given by the non-uniform grid spacing finite difference equation:

$$\frac{C_p^{t+\Delta t}-C_p^{t}}{\Delta t}=D_I\left(\frac{\dfrac{C_b^t-C_p^t}{\Delta\varepsilon}-\dfrac{C_p^t-C_f^t}{\varepsilon}}{\dfrac{\Delta\varepsilon+\varepsilon}{2}}+\frac{\dfrac{C_c^t-C_p^t}{\Delta\xi}-\dfrac{C_p^t-C_g^t}{\xi}}{\dfrac{\Delta\xi+\xi}{2}}\right) \qquad (6\text{-}21)$$

C_p^t, C_g^t and C_f^t are the solute concentrations at normal points at prior time , and therefore are known during numerical calculation. C_b^t is

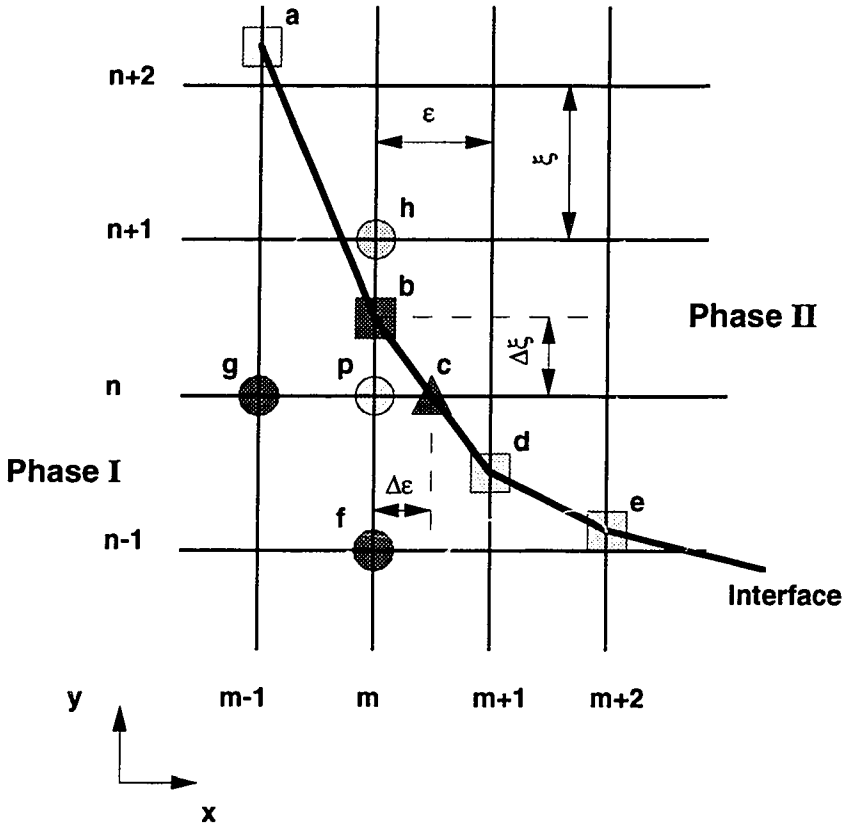

Fig. 6-4 Finite difference grid showing the interface line a-b-d-e and its surrounding region.

the interface concentration in Phase I and is calculated using Eqs. (6-18) and (6-19) and the following discrete equations,

$$\left(\frac{\partial^2 Y}{\partial x^2}\right)_m \approx \frac{Y_{m-1}-2Y_m+Y_{m+1}}{\xi^2} \tag{6-22}$$

$$\left(\frac{\partial Y}{\partial x}\right)_m \approx \frac{Y_{m+1}-Y_{m-1}}{2\xi} \tag{6-23}$$

C_d^t is calculated in a similar manner. C_c^t can be calculated by interpolating between points b and d. Once C_b^t and C_c^t are calculated, $C_p^{t+\Delta t}$ can be determined along with the values of C_f^t, C_g^t and C_p^t.

The interface position, $Y_m^{t+\Delta t}$, at point b in Fig. 6-4 can be calculated using the finite difference form of Eq. (6-4),

$$(C_{YI}-C_{YII})\frac{Y_m^{t+\Delta t}-Y_m^t}{\Delta t} = \left(-D_I\frac{C_b^t-C_p^t}{\Delta\varepsilon}+D_{II}\frac{C_h^t-C_b^t}{\varepsilon-\Delta\varepsilon}\right)\left\{1+\left(\frac{Y_{m+1}^t-Y_{m-1}^t}{2\xi}\right)^2\right\} \tag{6-24}$$

The solute concentration at other grid points and the interface location at other grid lines are determined in the similar way. The time step used in this calculation is:

$$\Delta t < \frac{1}{20}\frac{\varepsilon^2\xi^2}{\varepsilon^2+\xi^2}\frac{1}{D'} \tag{6-25}$$

where D equals D_I or D_{II}.

6.1.4. Parameters Employed in Numerical Calculations

A liquid-solid system (TLP-bonding of nickel using Ni-19 at.% P filler metal) is considered in the present thesis. However, it is worth pointing out that the numerical model developed above can also be applied to solid-solid or solid-gas systems. The diffusion coefficients and the equilibrium solute concentrations employed in this chapter are similar to those employed in Chapter 3 system (see Table 3-1). The grain size is assumed to be 40 μm. The initial thickness of the filler metal is 40 μm. The grain boundary energy γ_{gb} is 0.848 J/m^2 (reported as the free energy of the large angle random grain boundaries of nickel [Murr, 1975]). The γ_{gb}/γ_{int} ratio in pure metals is estimated based on experimental results to be 2.22 [Miller and Chadwick, 1967]. In the present study, both γ_{gb} and γ_{int} are assumed to vary from 0.424-0.848 J/m^2, and the γ_{gb}/γ_{int} ratio is assumed to vary from 1 to 2.

6.2. Results

The numerical model developed above has been applied to TLP-bonding of nickel base metal using Ni-19 at.% P filler metal. Figs. 6-5 and 6-6 show evolution of the liquid-solid interface profile at the bonding temperature. Based on Fig. 6-5, the liquid-solid interface is almost planar during the base metal dissolution stage, and liquid penetration at the grain boundary region is only apparent near the end of the dissolution process. Based on Fig. 6-6, liquid penetration becomes more pronounced when the holding time increases during the

isothermal solidification stage. The penetration depth increases to more than 10 μm -- large enough to be observed using conventional optical microscopy and scanning electron microscopy. These indications are comparable with the experimental results produced in this thesis (see Fig. 3-6 to 3-8). In this connection, Kokawa et al [1992] also indicated that the liquid penetration could not be observed during the dissolution process, but became more pronounced when the holding time increased during the isothermal solidification stage of TLP-bonding. The horizontal broken lines in Fig. 6-6 indicate the calculated displacement of the liquid-solid interface when the effect of grain boundary-related factors are neglected. It is clear that the width of the liquid phase in the bulk region far from the grain boundary (represented by the width at the symmetry axis) is smaller when the

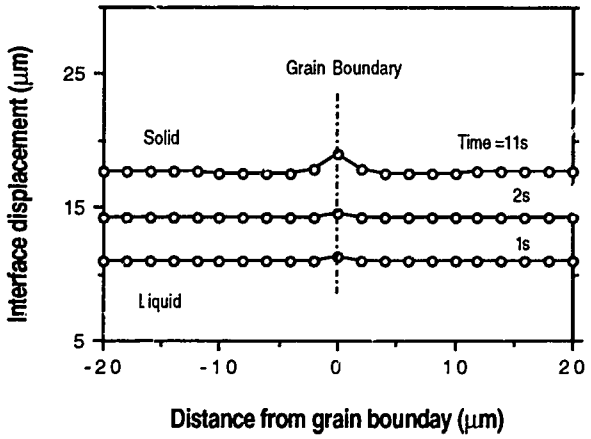

Fig. 6-5 Evolution of the profile of the liquid-solid interface during the dissolution stage.

effect due to the grain boundary energy and liquid-solid interfacial energy are taken into account. It follows that the isothermal solidification process in the bulk region is accelerated when the effects of the grain boundary energy and the liquid-solid interfacial energy are taken into account.

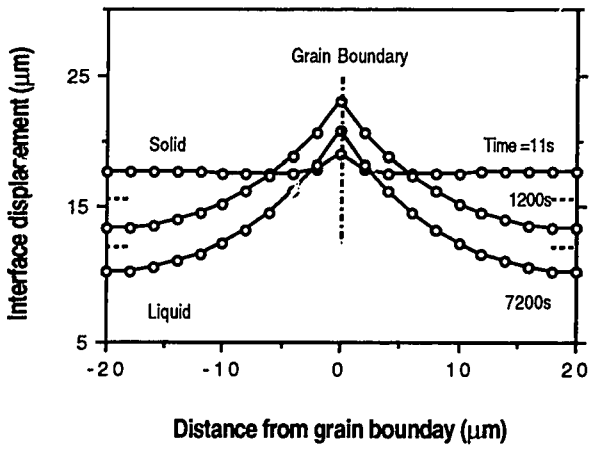

Fig. 6-6 Evolution of the profile of the liquid-solid interface during the isothermal solidification stage.

The influence of the grain boundary energy on liquid penetration at the grain boundary region is shown in Fig. 6-7. In this figure, the liquid-solid interfacial energy is maintained at 0.424 J/m^2, and the grain boundary energy is varied from 0.424 to 0.848 J/m^2. It is quite clear from Fig. 6-7 that the penetration depth is increased and the

angle at which the liquid-solid interface intersects the grain boundary becomes sharper when the grain boundary energy is increased. Kokawa et al [1992] observed that the liquid penetration at large angle random grain boundary regions was much more pronounced than that observed at the ordered grain boundaries (small angle grain boundaries and twin boundaries). Since a large angle random grain boundary has higher energy than an ordered grain boundary, the calculated results in Fig. 6-7 correspond well with the experimental observations made by Kokawa et al [1992].

Liquid penetration at the grain boundary region is also strongly influenced by the liquid-solid interfacial energy (Fig. 6-8). Liquid penetration becomes more pronounced when the solid-liquid interfacial energy is decreased. It follows that only the γ_{gb}/γ_{int} ratio, not the individual values of γ_{int} or γ_{gb}, determine the shape of solid-liquid interface (see Fig. 6-7 and Fig. 6-8). The reduction in liquid penetration is very small (less than one per cent) when the grain boundary energy decreases by 50 percent (see the curves in Figs. 6-7 and 6-8 where $\gamma_{gb}/\gamma_{int}=1$).

It is apparent that liquid penetration at grain boundary regions during TLP-bonding of Nickel using Ni-19 at.% P filler metal can be numerically modelled by taking into account factors such as the grain boundary energy and the liquid-solid interfacial energy.

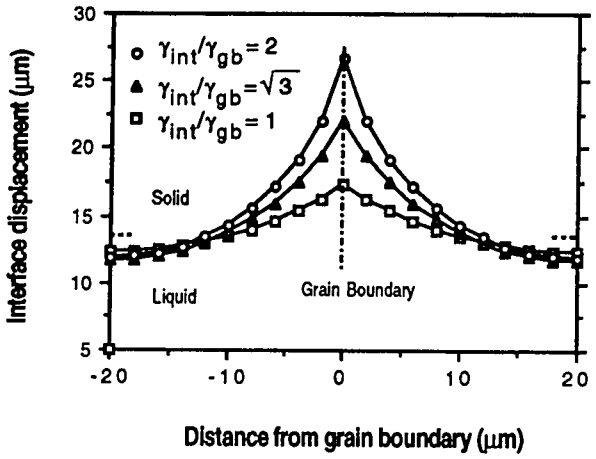

Fig. 6-7 Effect of the grain boundary energy on the profile of the liquid-solid interface during isothermal solidification (γ_{int} = 0.424 Jm^{-2}).

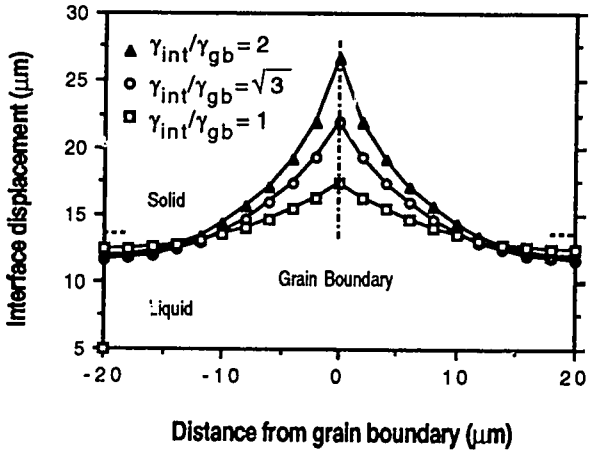

Fig. 6-8 Effect of the liquid-solid interfacial energy on the profile of the liquid-solid interface during isothermal solidification (γ_{gb} = 0.848 Jm^{-2}).

6.3. Future Work on the Grain Boundary Grooving Model

Evolution of grain boundary grooves at the liquid-solid interface during TLP-bonding of nickel using Ni-19 at.% P has been explained using the model developed in this chapter. This model can be also applied to the other two-phase diffusion-controlled processes, assuming that solutions can be formed for two or three-dimensional, diffusion-controlled and non-steady-state moving interface problems. All transport mechanisms will participate the diffusion process, namely, volume diffusion in each phase, grain boundary diffusion and interfacial diffusion. The driving forces for diffusion involves the concentration gradients in both phases, and the chemical potential gradients that result from the curvature gradient, and the balance of grain boundary free energy and interfacial energy at the grain boundary triple junction. Other factors, such as grain boundary segregation, will also strongly affect the process kinetics. The following section will describe the grain boundary diffusion and interfacial diffusion relation that could be employed in formulation of a general model for grain boundary grooving.

6.3.1. Increased diffusivity at Grain Boundary Regions

Grain boundary diffusion depends on the relation (also see Chapter 5):

$$\frac{\partial C}{\partial t} = D_{gb}\frac{\partial^2 C}{\partial y^2} + \frac{D_{II}}{k\delta}\left(\frac{\partial C}{\partial x}\right)_{x=+\delta/2} - \frac{D_{II}}{k\delta}\left(\frac{\partial C}{\partial x}\right)_{x=-\delta/2}, \qquad |x| = \frac{\delta}{2} \tag{6-26}$$

where D_{gb} are the diffusion coefficients at the grain boundary, δ is the grain boundary thickness, and k is a segregation-related factor.

Interface movement at the grain boundary triple junction is determined by the following relation:

$$(C_{YI}-C_{YII})\frac{dY}{dt} = \left\{-D_I\left(\frac{\partial C_1}{\partial y}\right)_{y=Y} + D_{gb}\left(\frac{\partial C_{gb}}{\partial y}\right)_{y=Y}\right\}\left\{1+\left(\frac{\partial Y}{\partial x}\right)^2\right\}. \qquad (6\text{-}27)$$

The effect of increased diffusivity at grain boundaries and of grain boundary segregation are accounted for using the above equations. However, according to the calculation experience in this study, an extremely long calculation time is required if an explicit finite difference scheme is employed to solve the grain boundary diffusion equations. In effect, the principal difficulty will be in solving the grain boundary equations using an implicit finite difference scheme.

A change of D_{gb} will affect the rate of interface movement at the grain boundary triple junction (see Eq. (6-27)). For example, let us consider the situation during the isothermal solidification stage of TLP-bonding. When D_{gb} increases, the term dY/dt will decrease. This means that the interface will move faster towards the joint centerline. It follows that the above equations can qualitatively explain how increased diffusivity at grain boundaries could speed up interface movement and hence the process kinetics.

6.3.2. Interfacial Diffusion

As can be seen from Eqs. (6-16) and (6-19), the liquid-solid interfacial energy produce a chemical potential gradient for solute along the liquid-solid interface. This chemical potential gradient produces diffusion flow along the liquid-solid interface and consequently, gives rise to the migration of the liquid-solid interface as described by Mullins [1957]. When a compositional discontinuity occurs at the interface:

$$\Delta\mu = - \frac{K\gamma_{int}\Omega}{(C_{YI}-C_{YII})} \tag{6-28}$$

The chemical potential gradient along the interface will therefore be associated with the gradient of interfacial curvature. Such gradients will promote diffusion of solute atoms having an average velocity given by the Nernst-Einstein relation:

$$v= - \frac{D}{kT} \frac{\partial(\Delta\mu)}{\partial s} \tag{6-29}$$

where D is the coefficient of interfacial diffusion and s the length of the arc along the profile. The interface current J of atoms will be the product of v times the number of solute atoms per unit area:

$$J=- \frac{C_{int}D}{kT\Omega} \frac{\partial(\Delta\mu)}{\partial s} \tag{6-30}$$

If we refer to the conservation of mass [Mullins, 1975 and Takahashi et al, 1988], the velocity of interface motion in the normal direction will be:

$$V_n = \frac{\Omega \delta_{int}}{C_{YI}-C_{YII}} \frac{\partial J}{\partial s} \tag{6-31}$$

A simple geometrical projection of velocity $\frac{\partial Y}{\partial t}$ gives the relation:

$$V_n = \left\{1+\left(\frac{\partial Y}{\partial t}\right)^2\right\}^{-1/2} \frac{\partial Y}{\partial t} \tag{6-32}$$

and by using the relation $\frac{\partial}{\partial s} = \frac{\partial x}{\partial s}\frac{\partial}{\partial x}$, then:

$$\frac{\partial Y}{\partial t} = \left\{1+\left(\frac{\partial Y}{\partial t}\right)^2\right\}^{1/2} V_n$$

$$= \frac{D_{int} C_{int} \delta_{int}}{kT(C_{YI}-C_{YII})} \frac{\partial}{\partial x}\left[\left\{1+\left(\frac{\partial Y}{\partial x}\right)^2\right\}^{-1/2} \frac{\partial \Delta \mu}{\partial x}\right] \tag{6-33}$$

where D is the diffusion coefficient along the liquid-solid interface, C_{int} is the composition of the liquid-solid interface and w is the thickness of the liquid-solid interface. Composition C_{int} is taken as $(C_{YI}+C_{YII})/2$. The migration rate of the interface is therefore the sum of the migration rates given by Eqs. (6-4) and (6-33). It follows that the influence of interfacial diffusion can be taken into account.

6.4. Summary

A numerical model has been developed for the evolution of the grain boundary grooves during two-phase diffusion transformation. The driving force for the diffusion process results both from concentration gradients and from curvature gradients. The following factors are indicated in the model:

(1) solute diffusion in each phase;

(2) the excess chemical potential resulting from the interfacial curvature;

(3) the excess chemical potential resulting from the balance between the grain boundary energy and the interfacial energy at the grain boundary triple junction.

Application of this numerical model during TLP-bonding indicates that the model can correctly display the liquid-solid interface migration at grain boundary regions. The calculated liquid penetration depth is also comparable with the experimental observations. The numerical calculations also indicates the correct trends in the evolution of the liquid-solid interface profiles when the γ_{gb}/γ_{int} ratio varies. These results of the numerical model compare well with the microscopic observation made by Kokawa et al [1992].

Formulae that take grain boundary diffusion and interfacial diffusion into account during development of a general grain boundary grooving model have been presented. These formulations will produce a useful starting-point for the development of a general model that can

handle two or three-dimensional, diffusion-controlled moving interface problems.

Chapter 7

Conclusion

This thesis has examined numerical modelling of TLP-bonding and other two-phase, diffusion-controlled moving interface processes. The present study comprises four distinct sections:

(1) TLP-bonding of nickel base metal having different grain sizes (using Ni-19at.%P filler metal);

(2) Development of a one-dimensional numerical model, verification of the model by testing TLP-bonded single crystal base metal and development of the optimum parameters during TLP-bonding operations;

(3) Development of a numerical model indicating the influence of increased diffusivity at grain boundary regions and of grain boundary migration on the process kinetics in diffusion-controlled processes;

(4) Development of a numerical model explaining the evolution of grain boundary grooving (or liquid phase penetration during TLP-bonding) during two-phase, diffusion-controlled moving interface problems.

The principal conclusions are indicated below.

7.1. TLP-Bonding Experimentation

The influence of nickel base metal grain size on the process kinetics of isothermal solidification during TLP-bonding was examined. The eutectic width decreased linearly with the square-root of the

holding time in all nickel base metals investigated. The principal conclusions are:

1. The rate of isothermal solidification during TLP-bonding increases in the following order: single crystal, coarse-grained and fine-grained nickel. It follows that base metal grain boundary regions can speed up the overall solute transport rate during TLP-bonding.
2. Impurities in nickel base metal increase the rate of isothermal solidification during TLP-bonding.

7.2. Kinetic Modelling of Two-Phase Diffusion Processes

A fast and accurate, fully implicit, one-dimensional finite difference model was developed that simulates diffusion-controlled, two-phase, moving interface problems. The principal conclusions from this modelling phase are:

1. The computed results are in excellent agreement with the experimental results produced during TLP-bonding of single-crystal nickel using Ni-19at% P filler metal. In addition, the computed results show excellent agreement with previously published experimental results developed during the solution treatment of thin, multilayer α and β brass diffusion couples [Heckel et al, 1975]. Also, the numerical model developed in this study produced results that compare well with the output of the numerical models developed by Tanzilli and Heckel [1968], and Pabi [1979].
2. The one-dimensional model effectively simulates, in a continuous manner, liquid-solid interface migration during base metal dissolution,

liquid phase isothermal solidification and solute redistribution during homogenization during TLP-bonding operations.

3. The numerical model predicts the optimum joining parameters during TLP-bonding. The optimum conditions occur when the solute diffusivity in the liquid and in the solid phases increase, and when the highest bonding temperature is employed.

4. Base metal dissolution cannot be represented using a parabolic law assumption. Consequently, analytical modelling cannot be used to simulate base metal dissolution. However, the isothermal solidification stage can be readily estimated by assuming a linear relation between solid-liquid interface displacement and the square-root of the holding time at the bonding temperature. The values produced using numerical and analytical modelling are identical in this case. Also, an analytical solution can be used to estimate the solute concentration at the specimen centerline following a given holding period during the homogenization stage.

7.3. Numerical Model: Effect of Increased Diffusivity at Grain Boundary Regions and of Grain Boundary Migration

A numerical model was developed that indicates in a continuous manner the effect of increased diffusivity at grain boundary regions, and of grain boundary migration on the total amount of solute diffused and hence, on the process kinetics during two-phase diffusion-controlled problems. The principal conclusions are:

1. The influence of grain boundary regions on the total amount of solute diffused depends on the grain size, and the ratio of grain boundary

diffusion coefficient and lattice diffusion coefficient, D_{gb}/D_l. When the D_{gb}/D_l ratio is high (for temperatures in the range, $T < 0.5\text{-}0.75T_m$), the influence of grain size on the total amount diffused is marked and decreasing the grain size increases the total amount diffused. When the D_{gb}/D_l ratio is low (at high processing temperatures in the range, $T > 0.75T_m$), the influence of grain size on the total amount diffused is small.

2. The apparent diffusion coefficients in Type B and Type A kinetic regimes, and in the transition regime between Type B and Type A behavior, are calculated using the numerical model.

3. When $\sqrt{D_l t}$ is larger than the grain size, d, the numerical calculations support Hart's analysis [1957], that an apparent diffusion coefficient exists. This apparent diffusion coefficient can be approximated using the relation, $D_{app} = D_l\left(1 + \frac{\delta}{d}\frac{D_{gb}}{D_l}\right)$.

4. Grain boundary migration increases the total amount diffused during only part of the holding period. During this period, the total amount diffused increases, when the grain size, the D_{gb}/D_l ratio, and the rate of grain boundary migration increase. For short processing times, grain boundary migration has negligible effect on the total amount diffused and, for long holding times, the total amount diffused is also similar in stationary and migrating grain boundary situations.

7.4. Numerical Model: Grain Boundary Grooving

A numerical model was developed that indicates the evolution of the grain boundary grooves during two-phase diffusion-controlled

processes. The driving force for the diffusional process results from a combination of concentration and interfacial curvature gradients. The following factors are taken into account:

(1) volume diffusion in each phase;

(2) the excess chemical potential resulting from the gradient of interfacial curvature;

(3) the excess chemical potential resulting from the balance between the grain boundary energy and interfacial energy at the grain boundary triple junction.

The model correctly simulates solid-liquid interface migration at grain boundary regions during TLP-bonding. The principal results are: The calculated liquid penetration depth at grain boundary regions is comparable with direct experimental observations in TLP-bonded nickel base metal. The numerical calculations indicate the correct trends during evolution of the liquid-solid interface profile. The liquid penetration depth increases when the γ_{gb}/γ_{int} ratio increases. These results are in close correspondence with the microscopical observations made by Kokawa et al (1992).

Additionally, a useful starting-point for the development of a general model capable of handling two or three-dimensional, diffusion-controlled moving interface problems has been presented. This general formulation accounts for all diffusion mechanisms, namely, volume diffusion in both phases, interfacial diffusion and grain boundary diffusion.

References

Allen, B.C. 1966. *Trans. Metall. Soc. AIME*, 236, 915-924

Allen, D.J. 1982, *Scripta Metall.*, 16, 5-9

Allen, M.B., Herrera, I. and Pinder, G.F. 1988. Numerical Modelling in Science and Engineering, John Wiley & Sons, New York

Aust, K.T. and Chalmers, B. 1970. *Metall. Trans.*, 1, 1095-1104

Balluffi, R.W. 1982. *Metall. Trans.* 13A, 2069-2095

Basterfield, J., Miller, W.A. and Weatherly, G.C. 1970. *Can. Met. Quart.*, 8, 131-144

Battle, T.P. and Pehlke, R.D. 1990. *Metall. Trans.*, 21B, 357-374

Benoist, P. and Martin, G. 1975. *J. Phys.*, 36, (Colloque C4), 213

Bernardini, J. and Martin, G. 1976. *Scripta Metall.*, 10, 833

Bernstein, L. 1966. *J. Electrochemical Soc.*, 113, 1282-1288

Bernstein, L. and Bartholomew, H. 1966. Trans. *Metall. Soc. AIME*, 236, 405-412

Bhanumurthy, K., Kale, G.B., Khera, S.K. and Asundi, M.K. 1990. *Metall. Trans.*, 21A, 2897-2903

Binder, K. 1992. in The Monte Carlo Method in Condensed Matter Physics,(ed. K. Binder), Springer-Verlag, Berlin, 1-19

Binh, V.T., Chaudier, M., Couturier, J.C., Uzan, R. and Drechsler, M. 1976. *Surface Sci.*, 57, 184-204

Cahn J.W. and Balluffi, R.W. 1979. *Scripta Metall.*, 13, 499-502

Campbell, D.R. 1974. *Bull. Amer. Phys. Soc.*, 19, 347, also see Ref. 2.

Cannon, R.F. and Stark, J.P. 1969. *J. Appl. Phys.*, 40, 4361

Cermak, J. 1990. Phys. Stat. Sol. (A) 120, 351- 361

Crank, J. 1975. The Mathematics of Diffusion, 2nd edition, Oxford University Press, New York

Crank, J. 1984. Free and moving boundary problems, Oxford University Press, Oxford, U.K.

Crusius, S., Inden, G., Knoop, U., Hoglund, L. and Agren, J. 1992. *Z. Metallkd.*, 83, 673-678

Danckwerts, P.V. 1950. *Trans. Faraday Soc.*, 46, 701-712

Duvall, D.S., Owczarski, W.A. and Paulonis, D.F. 1974. *Welding J.*, 203-214

Fisher, J.C. 1951. *J. Appl. Phys.*, 22, 74 -77

Flynch, J.F., Feinstein L. and Huggins, R.A. 1959. *Welding J.*, 85-89

Fox, L. 1975. in Moving Boundary Problems in heat Flow and Diffusion, eds. Ockendon and Hodgkins, 210-241

Gale, W.F. and Wallach, E.R., 1991. *Metall. Trans.*, 22A, 2451-2457

Gerald, C.F. and Wheatly, P.O. 1989. Applied numerical analysis, 4th ed., Addison-Wesley Publishing Company, California, U.S.A..

Gibbs, G.B. 1966. *Phys. Status Solidi*, 2, K27-29

Gilmer, G.H. and Farrell, H.H. 1976a. *J. Appl. Phys.*, 47, 3792-3798

Gilmer, G.H. and Farrell, H.H. 1976b. *J. Appl. Phys.*, 47, 4373-4380

Gjostein, N.A. 1961. *Trans. Metall. Soc. AIME*, 221, 1039-1046

Glaeser, A.M. and Evans, J.W. 1986. *Acta. Metall.*, 8, 1545-1552

Gupta, D., Campbell, D.R. and Ho, P.S. 1978. in Thin Films Interdiffusion and Reactions, (ed. J.M. Poate, K.N. Tu and I.W. Mayer), Wiley, New York, 161-242

Gust, W., Hintz, M.B., Lodding, A. and Odelius, H. 1982. *Acta Metall.*, 30, 75-82

Hackney, S.A. and Ojard, G.C. 1988. *Sripta Metall.*, 22, 1731-1735

Hardy, S.C., McFadden, G.B. and Coriell, S.R. 1991. *J. Crystal Growth*, 114, 467-480

Harrison, L.G. 1961. *Trans. Faraday Soc.*, 57, 1191-1199

Hart, E.W. 1957. *Acta Metall.*, 5, 597

Heckel, R.W., Hickl, A.J., Zaehring, R.J. and Tanzilli, R.A. 1972. *Metall. Trans.*, 3, 2565-2569

Herring, C. 1950. *J. Appl. Phys.*, 21, 301-303

Herring, C. 1951. in The Physics of Powder Metallurgy, (ed. W.E. Kingston), McGraw-Hill Book Co., New York, 143

Hickl, A.J. and Heckel, R.W. 1975. *Metall. Trans.*, 6A, 431-440

Hillert, M. and Purdy, G.R. 1978. *Acta Metall.*, 26, 333-340

Ho, E. and Weatherly, G.C. 1975, *Acta Metall.*, 23, 1451-1460

Ikawa, H. and Nakao, Y. 1977. *Trans. Jpn. Weld. Soc.*, 8, 3-7

Jahnke, B. and Demny, J. 1983. *Thin Solid Films*, 110, 225-235

Jost, W. 1960. Diffusion in Solids, Liquids, Gases, Academic Press Inc., Publishers, New York

Kang, C.Y. 1988. Doctoral Thesis, Osaka University

Karlsson, B. and Larsson, L.-E. 1975. *Mater. Sci. Eng.*, 20, 161-170

Kaysser, W.A., Huppmann, W.J. And Petzow, G. 1980. *Powder Metallurgy*, 86-91

King, A.H. 1987. *Internat. Mater. Rev.*, 32, 173-189

Kidson, G.V. and Miller, G.D. 1964. *J. Nuclear Mater.*, 12, 61-69

Kokawa, H., Lee, C.H. and North, T.H. 1991. *Metall. Trans.*, 22A, 1627-1631

Lanam, R.D. and Heckel, R.W. 1971. *Metall. Trans.*, 2, 2255-2266

Langer, J.S. and Sekerka, R.F. 1975. *Acta Metall.*, 23, 1225-1237

Lazaridis, A. 1969. Doctoral Thesis, Columbia University

Lazaridis, A. 1970. *Int. J. Heat Mass Transfer*, 13, 1459-1477

Lax, P.D. and Richtmyer, R.D. 1956. *Commun. Pure Appl. Math.*, 9, 267-293

Le Blance, A. and Mevrel, R., 1990. in High Temperature Materials for Power Engineering, Liege, Belgium, 24-27 September, 1451-1460

Le Claire, A.D. 1963. *British J. Appl. Phys.*, 14, 351-356

Levine, H.S. and Mac Callum, C.J. 1960. *J. Appl. Phys.*, 31, 595

Lidiard A.B. and Tharmalingam, K. 1959. *Disc. Faraday Soc.*, 28, 64-68

Liu, D., Miller, W.A. and Aust, K.T. 1989. *Acta Metall.*, 37, 3367-3378

Liu, S., Olson, D.L., Martin, G.P. and Edward, G.R. 1991. *Welding J.*, 70, 207s-215s.

Lynch, J.F., Feinstein, L. and Huggins, R.A. 1959. *Welding J.*, 85s-89s

MacDonald, W.D. and Eagar, T.W. 1992. *Annu. Rev. Mater. Sci.*, 22, 23-46

Massalski, T.B., ed. 1986. Binary Phase Diagrams, ASM Metals Park, NY

Miller W.A. and Chadwick, G.A. 1967. *Acta Metall.*, 15, 607-614

Mishin, Yu. M. and Razumovskii, I.M. 1992, *Acta. Metall.*, 40, 839-845

Mullins, W.W. 1957. *J. Appl. Phys.*, 28, 333-339

Mullins, W.W. 1958, *Acta Metall.*, 6, 414-427

Mullins, W.W. 1960, *Trans. Met. Soc. AIME*, 218, 354-361

Murray, W.D. and Landis, F. 1959. *J. Heat Transfer*, Trans. of ASME, 81C, 106-112

Nakao, Y., Nishimoto, K., Shinozaki, K., and Kang, C.Y. 1990. Joining of Advanced Materials, (Ed. T.H. North), Chapman and Hall, 129-144

Nakagawa, H., Lee, C.H. and North, T.H. 1991. *Metall.Trans.*, 22A, 543-555

Nash, P. (Editor). 1991. Phase diagrams of binary nickel alloys, ASM International, Materials Park, OH, 235

Niemann, J.T. and Garret, R.A. 1974. *Welding J.*, 175-184

Noye, J. 1982. in Numerical Solution of Partial Differential Equations (ed. J. Noye), North-Holland Publishing Company. New York, 1-137

Ohno, A. 1889. Proc. Metallurgical Processes for the Year 2000 and Beyond, TMS Vegas, NV, 155

Onzawa, T., Mitsunaga, Y., Tamura, A. and Morikawa, M. 1978. *J. Japan Weld Soc.*, 47, 161-166.

Pabi, S.K. 1979. *Phys. Stat. Sol.*, (a) 51, 281-289

Patel, P.D. 1968. *AIAA J.*, 6, 2454

Porter, D.A. and Easterling, K.E. 1992. Phase Transformations in Metals and Alloys, 2nd ed., Chapman & Hall, New York

Peterson, N.L. 1983. *Internat. Met. Rev.*, 28, 65-90

Ramirez, J.E. and Liu, S. 1992. *Welding J.*, 365-375

Richtmyer, R.D. 1957. Different methods for initial-value problems, Interscience Publishers, Inc., New York.

Robertson, W.M. 1965. *Trans. Metall. Soc. AIME*, 233, 1232-1236

Robertson, W.M. 1971. *J. Appl. Phys.*, 42, 463

Rubinstein, L.I. 1971. Trans. Math. Monographs 27, Am. Math. Soc., Providence, R.I.

Sakamoto, A., Fujiwara, C., Hattori, T. and Sakai, S. 1989. *Welding J.*, 63-71

Sekerka, R.F., Jeanfils, C.L. and Heckel, R.W. 1975. Lectures on the Theory of Phase Transformations, (ed. H.I. Aaronson), AIME, New York, 117-169

Sekerka, R.F. 1980. Proc. of Physical Metallurgy of Metals Joining Conf., (Eds. R. Kossowsky and M.E. Glicksman), TMS-AIME, St. Louis, Mo, 1-3

Shewmon P.G. 1989. Diffusion in Solids, TMS, Warrendale

Smith, S.S. 1948. *Trans. Metall. Soc. AIME*, 175, 15

Smidoda, K., Gottschalk, W. and Gleiter, H. 1978. *Acta Metall.*, 26, 1833-1836

Srinivasan, S.R. and Trived, R. 1973. *Acta Metall.*, 21, 611-620

Steidel, C.A., Li, Che-Yu, and Spencer, C.W. 1964. *Trans. Met. Soc. AIME*, 230, 85-89

Straumal, B., Muschik, T., Gust, W. and Predel, B. 1992. *Acta Metall.*, 40, 939-945

Suzuoka, T. 1961. *Trans. Jap. Inst. Metall.* 2, 25-33

Suzuoka, T. 1964. *J. Phys. Soc. Jap.*, 19, 839

Takahashi, Y., Ueno, F. and Nishiguchi, K. 1988. *Acta. Metall.*, 36, 3007-3018

Tanzilli, R.A. and Heckel, R.W. 1968. *Trans. AIME*, 242, 2313-2321

Tanzilli, R.A. and Heckel, R.W. 1971. *Metall. Trans.*, 2, 1779-1784

Tuah-Poku, I., Dollars, M. and Massalski, T.B. 1988. *Metall. Trans.*, 19A, 675-686

Vogel, H.J. and Ratke, L. 1991, *Acta Metall.*, 39, 641-649

Wells, R.R. 1976. *Welding J.*, 20s-27s

Welty, J.R., Wicks, C.E. and Wilson, R.E. 1984. Fundamentals of Momentum, Heat, and Mass Transfer, John Wiley & sons, Inc., 483

Whipple, R.T.P. 1954. *Phil. Mag.*, 45, 1225-1236

Woodruff, D.P. 1973. The Solid-Liquid Interface, Cambridge University Press, London

Appendix I

Analytical Solution of the Isothermal Solidification during TLP-Bonding

From the analysis in Chapters 3 and 4, we can get some important information about the isothermal solidification during TLP-bonding: the solute concentration in the liquid phase is mainly constant and the solute diffusivity in the solid is limited compared with the base metal dimensions. It follows that diffusion in the liquid can be ignored and the solid phases can again be approximated as semi-infinite mediums. Therefore, the problem become a semi-infinite one-phase diffusion problem.

(1) Calculation of Rate Constant β

The following is similar to Danckwerts' derivation when a general solution is indicated for a diffusion problem which involves two phases separated by a moving planar interface.

Assuming two phase meet at the moving interface Y(t),

$$\frac{\partial C_S(y,t)}{\partial t} = D_S \frac{\partial^2 C_2(y,t)}{\partial y^2}, \qquad Y(t) \le y \le \infty \tag{a1}$$

When the error function solution is applied to the solid phase,

$$C_S(y,t) = A_1 + A_2 \operatorname{erf}\left(\frac{y}{2\sqrt{D_S t}}\right). \tag{a2}$$

Using the appropriate boundary conditions, we obtain:

$$C_S(\infty,t) = A_1 + A_2 = C_M. \tag{a3}$$

At the moving interface, we have:

$$C_S(Y,t) = A_1 + A_2 \operatorname{erf}\left(\frac{Y}{2\sqrt{D_S t}}\right) = C_{\alpha L}. \tag{a4}$$

From Eqs. (a3) and (a4),

$$A_1 = C_M - \frac{C_M - C_{\alpha L}}{1 - \operatorname{erf}\left(\frac{Y}{2\sqrt{D_S t}}\right)}, \tag{a5}$$

$$A_2 = \frac{C_M - C_{\alpha L}}{1 - \operatorname{erf}\left(\frac{Y}{2\sqrt{D_S t}}\right)}, \tag{a6}$$

$$C_S(y,t) = C_M - \frac{C_M - C_{\alpha L}}{1 - \operatorname{erf}\left(\frac{Y}{2\sqrt{D_S t}}\right)} + \frac{C_M - C_{\alpha L}}{1 - \operatorname{erf}\left(\frac{Y}{2\sqrt{D_S t}}\right)} \operatorname{erf}\left(\frac{y}{2\sqrt{D_S t}}\right). \tag{a7}$$

Since Eqs. (a4)-(a6) have to be satisfied for all values of t, Y must be proportional to $\sqrt{t}$, i.e.,

$$Y = 2\beta\sqrt{t}, \tag{a8}$$

and then,

$$\frac{dY(t)}{dt} = \frac{\beta}{\sqrt{t}}. \tag{a9}$$

Substituting Eqs. (a7) and (a9) in the equation governing interface movement,

$$(C_{L\alpha} - C_{\alpha L})\frac{dY(t)}{dt} = D_S\left(\frac{\partial c_S(y,t)}{\partial y}\right)_{y=Y(t)}. \tag{a10}$$

we can get

$$(C_{L\alpha} - C_{\alpha L})\frac{\beta}{\sqrt{t}} = D_S\frac{C_M - C_{\alpha L}}{1-\mathrm{erf}\left(\frac{\beta}{\sqrt{D_S}}\right)}\frac{\exp\left(-\frac{\beta^2}{D_S}\right)}{\sqrt{\pi D s t}}. \tag{a11}$$

Then

$$(C_{L\alpha} - C_{\alpha L})\beta\sqrt{\pi} + \frac{\sqrt{D_S}(C_{\alpha L} - C_M)}{1-\mathrm{erf}\left(\frac{\beta}{\sqrt{D_S}}\right)}\exp\left(-\frac{\beta^2}{D_S}\right) = 0. \tag{a12}$$

This equation can also derived by substituting $C_{-\infty} = C_{L\alpha}$ and $C_{\infty} = C_M$ into Eq. (2-31). In the papers by Tuah-Poku et al [1988] and by Liu et al [1991], the term $\exp\left(-\frac{\beta^2}{D_S}\right)$ is under the fraction and this may be due to a misprint.

(2) Estimation of the Completion Time for Isothermal Solidification

By assuming:

$$\beta = G\sqrt{D_S}, \tag{a13}$$

the Eq. (a12) becomes:

$$\frac{[1-\mathrm{erf}(G)]G\sqrt{\pi}}{\exp(-G^2)} = \frac{C_{\alpha L}-C_M}{C_{L\alpha}-C_{\alpha L}}. \tag{a14}$$

Therefore, G is a factor related to the solute distribution. When $G \to 0$, then $\mathrm{erf}(G) \to 1$, Eq. (a-7) becomes:

$$c_S(y,t) = C_M - \frac{C_M-C_{\alpha L}}{1-\mathrm{erf}(G)} + \frac{C_M-C_{\alpha L}}{1-\mathrm{erf}(G)}\,\mathrm{erf}\left(\frac{y}{2\sqrt{D_S t}}\right)$$

$$= C_{\alpha L} + (C_M-C_{\alpha L})\,\mathrm{erf}\left(\frac{y}{2\sqrt{D_S t}}\right). \tag{a15}$$

This is the same as Eq. (2-12). Therefore, if G is small, the isothermal solidification can modelled by the model of an exchange experiment. The total amount diffused into the solid phase, M_t, can calculated by Eq. (2-14):

$$M_t = 2(C_{\alpha L}-C_M)\sqrt{\frac{D_S t}{\pi}}. \tag{a16}$$

When this amount equals the initial solute content in the liquid phase when the isothermal solidification starts, the isothermal solidification stage will be complete. By assuming the solute amount diffused into the base metal is negligible during the dissolution stage, this initial solute content in the liquid phase equals $\frac{W_0 C_F}{2}$, then,

$$\frac{W_0 C_F}{2} = 2(C_{\alpha L}-C_M)\sqrt{\frac{D_S t}{\pi}}, \tag{a17}$$

therefore, the completion time for the isothermal solidification is:

$$t_S = \frac{\pi}{16 D_S}\left(\frac{C_F W_0}{C_{\alpha L}-C_M}\right)^2. \tag{a18}$$

When C_M=0, the above equation becomes:

$$t_S = \frac{\pi}{16 D_S}\left(\frac{C_F W_0}{C_{\alpha L}}\right)^2. \tag{a19}$$

This is also given in the paper by Tuah Poku et al [1988], but the derivation there is less rigorous. The crucial point is that the above equation is only valid when G is small.

Appendix II

Consistency Analysis of the Finite Difference Approximation for the Grain Boundary Diffusion Equation

The finite difference equation of the grain boundary diffusion equation (5-2) is:

$$\frac{C_{i,j}^{t+\Delta t}-C_{i,j}^{t}}{\Delta t} = D_{gb}\frac{C_{i,j+1}^{t}-2C_{i,j}^{t}+C_{i,j-1}^{t}}{(\Delta y)^2} + \frac{D_l}{k\delta}\frac{-3C_{i,j}^{t}+4C_{i+1,j}^{t}-C_{i+2,j}^{t}}{2\Delta x}$$

$$-\frac{D_l}{k\delta}\frac{3C_{i,j}^{t}-4C_{i-1,j}^{t}+C_{i-2,j}^{t}}{2\Delta x}. \qquad \text{(a20)}$$

Using Taylor series expansion, we can get:

$$\frac{[C_{i,j}^{t} + \frac{\partial C_{i,j}^{t}}{\partial t}\Delta t + \frac{1}{2!}\frac{\partial^2 C_{i,j}^{t}}{\partial t^2}\Delta t^2 + \cdots] - C_{i,j}^{t}}{\Delta t}$$

$$= \frac{D_{gb}}{\Delta y^2}\{[C_{i,j}^{t} + \frac{\partial C_{i,j}^{t}}{\partial y}\Delta y + \frac{1}{2!}\frac{\partial^2 C_{i,j}^{t}}{\partial y^2}\Delta y^2 + \frac{1}{3!}\frac{\partial^3 C_{i,j}^{t}}{\partial y^3}\Delta y^3 + \cdots] - 2C_{k,j}^{t}$$

$$+[C^t_{i,j} - \frac{\partial C^t_{i,j}}{\partial y}\Delta y + \frac{1}{2!}\frac{\partial^2 C^t_{i,j}}{\partial y^2}\Delta y^2 - \frac{1}{3!}\frac{\partial^3 C^t_{i,j}}{\partial y^3}\Delta y^3 + \cdots]\}$$

$$+\frac{D_l}{\delta\Delta x}\{-1.5C^t_{i,j} + 2[C^t_{i,j} + \left(\frac{\partial C^t_{i,j}}{\partial x}\right)_{x=+\delta/2}\Delta x + \frac{1}{2!}\left(\frac{\partial^2 C^t_{i,j}}{\partial x^2}\right)_{x=+\delta/2}\Delta x^2$$

$$+\frac{1}{3!}\left(\frac{\partial^3 C^t_{i,j}}{\partial x^3}\right)_{x=+\delta/2}\Delta x^3 + \cdots] - 0.5[C^t_{i,j} + \left(\frac{\partial C^t_{i,j}}{\partial x}\right)_{x=+\delta/2}2\Delta x$$

$$+\frac{1}{2!}\left(\frac{\partial^2 C^t_{i,j}}{\partial x^2}\right)_{x=+\delta/2}(2\Delta x)^2 + \frac{1}{3!}\left(\frac{\partial^3 C^t_{i,j}}{\partial x^3}\right)_{x=+\delta/2}(2\Delta x)^3 + \cdots]\}$$

$$+\frac{D_l}{\delta\Delta x}\{-1.5C^t_{i,j} + 2[C^t_{i,j} - \left(\frac{\partial C^t_{i,j}}{\partial x}\right)_{x=-\delta/2}\Delta x + \frac{1}{2!}\left(\frac{\partial^2 C^t_{i,j}}{\partial x^2}\right)_{x=-\delta/2}\Delta x^2$$

$$-\frac{1}{3!}\left(\frac{\partial^3 C^t_{i,j}}{\partial x^3}\right)_{x=-\delta/2}\Delta x^3 + \cdots] - 0.5[C^t_{i,j} - \left(\frac{\partial C^t_{i,j}}{\partial x}\right)_{x=-\delta/2}2\Delta x$$

$$+\frac{1}{2!}\left(\frac{\partial^2 C^t_{i,j}}{\partial x^2}\right)_{x=-\delta/2}(2\Delta x)^2 - \frac{1}{3!}\left(\frac{\partial^3 C^t_{i,j}}{\partial x^3}\right)_{x=-\delta/2}(2\Delta x)^3 + \cdots]\}. \quad \text{(a21)}$$

Therefore:

$$\frac{\partial C^t_{i,j}}{\partial t} + \frac{1}{2}\frac{\partial^2 C^t_{i,j}}{\partial t^2}\Delta t + O(\Delta t^2) = D_{gb}\frac{\partial^2 C^t_{i,j}}{\partial y^2} + D_{gb}\frac{1}{12}\frac{\partial^4 C^t_{i,j}}{\partial y^4}\Delta y^2 + O(\Delta y^3)$$

$$+\frac{D_l}{k\delta}\left(\frac{\partial C^t_{i,j}}{\partial x}\right)_{x=+\delta/2} - \frac{D_l}{k\delta}\frac{1}{3!}\left(\frac{\partial^3 C^t_{i,j}}{\partial x^3}\right)_{x=+\delta/2}\Delta x^2 + O(\Delta x^3)$$

$$+\frac{D_l}{k\delta}\left(\frac{\partial C^t_{i,j}}{\partial x}\right)_{x=-\delta/2} + \frac{D_l}{k\delta}\frac{1}{3!}\left(\frac{\partial^3 C^t_{i,j}}{\partial x^3}\right)_{x=-\delta/2}\Delta x^2 + O(\Delta x^3)$$

(a22)

This equation simplifies to

$$\frac{\partial C^t_{i,j}}{\partial t} = D_{gb}\frac{\partial^2 C^t_{i,j}}{\partial y^2} + \frac{D_l}{k\delta}\left(\frac{\partial C^t_{i,j}}{\partial x}\right)_{x=+\delta/2} + \frac{D_l}{k\delta}\left(\frac{\partial C^t_{i,j}}{\partial x}\right)_{x=-\delta/2} + E^t_{i,j}. \qquad \text{(a23)}$$

$$E^t_{i,j} = \frac{1}{2}\frac{\partial^2 C^t_{i,j}}{\partial t^2}\Delta t + D_{gb}\frac{1}{12}\frac{\partial^4 C^t_{i,j}}{\partial y^4}\Delta y^2 - \frac{D_l}{k\delta}\frac{1}{3!}\left(\frac{\partial^3 C^t_{i,j}}{\partial x^3}\right)_{x=+\delta/2}\Delta x^2$$

$$+\frac{D_l}{k\delta}\frac{1}{3!}\left(\frac{\partial^3 C^t_{i,j}}{\partial x^3}\right)_{x=-\delta/2}\Delta x^2 + O(\Delta t^2) + O(\Delta y^3) + O(\Delta x^3).$$

(a24)

Eq. (a20) is therefore consistent with the G.B. diffusion equation , because the truncation error $E^t_{k,j}\rightarrow 0$, when $\Delta t\rightarrow 0$, $\Delta y\rightarrow 0$ and $\Delta x\rightarrow 0$. It has truncation error $O(\Delta t+\Delta y^2+\Delta x^2)$.

Appendix III

Stability Consistency of the Finite Difference Approximation for the Grain Boundary Diffusion Equations

Rearranging the finite difference equation (a20):

$$C_{i,j}^{t+\Delta t}-C_{i,j}^{t} = f_{gby}(C_{i,j+1}^{t}-2C_{i,j}^{t}+C_{i,j-1}^{t}) + f_{gbx}(-1.5C_{i,j}^{t}+2C_{i+1,j}^{t}-0.5C_{i+2,j}^{t}) - f_{gbx}(1.5C_{i,j}^{t}-2C_{i-1,j}^{t}+0.5C_{i-2,j}^{t}), \quad (a25)$$

where $f_{gby} = \frac{\Delta t D_{gb}}{(\Delta y)^2}$ and $f_{gbx} = \frac{\Delta t D_l}{\delta \Delta x}$. The stability of Equation (a25) may be determined by application of the von Neumann method in the following way. Each Fourier component of the error distribution at the time t may be written:

$$\xi_{i,j}^{t} = (G)^t e^{i^c(m_x i\Delta x + m_y j\Delta y)}, \quad (a26)$$

where $(G)^t$ is the complex amplitude at time level t of the particular finite Fourier component whose wave numbers in the x and y direction are m_x and m_y, and where $i^c=\sqrt{-1}$. Defining the x and y phase angles by $\beta_x=\pi m_x \Delta x$ and $\beta_y=\pi m_y \Delta y$, Eq. (a26) then becomes:

$$\xi_{k,j}^{t} = (G)^{t} e^{i^{c}(k\beta_x + j\beta_y)}. \qquad (a27)$$

Substitution of Eq. (a27) into the error equation corresponding to the finite difference equation (a25) gives, on division by $(G)^{t} e^{i^{c}(k\beta_x + j\beta_y)}$,

$$G^{\Delta t}-1 = f_{gby}[\cos\beta_y - i^{c}\sin\beta_y - 2 + \cos\beta_y + i^{c}\sin\beta_y]$$

$$+f_{gbx}[-0.5(\cos 2\beta_x - i^{c}\sin 2\beta_x)+2(\cos\beta_x - i^{c}\sin\beta_x)-3$$

$$-0.5(\cos 2\beta_x - i^{c}\sin 2\beta_x)+2(\cos\beta_y + i^{c}\sin\beta_y)], \qquad (a28)$$

then,

$$G^{\Delta t} = 1-4f_{gby}\sin^2\left(\frac{\beta_y}{2}\right) - 8f_{gbx}\sin^2\left(\frac{\beta_x}{2}\right). \qquad (a29)$$

Because G is real, the stability requirement $|G^{\Delta t}| \le 1$ becomes

$$-1 \le 1-4f_{gby}\sin^2\left(\frac{\beta_y}{2}\right) - 8f_{gbx}\sin^2\left(\frac{\beta_x}{2}\right) \le 1. \qquad (a30)$$

This is satisfied, and Eq. (a25) is stable, if

$$2f_{gby} + 4f_{gbx} \le 1. \qquad (a31)$$

Therefore the criterion for the calculation time step is

$$\Delta t \leq \frac{1}{2\left(\frac{D_{\phi b}}{(\Delta y)^2} + \frac{2D_l}{\delta \Delta x}\right)}. \qquad \text{(a32)}$$